Coastal and Inland Aquatic Data Products for the Hyperspectral Infrared Imager (HyspIRI)

A Preliminary Report by the HyspIRI Aquatic Studies Group (HASG)

26 February 2015

Authors

Abelev, Andrei	Naval Research Laboratory
Babin, Marcel	Unité Mixte Internationale Takuvik, Université Laval
Bachmann, Charles	Rochester Institute of Technology
Bell, Thomas	University of California at Santa Barbara
Brando, Vittorio	IREA, Consiglio Nazionale delle Ricerche
Byrd, Kristin	U.S. Geological Survey
Dekker, Arnold	CSIRO Land and Water
Devred, Emmanuel	Unité Mixte Internationale Takuvik, Université Laval
Forget, Marie-Hélène	Unité Mixte Internationale Takuvik, Université Laval
Goodman, James	HySpeed Computing
Guild, Liane	NASA Ames Research Center
Hochberg, Eric	Bermuda Institute of Ocean Sciences
Hu, Chuanmin	University of South Florida
Jo, Young-Heon	Pusan National University
Kelly, Maggi	University of California, Berkley
Klemas, Victor	University of Delaware
Lee, Zhongping	University of Massachusetts, Boston
Moisan, Tiffany	NASA, Wallops
Moses, Wesley	Naval Research Laboratory
Muller-Karger, Frank	University of South Florida
Palacios, Sherry	NASA Ames Research Center
Philpot, Bill	Cornell University
Turpie, Kevin*	University of Maryland, Baltimore County
Toro-Farmer, Gerardo	University of South Florida
Yu, Qian	University of Massachusetts, Amherst

* - Contributing Editor

HASG Members

Abelev, Andrei	Naval Research Laboratory
Babin, Marcel	Unité Mixte Internationale Takuvik, Université Laval
Bachmann, Charles	Rochester Institute of Technology
Barreto, Maritza	University of Puerto Rico
Bell, Thomas	University of California at Santa Barbara
Bissett, Paul	Florida Environmental Research Institute
Blanco, Alfonso	George Mason University, EPA
Boss, Emmanuel	School of Marine Science, University of Maine
Bracher, Astrid	Institute of Environmental Physics, University of Bremen
Brando,Vittorio	IREA, Consiglio Nazionale delle Ricerche
Byrd, Kristin	U.S. Geological Survey
Campbell, Petya	University of Maryland, Baltimore County
Choi, Jung-Kuk	Korea Institute of Ocean Science & Technology (KIOST)
Craig, Susanne	Bedford Institute of Oceanography, Dalhousie University
Dekker, Arnold	CSIRO Land and Water
Devred, Emmanuel	Unité Mixte Internationale Takuvik, Université Laval
Dierssen, Heidi	University of Connecticut
Ferreira, Ana Rita	Upwelling | Blue Innovation
Forget, Marie-Hélène	Unité Mixte Internationale Takuvik, Université Laval
Gao, Bo-Cai	Naval Research Laboratory
Goodman, James	HySpeed Computing
Guild, Liane	NASA Ames Research Center
Hill, Victoria	Old Dominion University
Hochberg, Eric	Bermuda Institute of Ocean Sciences
Hu, Chuanmin	University of South Florida
Jo, Young-Heon	Pusan National University
Kelly, Maggi	University of California, Berkley
Kiefer, Dale	University of Southern California
Klemas, Victor	University of Delaware
Knaeps, Els	Flemish Institute for Technological Research (VITO)
Knight, Benjamin	Cawthron Institute
Kudela, Raphael	University of California, Santa Cruz
Lee, Zhongping	University of Massachusetts, Boston
Martinez Vincente, Victor	Plymouth Marine Laboratory
Minnett, Peter	RSMAS, University of Miami
Moisan, Tiffany	NASA Wallops
Moses, Wesley	Naval Research Laboratory
Muller-Karger, Frank	University of South Florida
Palacios, Sherry	ORAU, NASA Ames Research Center
Park, Youngje	Korea Institute of Ocean Science & Technology (KIOST)
Philpot, Bill	Cornell University
Purkis, Sam	Oceanographic Center, NOVA Southeastern University
Roffer, Michell A.	Roffer's Ocean Fishing Forecasting Service, Inc.
Roper, William	George Mason University

Salem, Foudan	George Mason University
Schaeffer, Blake A.	U.S. Environmental Protection Agency
Siegel, Dave	University of California at Santa Barbara
Sheng, Yongwei	Dept of Geography, UCLA
Sterckx, Sindy	Flemish Institute for Technological Research (VITO)
Stumpf, Richard	NOAA
Toro-Farmer, Gerardo	University of South Florida
Torres Perez, Juan	BAERI, NASA Ames Research Center
Tzortiou, Maria	University of Maryland
Yu, Qian	University of Massachusetts, Amherst
Zimmerman, Richard	Old Dominion University
Zuloaga, Santiago	Imaer Tecnica

Table of Contents

Executive Summary

The HyspIRI Aquatic Studies Group (HASG) has developed a conceptual list of data products for the HyspIRI mission to support aquatic remote sensing of coastal and inland waters. These data products were based on mission capabilities, characteristics, and expected performance. The topic of coastal and inland water remote sensing is very broad. Thus, this report focuses on aquatic data products to keep the scope of this document manageable. The HyspIRI mission requirements already include the global production of surface reflectance and temperature. Atmospheric correction and surface temperature algorithms, which are critical to aquatic remote sensing, are covered in other mission documents. Hence, these algorithms and their products were not evaluated in this report. In addition, terrestrial products (e.g., land use/land cover, dune vegetation, and beach replenishment) were not considered. It is recognized that coastal studies are inherently interdisciplinary across aquatic and terrestrial disciplines. However, products supporting the latter are expected to already be evaluated by other components of the mission. The coastal and inland water data products that were identified by the HASG, covered six major environmental and ecological areas for scientific research and applications: wetlands, shoreline processes, the water surface, the water column, bathymetry and benthic cover types. Accordingly, each candidate product was evaluated for feasibility based on the HyspIRI mission characteristics and whether it was unique and relevant to the HyspIRI science objectives.

For each of the six major environmental and ecological areas of aquatic data products, several key example data products were identified (Table ES.1). These were assigned priority ranking based on three major factors. The first factor was the uniqueness of the measurement to the HyspIRI mission characteristics and objectives. In certain cases, products could be identified as not being easily generated on global scales via any other orbiting remote sensing asset planned by the US government. The second factor was the urgency for such data products in the support of scientific research and application in the six major aquatic environmental and ecological areas. This involved assessing how well the data products would directly and immediately contribute to the HyspIRI science questions or were tied to objectives identified by the 2007 Decadal Survey. In addition, the importance or urgency to science research and applications was also considered, even if not clearly defined by the mission science questions or Decadal Survey. The third factor was the feasibility or ease of implementation of each data product, i.e., what are the chances that accurate results would be obtained? Combining these three criteria through a continued dialogue, a subjective priority was assigned to key candidate products and applications. Assessment of aquatic data products for the six major areas are discussed in detail in Section 2 of this report and synthesized in Section 3.

Two main challenges face the coastal and inland aquatic remote sensing community in developing the data products described in this report. First, community-owned Level-2, -3, or -4 algorithms must be shown to generate products on synoptic scales using HyspIRI Level-1 or Level-2 surface reflectance or temperature data. Second, it must also be shown that these community-generated data products will be of sufficient

quality to achieve science objectives, especially those that are aligned with answering the mission science questions. To address these two challenges, recommendations are provided in the last section of this report. However, these recommendations are by no means exhaustive. A collaborative dialogue will need to be continued amongst algorithm developers, researchers in the field, mission engineering teams, and project and program management. The HASG can serve as a forum to facilitate this discussion throughout the algorithm development phase of the mission. Finally, remote sensing over coastal and inland waters present HyspIRI with unique, yet tractable, challenges. Thus, it is recommended that NASA support some preparatory algorithm development, including leveraging other efforts (e.g., the Pre-Aerosol, Clouds, and ocean Ecosystem (PACE) mission) and other resources when possible.

To that end, it is recommended that HyspIRI community efforts be synergized with other efforts in the greater coastal and inland remote sensing community. A community-wide dialogue could be facilitated through the HASG by providing a forum for development efforts supporting other hyperspectral or coastal and inland water remote sensing endeavors. In addition, it is important that the HASG leadership inform the mission project and program management of community developments, interests, and recommendations. Finally, the HASG could facilitate a dialogue with the mission engineering team to develop a complete understanding of instrument characteristics, calibration, and project-owned Level-2 algorithm function and characteristics. It is expected that this exchange could be collaborative, but moderated by project management, as necessary. Further recommendations regarding this relationship are provided in Section 4 of this report.

Table ES. 1 - Products and Prioritization. Summary of the key data products or applications for sections 2.1 – 2.6 of this report. For each data product or application, a priority is assigned, from 1 to 4 (1 being the highest priority), which is based on the uniqueness to the HyspIRI mission, the urgency and compelling nature, and the feasibility of each proposed product.

Category	Data Product	Priority
1. Wetlands	**Wetland Delineation and Type**	**1**
	Fraction of Vegetation Cover (sub-pixel)	**2**
	Fraction of Water Cover (sub-pixel)	**2**
	Fraction of Exposed Soil (sub-pixel)	**2**
	Sub-aerial Biomass	**3**
	Species Map	**3**
	Vegetation and Water Indices	**3**
	Evaporation Rates	**3**
	Soil Water Content	**3**
	Substrate Type	**4**
	Substrate Grain Size	**4**
	Substrate Bearing Strength	**4**
2. Coastlines / Ice Margins	Groundwater Discharge and Eco Response	**2**
	Ice Margin Phytoplankton Pigments	**2**
	Floods and Coastlines Maps (Episodic)	**3**
3. Water Surface Features	**Water Surface Temperature***	**1**
	Floating Material Type Map	**2**
	Floating Material Density	**2**
	Total Mass	**3**
4. Water Column	Apparent Optical Properties	
	-Remote Sensing Reflectance (R_{rs})*	**1**
	-Diffuse Attenuation Coefficient (K_d)	**3**
	Inherent Optical Properties	
	-Absorption (a)	**3**
	-Particle Backscatter (b_p)	**3**
	Fluorescence Line Height	**2**
	Total Suspended Matter (TSM)	**3**
	Total Suspended Sediment (TSS)	**3**
	CDOM	**3**
	Chlorophyll *a* Concentration	**3**
	Other Pigment Concentrations	**3**
	Phytoplankton Functional Type	**3**
5. Bathymetry	**Depth**	**1**
6. Benthos	**Benthic Cover Type (Coral, Algae, SAV, etc.)**	**1**
	Species Maps	**3**

*** Project Supported Data Products**

1. Introduction

1.1 Background

Coastal ecosystems are among the most productive ecosystems in the world, playing a major role in water, carbon, nitrogen and phosphorous cycles between land and sea. Furthermore, coastal regions are home to about two thirds of the world's population (Cracknell, 1999). In the USA, coastal counties alone contribute nearly 40% of the country's Gross Domestic Production (Kildow, *et al*., 2009). The social and economic well-being of human communities living in these regions depends significantly on the health of the surrounding coastal ecosystem. Studies of coastal and inland aquatic ecosystems and water quality are critical to understanding and protecting these valuable resources. These marginal regions between land and sea support valuable ecotones that are highly vulnerable to shifts in the environment, whether from climate change and its consequences (e.g., sea level rise), human activities (e.g., eutrophication or changes to existing watershed hydrology), or natural disturbances (e.g., storms or tsunamis). As these drivers of change can occur on large scales or even globally, spaceborne remote sensing is a key tool for studying these environments.

As coastal aquatic ecosystems exhibit extreme variations in areal extent, spatial dynamics, and bio-optical complexity, studying and monitoring their biophysical features and processes require imagery with high spatial and spectral resolutions (Klemas, 2013). Lee *et al.*, (2007) have suggested a minimum requirement of 17 spectral bands (see Table 2 in their paper) located between 400 and 800 nm to observe subtle changes in the remote sensing reflectance of water alone, given the great variability in the influence of turbidity, bottom reflectance, and complex atmospheric conditions. Adding interdisciplinary studies of emergent communities, shorelines, floating substances and benthic communities increases the required number and range of bands substantially. The National Research Council report titled "Earth Science and Applications from Space: National Imperatives for the Next Decade and Beyond" (2007), also known as the "Decadal Survey," defined the need for a global mission for studying coastal aquatic ecosystems using a spaceborne hyperspectral sensor. Recent advances in sensor technology have enabled the development and launch of spaceborne hyperspectral sensors, which has opened a new era in the remote sensing of inland, estuarine, and coastal environments. Remote sensing retrievals can benefit from more spectral information, making it possible to acquire more information over a greater range of conditions and reduce the effect of noise in the data by choosing different, but correlated, regions of the spectrum, or using information from a combination of bands with a known relationship. Hyperspectral sensors open the possibility of the retrieval of a large number of aquatic biophysical products, such as phytoplankton concentration, concentration of dissolved organic matter, diffuse attenuation coefficient, backscattering coefficient, suspended sediment concentration, or phytoplankton community structure. In 2000, the National Aeronautics and Space Administration (NASA) launched the first spaceborne hyperspectral sensor, Hyperion, with 220 contiguous spectral bands. In 2001, the European Space Agency launched the

Compact High Resolution Imaging Spectrometer (CHRIS), a programmable sensor with up to 63 bands. The Naval Research Laboratory built and launched the Hyperspectral Imager for the Coastal Ocean (HICO) in 2009. Except for HICO, none of the spaceborne hyperspectral sensors launched so far were designed to have a Signal-to-Noise Ratio (SNR) that is optimized for the optically complex coastal aquatic environment. HICO is a low cost, prototype sensor that was developed as a demonstration mission with on-demand image acquisition, but was not designed to be capable of providing global coverage on a regular basis.

The Decadal Survey has recommended the development of the Hyperspectral Infrared Imager (HyspIRI) mission. Although originally developed as a terrestrial ecosystem mission, HyspIRI is well suited to produce global maps of coastal ecosystems, which can improve our understanding of how coastal processes and ecologies are distributed and structured, and how they function. To that end, this document reports input from the HyspIRI Aquatic Study Group (HASG), which was chartered to solicit and compile input from the hyperspectral coastal and inland remote sensing community. The resulting report explores potential data products to be generated by the community using measurements taken from the HyspIRI mission. The focus is primarily on coastal systems, though inland water studies are equally important. The potential application of hyperspectral remote sensing of inland waters is well covered in an Australian government report (Dekker and Hestir, 2012).

1.2 HyspIRI Mission Concept

As shown in Table 1.1, the current design plan for HyspIRI includes a hyperspectral Visible Short Wave Infrared (VSWIR) imaging spectrometer with 213 spectral channels between 0.38 and 2.5 μm at 0.01 μm spectral resolution, and a multispectral Thermal Infrared (TIR) imager with eight spectral channels (one centered at 4 μm and seven located between 7.5 and 12 μm). Both instruments will have a spatial resolution of 60 m at nadir. The spacecraft is planned to fly in a polar orbit, crossing the equator at 11:00 a.m. local time in its ascending node. The equatorial revisit times will be 19 days and five days for the VSWIR and TIR instruments, respectively (Roberts *et al.*, 2012). The instrument will have a 14-bit radiometric resolution, 2% polarization sensitivity, and a 4° westward tilt to reduce specular solar reflectance.

Figure 1.1 compares the spectral resolution and range of HyspIRI's VSWIR spectrometer to those of traditional spaceborne ocean color instruments used for open-ocean remote sensing. With more than 30 bands in the spectral range 400–800 nm, HyspIRI would be capable of capturing subtle changes in the reflectance due to bio-optical variations in the water, and provide new information that cannot be obtained from current multispectral sensors. For example, the spectral bands between 710 and 750 nm will provide critical information necessary for accurately retrieving high concentrations of chlorophyll-*a* (chl-*a*) (Moses *et al.,* 2009). The high spectral resolution of HyspIRI would also result in redundancy of information due to a strong correlation between some bands, which would improve retrievals of water column properties when the measurements contain errors (IOCCG, 1998). Using the high spectral resolution of HyspIRI, we can expect to improve the accuracy of existing multispectral products (e.g.,

chl-*a* concentration, inherent optical properties, *etc.*), and also derive new products that could not be retrieved using multispectral sensors (e.g., pigment composition).

Table 1.1 Key characteristics of the HyspIRI mission.

	VSWIR	**TIR**
Spectral Range	380 – 2500 nm	3.98, 7.35, 8.28, 9.07, 10.53, 11.33, and 12.05 μm
Spectral Bandwidth	10 nm, uniform over range	0.084, 0.32, 0.34, 0.35, 0.36, 0.54, 0.54, and 0.52 μm
Radiometric Resolution	14-bit	14-bit
Angular Field of View	12°	51°
Altitude	700 km	700 km
Swath Width	145 km	600 km
Cross Track Samples	>2400	10,000
Spatial Resolution	60 m (Depth < 50m) 1 km (Depth > 50m)	60 m (Depth < 50m) 1 km (Depth > 50m)
Spatial Range	>145 km	600 km
Samples	2400	10,000
Orbit	Polar Ascending	Polar Ascending
Equatorial Crossing	11:00 a.m.	11:00 a.m.
Altitude	700 km	
Equatorial Revisit	19 days	5 days
Rapid Response	3 days	3 days
Tilt	4° West	4° West

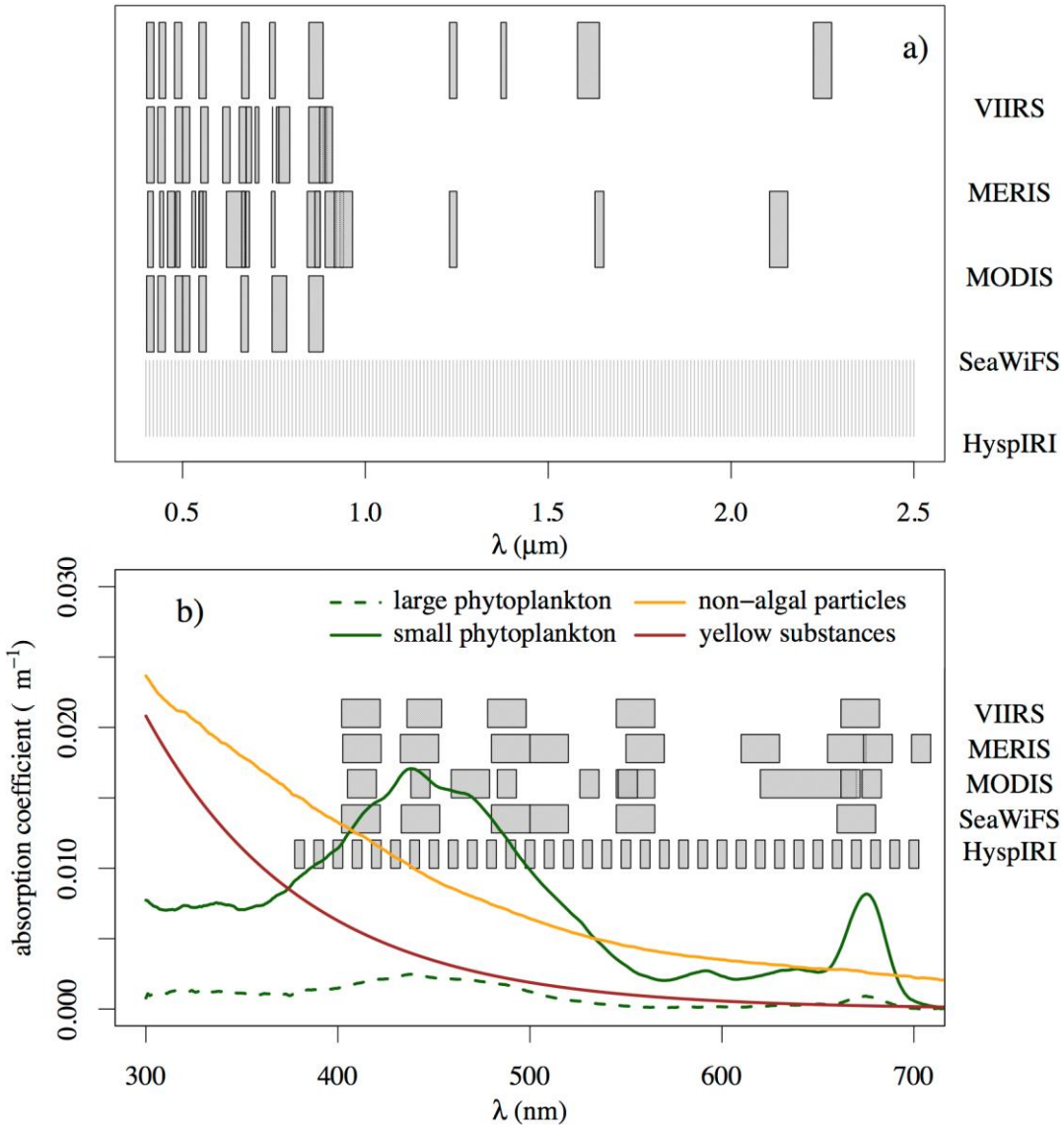

Figure 1.1 (a) Spectral coverage of HyspIRI and standard ocean color sensors in the VSWIR region; (**b**) Absorption coefficients of phytoplankton (small and large cells), non-algal particles, yellow substances and the spectral coverage of the aforementioned sensors in the visible region. All bands are shown for the MODerate Imaging Spectroradiometer (MODIS) and MERIS (MEdium Resolution Imaging Spectrometer), some of which overlap. However, only the moderate resolution bands are shown for VIIRS (Visible Infrared Imaging Spectrometer).

Observations of the visible portion of the water-leaving radiance from a spaceborne platform started at the end of the 1970s with the launch of the Coastal Zone Color Scanner (CZCS) on Nimbus-7. CZCS had a spatial resolution of 825 m at nadir and five channels spanning 443–750 nm. The sensor was primarily used to map the biomass of the ocean, which was achieved with great success (Yentsch, 2013). Following CZCS, a number of multispectral sensors have been launched by various space agencies, with a number of bands in the visible and infrared regions, such as the Ocean Color Monitor

(OCM), with eight bands, and the Global Imager (GLI), with 36 bands. The spatial resolution at nadir of such multispectral ocean color sensors has ranged from 250 m (e.g., the MODerate spectral resolution Imaging Spectroradiometer (MODIS)) to a few kilometers (e.g., the POLarization and Directionality of the Earth's Reflectances (POLDER) instrument, with 6 km spatial resolution).

The spectral range of HyspIRI includes wavelengths between 1 and 2.5 μm, which are important for atmospheric correction and can be used to significantly improve the retrieval of surface reflectance in coastal and inland waters. The projected SNR of HyspIRI is better than that of Hyperion, comparable to that of HICO, and is considered reasonably adequate for accurately retrieving hyperspectral reflectance from water surface for typical coastal or inland water conditions. Even with a temporal revisit cycle as long as 19 days, the regular global coverage offered by HyspIRI at high spatial and spectral resolutions will support studies of global coastal waters that require detailed information about the spatial extent and distribution of surface, sub-surface, or bottom features. This report also discusses the retrieval of various optical and bio-optical properties routinely measured by multispectral ocean color sensors, and explains the improvements that could be achieved through hyperspectral measurements from sensors such as HyspIRI.

1.3 Identifying Candidate Remote Sensing Products

In order to develop this report, community input was compiled from the literature and through discussions of the HASG. This input was subsequently documented in this report by a smaller team of writers, and the resulting manuscript was then reviewed by the HASG. The object was to first identify all manners of aquatic hyperspectral data products (including some details or examples of their use) that can be obtained through the HyspIRI mission and are necessary to address the HyspIRI aquatic science questions (see Table 1.2). The team then considered the requirements of algorithms that would be supported by HyspIRI's capabilities. This led to a more realistic identification of the challenges associated with each potential product. To aid NASA project and program management, these products were then prioritized based on their uniqueness to the mission characteristics, their compelling nature or relevance to the mission science objectives and their overall feasibility.

Most of the focus was placed on hyperspectral applications of HyspIRI VISWIR spectroscopy, particularly including classification algorithms and spectral component decomposition. In addition, some algorithms that rely on only a few bands were also considered. In some cases, this was merely to explore how hyperspectral data products would improve our understanding of coastal and inland water processes. Some multi-band algorithms were included with the supposition that contemporaneous, co-registered multi-band products would enhance the application of data products based on hyperspectral data. In addition, the rich spectral data offered by the spectrometer facilitate the use of adaptable multispectral algorithms, and support a greater variety of potential multi-band algorithms, which addresses the great diversity of spectral signatures found along the water/land interface. The use of the HyspIRI thermal bands were likewise considered.

Table 1.2. HyspIRI Science Questions (copied from http://hyspiri.jpl.nasa.gov/science). The VQ questions are primarily related to VSWIR data, the TQ questions are related to TIR data, and the CQ questions are related to VSWIR-TIR combined data products.

No.	Question
VQ1.	What is the global spatial pattern of ecosystem and diversity distributions and how do ecosystems differ in their composition or biodiversity?
VQ2.	What are the seasonal expressions and cycles for terrestrial and aquatic ecosystems, functional groups, and diagnostic species? How are these being altered by changes in climate, land use, and disturbance?
VQ3.	How are the biogeochemical cycles that sustain life on Earth being altered/disrupted by natural and human-induced environmental change? How do these changes affect the composition and health of ecosystems and what are the feedbacks with other components of the Earth system?
VQ4.	How are disturbance regimes changing and how do these changes affect the ecosystem processes that support life on Earth?
VQ5.	How do changes in ecosystem composition and function affect human health, resource use, and resource management?
VQ6.	What are the land surface soil/rock, snow/ice and shallow-water benthic compositions?
TQ1.	How can we help predict and mitigate earthquake and volcanic hazards through detection of transient thermal phenomena?
TQ2.	What is the impact of global biomass burning on the terrestrial biosphere and atmosphere, and how is this impact changing over time?
TQ3.	How is consumptive use of global freshwater supplies responding to changes in climate and demand, and what are the implications for sustainable management of water resources?
TQ4.	How does urbanization affect the local, regional and global environment? Can we characterize this effect to help mitigate its impact on human health and welfare?
TQ5.	What is the composition and temperature of the exposed surface of the Earth? How do these factors change over time and affect land use and habitability?
CQ1.	How do inland, coastal, and open ocean aquatic ecosystems change due to local and regional thermal climate, land-use change, and other factors?
CQ2.	How are fires and vegetation composition coupled?
CQ3.	Do volcanoes signal impending eruptions through changes in the temperature of the ground, rates of gas and aerosol emission, temperature and composition of crater lakes, or health and extent of vegetation cover?
CQ4.	How do species, functional type, and biodiversity composition within ecosystems influence the energy, water and biogeochemical cycles under varying climatic conditions?
CQ5.	What is the composition of exposed terrestrial surface of the Earth and how does it respond to anthropogenic and non-anthropogenic drivers?
CQ6.	How do patterns of human environmental and infectious diseases respond to leading environmental changes, particularly to urban growth and change and the associated impacts of urbanization?

2. Survey of Hyperspectral Aquatic Data Products

2.1 Wetland Cover Classification and Mapping

Wetlands are highly productive systems that act as critical habitats for a wide variety of life and provide numerous ecosystem services. They are at risk globally due to a range of factors including agricultural and urban expansion, eutrophication, pollution, and sea level rise. Mapping wetlands continues to be a national priority in the U.S. Global efforts to monitor wetlands are increasing. This section provides a brief review of past and present success at mapping wetland type and function (e.g., saltwater, brackish water, freshwater, wooded, scrub-shrub, mangroves, and marshes) via remote sensing across spatial and spectral scales, and highlights areas in which the hyperspectral capability, spatial resolution, swath-width and signal-to-noise ratio of HyspIRI meet most of the requirements for mapping wetland vegetation type and function at regional to global scales.

Wetlands and estuaries are highly productive and act as critical habitats for a wide variety of plants, fish, shellfish, and other wildlife. Wetlands also provide flood protection, protection from storm and wave damage, water quality improvement through filtering of agricultural and industrial waste, and recharge of aquifers (Miller and Fujii 2010, Morris *et al*., 2002; Odum, 1993). Wetlands have been exposed to a wide range of stress-inducing alterations, including dredge and fill operations, hydrologic modifications, pollutant run-off, eutrophication, impoundments, invasion by other plant species, and fragmentation by roads and ditches. There is also considerable concern regarding the impact of climate change on coastal wetlands, especially due to relative sea level rise, increasing temperatures and changes in precipitation (Church and White, 2006; McInnes *et al*., 2003). At the same time, coastal wetlands (along with mangroves and seagrasses) represent a significant carbon pool. The carbon stocks and future cumulative carbon storage in these wetlands are referred to as "Blue Carbon," and play an important role in managing atmospheric carbon (Pendleton et al. 2012). To plan for wetland protection and responsible development, there is a need to map and monitor changes in saltwater, freshwater and wooded wetlands at local, regional, and global scales. Much has been done since the early 1980s to map wetlands with remote sensing. Early work with multispectral imagery has been augmented with recent use of hyperspectral imagery. Dynamic global vegetation models offer explicit representations of the land surface through time and have been used to research large-scale hydrologic responses to climate change (Murray *et al*., 2012).

Knowledge of latent and sensible heat fluxes and soil moisture is important to monitoring plant growth and productivity, land degradation and desertification, numerical modeling and prediction of atmospheric and hydrological cycles, and improving the accuracy of weather forecast models. The combined use of satellite data from optical and thermal infrared radiometers has shown promise for the retrieval of latent and sensible

heat fluxes, as well as soil surface moisture variations (Petropoulos *et al*., 2009; Sandholt *et al.*, 2002).

Science Questions Addressed

The wetland data products obtained from the HyspIRI mission will help address the following science questions (from Table 1.2):

VQ1. What is the global spatial pattern of ecosystem and diversity distributions and how do ecosystems differ in their composition or biodiversity?

VQ2. What are the seasonal expressions and cycles for terrestrial and aquatic ecosystems, functional groups, and diagnostic species? How are these being altered by changes in climate, land use, and disturbance?

VQ3. How are the biogeochemical cycles that sustain life on Earth being altered/disrupted by natural and human-induced environmental change? How do these changes affect the composition and health of ecosystems and what are the feedbacks with other components of the Earth system?

CQ1. How do inland, coastal, and open ocean aquatic ecosystems change due to local and regional thermal climate, land-use change, and other factors?

CQ4. How do species, functional type, and biodiversity composition within ecosystems influence the energy, water and biogeochemical cycles under varying climatic conditions?

CQ6. How do patterns of human environmental and infectious diseases respond to leading environmental changes, particularly to urban growth and change and the associated impacts of urbanization?

Candidate Products or Applications

Saltwater and Brackish Marsh Vegetation

Salt marshes are widely distributed along many of the world's coasts and are often dominated by specifically adapted species of grasses, sedges, and rushes that tend to form monospecific canopies across regions with a high salinity gradient. For instance, smooth cordgrass (*Spartina alterniflora*) tends to dominate the eastern North American seaboard and the Gulf of Mexico. The relative purity and size of some salt marshes and aquatic nature of the substrate make it possible to map them from satellites. Multispectral medium resolution satellite imagers, such as Landsat TM and Satellite Pour l'Observation de la Terre (SPOT), and high resolution satellites, such as IKONOS® and QuickBird, have been effective primarily for mapping wetland location and extent (Gilmore *et al.*, 2010; Jensen, 1998; Klemas, 2011; Lunetta and Balogh, 1999; Lyon and McCarthy, 1995; Wang, 2010), as well as vegetation pattern and condition (Ramsey and Rangoonwala, 2005; Kelly *et al*., 2011; Tuxen *et al.*, 2008; Tuxen *et al.*, 2011) at local or regional scales.

Efforts have been made to assess and monitor coastal marshes in order to improve our understanding of their essential services and to aid in their management (Dahl, 2011; Kelly and Tuxen, 2009; UNEP, 2006). Part of the process of managing degradation of

coastal marsh services includes identifying changes in marsh systems that would affect these services (Barbier, *et al.*, 2011). Studies of changes in ecological function and response are often limited to a small number of plots, and scientists must extrapolate findings to regional scales. Although monitoring widespread changes to these landscapes could assist researchers and policymakers in assessing and monitoring marsh deterioration or restoration, limited accessibility makes large-scale, *in situ,* evaluation challenging (Seher and Tueller, 1973). Remote sensing techniques offer an efficient approach to quantify changes in marsh vegetation (Klemas, 2013a; 2013b). The utility of remote sensing techniques has been explored for measuring quantities over large regions of wetlands, such as species and cover type (Artigas and Yang, 2005; Jensen, *et al.*, 1986; Jollineau and Howarth, 2008; Judd, *et al.*, 2007; Schmidt and Skidmore, 2003; Silvestri and S., 2003; Underwood, *et al.*, 2006; Zomer, *et al.*, 2009), canopy density or Leaf Area Index (LAI) (Sone, *et al.*, 2009; Wang, *et al.*, 2007; Xavier and Vettorazzi, 2004; Xiao, *et al.*, 2002), biomass (Klemas, 2013a; Mishra *et al.* 2012; Mutanga *et al*. 2012; Byrd *et al*. 2014), or quantities related to plant production and stress (Klemas, 2001; Mendelssohn, *et al.*, 2001; Ramsey and Rangoonwala, 2006; Tilley, 2003; Vaesen, *et al.*, 2001; Zhao, *et al.*, 2009). However, the optical properties of an inundated canopy can present new challenges for some of these techniques (Turpie, 2012; Turpie, 2013). Most attempts at mapping these vegetation biophysical characteristics have utilized multispectral sensors, largely due to ease of availability. Recent analysis of full spectrum field spectrometer data indicated that hyperspectral first derivative reflectance spectra can provide improved predictions of wetland vegetation biomass over simulated broadband spectra under low inundation conditions (Byrd *et al.* 2014). Further, biomass studies in forest and cropland have demonstrated the greater predictive capacity of hyperspectral imagery compared to multispectral sensors (Mariotto, *et al*. 2013, Thenkabail, *et al*. 2004), suggesting that hyperspectral data will improve biophysical models in wetlands as well.

The value of satellite imagery is illustrated in Figure 2.1.1, which shows an image of the Texas coast captured by the MODIS sensor on NASA's Terra satellite 13 days after Hurricane Ike made landfall on September 13, 2008. The storm's surge covered hundreds of kilometers of the Gulf Coast because Ike was a large storm, with tropical-storm-strength winds stretching more than 400 km from the center of the storm. Most of the shoreline in this region is coastal wetland. One can clearly distinguish the brown areas in the image, which are the result of the massive storm surge that Ike had pushed far inland over Texas and Louisiana, causing a major marsh dieback. The salty water burned the plants, leaving them wilted and brown. The brown line corresponds with the location and extent of the wetlands. North of the brown line, the vegetation gradually transitions to pale green farmland and dark green natural vegetation untouched by the storm's surge. The powerful tug of water returning to the Gulf also stripped marsh vegetation and soil off the land. Therefore, some of the brown seen in the wetlands may be deposited sediment. Plumes of brown water are visible as sediment-laden water drains from rivers and the coast in general. The muddy water slowly diffuses, turning pale green, green, and finally blue as it blends with clearer Gulf water (NASA/GSFC, 2010; Ramsey and Rangoonwala, 2005).

Figure 2.1.1 – The MODIS Spectroradiometer on NASA's Terra satellite captured this image with a spatial resolution of 250 m 13 days after Hurricane Ike came ashore. The brown areas in the image are the result of a massive storm surge that Ike pushed far inland over Texas and Louisiana, causing a major marsh dieback. Credits: NASA/GSFC.

Detailed mapping of species composition, dynamics, and plant vigor in complex salt marshes will require additional spectral data beyond what is found in multispectral imagery alone (Kelly and Tuxen, 2009). For example, the Airborne Visible and Infrared Imaging Spectrometer (AVIRIS) has been successfully used to map estuarine wetlands in the San Francisco Bay Area, California, USA (Rosso *et al*., 2005; Li *et al*., 2005), and Everglades National Park, Florida, USA (Hirano, *et al*., 2003), as well as other study areas. These early proof-of-concept studies using airborne hyperspectral imagers strongly suggest significant benefit from the use of data generated by HyspIRI.

Freshwater Marshes

Freshwater marshes are relatively patchy and floristically diverse, and have a more mixed vegetative cover, producing a more complex, composite spectral signature than most saltwater marshes. These systems have also been disproportionately altered due to agricultural and urban expansion. Therefore, for local studies, they often need to be observed at high spatial resolution. A cost-effective method is to cover large areas, such as the Amazon Basin system, with medium resolution (30-250 m) imagers, and focus on critical or rapidly changing sites using the high resolution sensors (Arai *et al.*, 2011). Hyperion and MERIS data have been used to classify Amazon water types (Lobo *et al*., 2012).

The evaporation flux from freshwater wetlands has been estimated using thermal infrared sensing data and parameterization of the surface energy balance (Jackson, 2005; Mohamed, 2004). For instance, in the upper Nile Sudd wetlands of Sudan, the spatially averaged evaporation over three years was found to vary between 1460 and 1935 mm/yr. This is substantially less than open water evaporation, and the wetland appears to be 70% larger than what was previously assumed. This new set of spatially distributed evaporation parameters from thermal infrared (IR) remote sensing forms an important dataset for calibrating a regional climate model enclosing the Nile Basin (Chen *et al*., 2002; Moffett, 2010; Mohamed *et al*., 2004).

The hydro-meteorological data for many of the world's freshwater marshes is still quite inadequate. The areal size of these marshes, the evaporation rates, and their influence on the micro and meso climate are still unresolved questions of their hydrology. The combination of HyspIRI's thermal infrared radiometer and imaging spectrometer will be effective for observing these hydrologic conditions of wetlands, including water levels and other hydro-meteorological properties.

Wooded and Scrub-Shrub Wetlands

Forested and scrub-shrub wetlands, characterized as woody communities, are regularly inundated and saturated during the growing season. Wooded wetlands often spectrally resemble wooded uplands and are therefore difficult to distinguish from wooded upland areas, especially in drier conditions. For this reason, wooded wetlands are often less accurately mapped than emergent wetlands, even with hyperspectral imagery (e.g. Hirano *et al*., 2003). More success has been reported when satellite images of wetlands at their highest water levels are analyzed (Ozesmi and Bauer, 2002), or by making use of multi-temporal imagery from Landsat. For example, Townsend and Walsh (2001) used Landsat Thematic Mapper (TM) images from different seasons (March–April, May–June, July–August) throughout a single year to exploit the phenological variability in forest wetlands in North Carolina, USA for mapping ecologically important vegetation types within the floodplain (Townsend and Walsh, 2001). Satellite imaging systems, such as the Advanced Very High Resolution Radiometer (AVHRR), Landsat TM, and MODIS, have been used to monitor deforestation and droughts of forest canopies of rain forests, including the Amazon (Anderson *et al*., 2010).

Mangroves

Mangroves help reduce the erosional impact of storms, serve as breeding and feeding grounds for juvenile fish and shellfish, trap silt that could smother offshore coral reefs, and cleanse water by the uptake of nutrients and pollutants. Mangroves, which once occupied 75% of tropical and subtropical coastlines, are now seriously threatened by coastal development and climate change, including sea level rise. In many countries, mangrove swamps are being cut to provide firewood or building material, and are being destroyed by development of shrimp ponds (Alongi, 2002; Pinet, 2009; Wang and Sousa, 2009).

Rapid losses of mangroves make it crucial to inventory and monitor the remaining mangroves to protect them from harmful development (Blasco, Aizpuru and Gers, 2001; Guanawardena and Rowan, 2005; Terchunian *et al*., 1986). Mapping and quantifying the

structure and biomass of mangrove ecosystems on a large scale is also important for studies of carbon storage, biodiversity, forest quality, and habitat suitability. Remote sensing has had a crucial role in monitoring mangroves, but the majority of applications have been limited to mapping areal extent and patterns of change.

Mangrove forests are patchy and have gaps in the canopy that expose moist soil or water. Therefore, high spatial resolution is required for mapping them in detail. Large scale mangrove mapping has been performed in the past using medium-resolution satellites such as Landsat-TM and SPOT (Gao, 1998; Kovacs, Wang and Blanco-Correa, 2001; Saito *et al*., 2003). SPOT multispectral data were shown to be suitable for mapping dense mangroves. On the other hand, sparse mangroves were less accurately mapped**,** due to the spectral interference of their mudflat background (Gao, 1998).

Although there have been few studies using satellite-based hyperspectral remote sensing to detect and map mangrove species, laboratory experiments have shown that discrimination among multiple species is possible (Heumann, 2011; Vaiphasa *et al*., 2005). Satellite-borne hyperspectral imagers, such as Hyperion, can detect fine differences in spectral reflectance. Similarly, HyspIRI may be able to map the spatial extent of mangroves and provide species discrimination on a global scale (Blasco, Aizpuru, and Din Ndango, 2005; Heumann, 2011). One of the challenges with species discrimination using hyperspectral sensors is that the gaps in the canopy expose the background moist soil or water, which "contaminates" the pure spectral reflectance signatures of the mangroves, unless the canopy is very dense.

Marsh Hydrology and Hydro-meteorology

Knowledge of latent and sensible heat fluxes, as well as soil water content, is important for many environmental applications, including monitoring plant water requirements, plant growth, irrigation, land degradation, and desertification. Such data are also significant in the numerical modeling and prediction of atmospheric and hydrologic cycles, and for improving the accuracy of weather forecast models. The combined use of satellite data from optical and thermal infrared radiometers has shown promise for the retrieval of latent and sensible heat fluxes and soil surface moisture variations within the top 5 cm of the soil depth (Ghilain *et al*., 2011; Marshall *et al*., 2013; Petropoulos *et al*., 2009).

Evapotranspiration is an important variable in water and energy balances of the earth's surface. Understanding the distribution of evapotranspiration is a key factor in hydrology, climatology, agronomy, and ecological studies. On a global scale, about 64% of precipitation on the continents is evapotranspired. Of this amount, about 97% is evapotranspired from land surfaces and 3% evaporated from open water (Rivas and Caselles, 2004). In some zones of the world, about 90% of the precipitation can be evapotranspired (Varni *et al*., 1999). Thus, most of the water from the hydrologic system is transpired and evaporated, showing the importance evapotranspiration.

Spatial patterns of evapotranspiration in marshes can now be calculated using satellite data with a minimum of ground meteorological data (Meijerink, 2002). Rivas and Caselles (2004) have shown that the evapotranspiration of vegetation in a large river

basin can be estimated by combining the surface temperature, as obtained from satellite images, with conventional weather information. Carlson (2007) prepared an overview of the Triangle Method for estimating surface evapotranspiration and soil moisture from satellite imagery. A review of methods using remotely sensed surface temperature data for estimating land surface evaporation is provided by Kalma *et al*. (2008).

Continuous reduction of water levels and man-made and natural modifications of wetland hydrology are causing wetland stress and losses in many parts of the world. These hydrologic changes influence vegetation species composition, distribution, and condition. In the worst case, this can lead to a drying out of the whole wetland (Chopra *et al*., 2001; Xin, 2004). The hydrological conditions of emergent wetland vegetation have been explored with the help of remotely sensed biophysical data, such as surface temperature and vegetation indices (NDVI). Using a digital elevation model and regression models, a relation between surface temperature and water stress has been established. Results show that surface temperature and NDVI can be used for a better understanding of hydrological conditions of wetlands (Banks *et al*., 1996; Bendjoudi *et al*., 2002; Petropoulos *et al*., 2009). Daily and 8-day composite products from MODIS have been used effectively to map floodplain and wetland inundation extent corresponding to peak flows of significant flood events (Chen et al., 2013). In comparison, HyspIRI's higher spatial resolution should provide even more accurate information.

Satellite data have been used to improve rainfall mapping and to monitor relationships between rainfall and vegetation responses. Vegetation and inundation dynamics and aspects of water quality of wetlands have been monitored in many parts of the tropics and elsewhere by using multispectral, thermal and radar imagery (Meijerink, 2002). To study the dynamics of regional vegetation responses in southern Africa to the dry El Nino years and intervening wetter years, Kogan (1989) used a Vegetation and Temperature condition index (VT) based on NDVI values after radiometric correction and the brightness temperature of the surface based on the AVHRR thermal channel. Effects of transpiration of healthy vegetation are included by the temperature component of the index. Kogan (1989) found that it took 5 – 6 weeks for the VT index to decrease to a level that indicates severe stress (VT = 10 – 20), whereas with adequate moisture, the index is around 60. The numerical value of VT can be used for multi-temporal studies and for comparing values from the VSWIR and TIR sensors of HyspIRI in different parts of the world.

Natural vegetation patterns, as observed in satellite images, can also be related to groundwater occurrences and groundwater flow systems (Meijerink, 2002). Locating groundwater discharge zones in surface water bodies can provide information about the groundwater flow system in wetlands and about the potential transport of contaminants. This information can aid in the design and emplacement of groundwater monitoring networks and determining remediation techniques. Knowing the areal extent of groundwater discharge to surface water can also be useful for selecting sampling sites and for estimating the environmental effects of contaminant migration. Thermal infrared imaging is an effective method for assessing large areas and getting information about

specific locations of groundwater discharge because the groundwater usually has a different temperature than the background surface water (Byers and Chmura, 2013; Xin, 2004). Simulated flooding patterns obtained from coupled surface water-groundwater models have been compared to patterns derived from satellite multispectral, thermal infrared and radar data that provided such model inputs as topography, aquifer thickness, channel positions, evapotranspiration and precipitation (Milzow *et al*., 2009).

Sand and Mudflats

In desert regions, some studies have shown that grain size information can be obtained from hyperspectral imagery (Okin and Painter, 2004; Ghrephat *et al.*, 2007). Hyperspectral imagery has been used to delineate coastal surface properties such as composition, moisture, and grain size. These are critical parameters for determining the substrate bearing strength (Bachmann *et al*., 2010). More recent studies have shown that sand density variations are observable in hyperspectral imagery (Bachmann *et al*., 2012), however, the exact relationship depends strongly on the sand constituent mixtures found in specific coast types (Bachmann *et al*., 2013). Although hyperspectral sensors only see the surface layers, statistics can be derived that relate the surface properties to the likely bearing strength of soils, making it possible to produce potential bearing strength maps on large scales. Initial validations have been performed relating airborne hyperspectral data to *in situ* spectral and geotechnical measurements through a spectral-geotechnical look-up table (Bachmann *et al*., 2010).

The most common methods for remotely sensing soil moisture are based on microwave radiometry. Approximate estimates of soil moisture have also been derived from satellite thermal infrared data. For instance, Shih and Jordan (1993) used Landsat TM band 6 thermal infrared imagery to monitor soil moisture conditions in southwestern Florida. The theoretical method of using daily temperature datasets to estimate root zone soil moisture was tested with field data. Results indicated that the percentage gravimetric soil moisture content in the 0-24 cm depth was inversely related to the soil surface temperature. TM band 6 images were overlaid in a Geographical Information System (GIS) onto four principal land-use categories (agricultural/irrigated, urban/clearings, forest/wetlands, and water), and used to assess four qualitative soil moisture conditions (water/very wet, wet, moist, and dry) within each land-use category (Shih and Jordan, 1993). In addition, liquid water absorption spectral features in hyperspectral imagery have also been related to surface layer concentrations and can also be used to retrieve surface moisture levels (Bachmann *et al*., 2012).

HyspIRI's hyperspectral and thermal infrared imagery may help extend estimates of substrate bearing strength and soil moisture to regional and global scales. This would be an important product for both civilian and military use.

Invasive Species in Wetlands

Wetlands can be invaded by plant species that displace native plants and degrade their habitat. Mapping tools are needed to document the location and extent of such invasive species. Pengra *et al.*, (2007) were able to map *Phragmites australis*, a tall grass that invades coastal marshes throughout North America, with Hyperion imagery in the wetlands of Green Bay, Wisconsin, USA. Artigas and Yang (2005) used hyperspectral

imagery from the Airborne Imaging Spectroradiometer for Applications (AISA) in New Jersey, USA to classify marsh conditions based on *in situ* reflectance spectra of dominant marsh species and seasonal spectra of *Phragmites australis*. Hestir *et al*., (2008) developed a regional-scale monitoring framework to map wetland weeds in the Sacramento–San Joaquin Delta, California, USA. They focused on terrestrial riparian weed, the perennial pepperweed (*Lepidium latifolium*), using an airborne hyperspectral imager (HyMAP) that collects data at 128 bands in the visible and near-infrared (VNIR; 0.45–1.5 µm) regions through the shortwave infrared (SWIR; 1.5–2.5 µm) region, at bandwidths that range from 10 nm in the VNIR region to 15–20 nm in the SWIR region. The spatial resolution of the data was 3 m, with a swath width of 1.5 km. At a field scale, Sonnentag *et al*., (2011) used multispectral webcam imagery to track perennial pepperweed in the Sacramento Delta in California. These studies suggest that HyspIRI would be useful for mapping invasive species and wetland change.

Challenges

Although darker than most terrestrial vegetation, wetlands are more reflective than most non-turbid, open water targets. However, these environments are still subject to sun glint (Hochberg *et al*., 2010). For coastal emergent vegetation, the issue of glint becomes much more complex. For example, in salt marshes, tidal emergent vegetation is typically erectophile, with small ponds and channels interspersed. These features typically range in spatial scale from a fraction of a meter to tens of meters. In these systems, glint would undoubtedly contribute to the remotely sensed signal measured by HyspIRI with its 60 m nadir pixel size. Naturally, the effect would vary with the solar illumination and sensor viewing angles, being more intense at low latitudes and growing worse with proximity to the summer solstice. Measurement and modeling capabilities for glint in wetlands lag those for shallow and deep oceans. Suitable models or measurement techniques have yet to be developed to quantify this effect because the relationship between surface roughness and various environmental factors are unknown (Turpie, 2012). At the same time, emergent vegetation has the benefit of providing useful, observable near-infrared (NIR) and SWIR spectral features, which can dominate glint.

Qualitatively, it is possible to demonstrate glint effects from multi-angle satellite images acquired by CHRIS/Proba. Figure 2.1.2 illustrates an example of the effect of glint on remote sensing reflectance observed over wetlands. With a nominal view zenith angle of 0°, glint is visually apparent in water bodies amongst the vegetated areas (Figure 2.1.2a). This glint is likely caused by capillary waves patterned by the local wind field. With a nominal view zenith angle of 55°, glint is much less visually apparent (Figure 2.1.2b). These visual glint patterns are supported by sample spectra. For the same region of wetland, the 0° nominal view angle spectra (Figure 2.1.3a) have higher reflectance values and are more variable than the 55° view angle spectra (Figure 2.1.3b).

Although using conventional techniques to separate glint from the vegetation spectral signal may appear to be challenging, the relatively strong signal from sub-aerial vegetation sufficiently dwarfs the glint, consequently presenting a smaller effect compared to that found with remote sensing retrievals of water column and benthic communities. In addition, wetland vegetation cover tends to reduce surface roughness from wind. Thus, the range of angles that are influenced by sun glint are reduced in

comparison to ocean water (Vanderbilt *et al*., 2002). The 11 a.m. equatorial crossing of the spacecraft and the 4° tilt of the HyspIRI instrument away from the sub-solar point should greatly reduce the effect of sun glint in these coastal and inland wetlands.

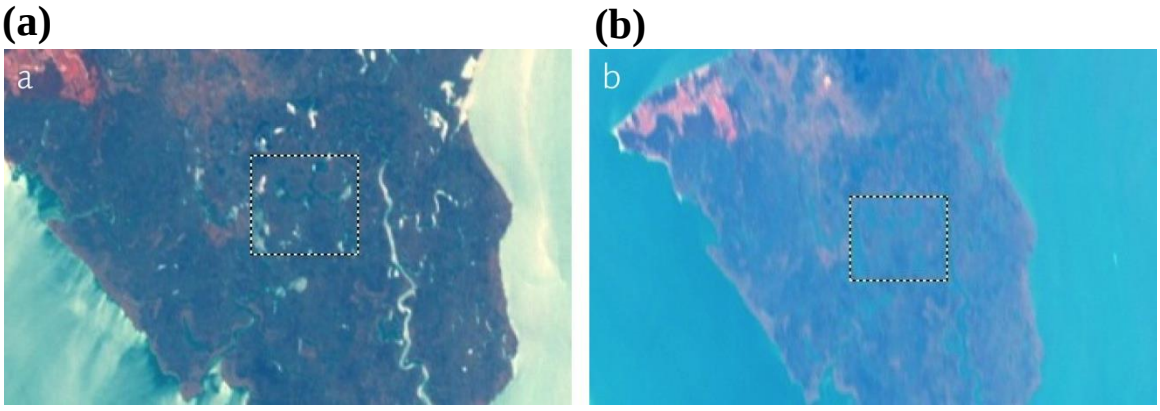

Figure 2.1.2 – Multi-angle CHRIS/Proba images of Fishing Bay Wildlife Management Area, Maryland. (a) At 0° nominal view zenith angle, glint is visually apparent on water bodies interspersed amongst sub-aerial vegetation. (b) At 55° nominal view zenith angle, glint is much less apparent. Boxes cover the same ground area in both (a) and (b). This region is extracted for statistics shown in Figure 2.1.3.

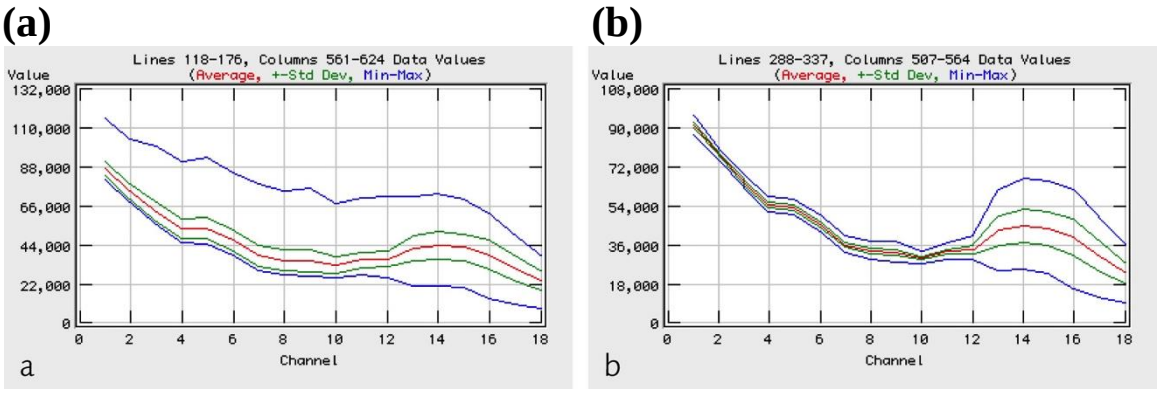

Figure 2.1.3 – Spectra extracted from regions highlighted by boxes in Figure 2.1.2. The ordinate axis is in units of radiance (μW m^{-2} nm^{-1} sr^{-1}) for the CHRIS/Proba instrument. (a) At 0° nominal view zenith angle, glint produces very high values across the spectrum, evidenced by the maximum spectral curve. (b) At 55° nominal view zenith angle, the glint effect is greatly reduced.

Another challenge with wetland species (e.g., mangroves) discrimination using hyperspectral sensors is that, unless the canopy is very dense, there will be gaps exposing moist soil or water, which will "contaminate" the pure spectral reflectance signatures of the vegetation. Some freshwater marshes may be too small and patchy to be resolved by HyspIRI or any other medium resolution satellite, and may require ancillary data. Furthermore, freshwater marshes can be floristically diverse and have a more mixed vegetative cover producing a more complex, composite spectral signature than most

saltwater wetlands. Finally, the optical properties of any inundated canopies will present additional challenges for some of these techniques (Turpie, 2012; Turpie, 2013).

Mission Relevance

Hyperspectral remote sensing data are required to map the location, type and spatial extent of wetlands, classify wetland vegetation species/types, or derive wetland productivity, hydrologic dynamics, and other critical biophysical and functional properties (Brando and Decker, 2003; Christian and Krishnayya, 2009; Hirano *et al*., 2003; Jensen *et al*., 2007; Papes *et al*., 2010; Pengra *et al*., 2007; Schmidt *et al*., 2004; Ustin *et al*., 2004; Yang *et al*., 2009; Zomer *et al*., 2009). For instance, using hyperspectral imagery and narrow-band vegetation indices, researchers have been able to not only discriminate some wetland species but also make progress on estimating biochemical and biophysical parameters of wetland vegetation, such as water content, biomass, leaf area index, and leaf constituents such as nitrogen (Adam *et al*., 2010; Artigas and Yang, 2006; Filippi and Jensen, 2006; Gilmore *et al*., 2008; Ozesmi and Bauer, 2002; Pengra *et al*., 2007; Tian *et al*., 2011; Wang, 2010).

The spaceborne imaging spectrometer Hyperion has been shown to be able to detect fine differences in spectral reflectance, allowing some wetland species discrimination (Brando and Decker, 2003; Christian and Krishnayya, 2009; Papes *et al*., 2010; Pengra *et al*., 2007). Hyperion collects data at 220 spectral bands with a spatial resolution of 30 m. However, Hyperion is a proof-of-concept mission and does not have a global mapping capability; it has a limited SNR; and the mission is nearing the end of its planned lifetime. Therefore, in the near future, HyspIRI, if successfully launched, may be the only U.S. spaceborne imaging spectrometer that provides the spatial and spectral resolution, swath width and SNR required for mapping wetlands at global scales.

HyspIRI's VSWIR and TIR sensors will be able to observe hydrologic and hydro-meteorological processes, including groundwater seepage, nitrogen load, water quality, evapotranspiration, etc. (Banks *et al*., 1996; Bendjoudi *et al*., 2002; Byers and Chmura, 2013; Chen *et al*., 2002; Meijerink, 2002; Moffett, 2010; Mohamed *et al*., 2004; Xin, 2004). Once the monitoring model for global wetlands using HyspIRI data is built and validated with field data, the hyperspectral and thermal infrared data can be used to survey and assess their condition in response to human-made disturbances, natural disasters and climate change in near-real time.

2.2 Land/Water Geomorphology

Science Questions Addressed

The land/water geomorphology data products retrieved from HyspIRI data will help address the following HyspIRI science questions (from Table 1.2).

VQ1. What is the global spatial pattern of ecosystem and diversity distributions and how do ecosystems differ in their composition or biodiversity?

VQ4. How are disturbance regimes changing and how do these changes affect the ecosystem processes that support life on Earth?

TQ5. How does urbanization affect the local, regional and global environment? Can we characterize this effect to help mitigate its impact on human health and welfare?
CQ5. What is the composition of exposed terrestrial surface of the Earth and how does it respond to anthropogenic and non-anthropogenic drivers?

CQ6. How do patterns of human environmental and infectious diseases respond to leading environmental changes, particularly to urban growth and change and the associated impacts of urbanization?

Candidate Products or Applications

Shoreline Changes and Floods (Disturbances)

Quantifying shoreline change requires accurate delineation of shoreline positions on image time-series where tidal influence is minimal. Several methods have been proposed and used to derive shoreline positions from passive remote sensing, which may be tested with HyspIRI VSWIR or similar data. These include a single-band method to use a threshold to separate land from water (Bayram *et al*., 2008), an edge filter method (Scott *et al*., 2003), and an unsupervised classification method such as the iterative self-organizing data analysis (ISODATA) classification (Armenakis *et al*., 2003). Similarly, other well-developed indices, including the Normalized Difference Vegetation Index (NDVI), defined as

$$\mathrm{NDVI} = (R_{\mathrm{NIR}} - R_{\mathrm{RED}})/(R_{\mathrm{NIR}} + R_{\mathrm{RED}}) \quad (1)$$

where R is reflectance, and Normalized Difference Water Index (NDWI), defined as

$$\mathrm{NDWI} = (R_{\mathrm{GREEN}} - R_{\mathrm{NIR}})/(R_{\mathrm{GREEN}} + R_{\mathrm{NIR}}) \quad (2)$$

are also used for water/land delineation as well as for flood mapping (McFeeters, 1996; Domenikiotis *et al*., 2003; Jain *et al*., 2005; Lunetta, 2006; Ouma & Tateishi, 2006; Xu, 2006). A recently developed index to delineate floating materials in the open ocean, namely the floating algae index (FAI, Hu, 2009), was also found effective in delineating the land-water interface (Feng *et al*., 2012) because of its relative tolerance to changing aerosols and solar/viewing geometry.

While each method has its own pros and cons, the fundamental principle is the same: water absorbs light strongly in the NIR and SWIR wavelengths, resulting in much reduced reflectance as compared with other wavelengths for the same image pixels or compared with other pixels for the same wavelengths. For example, the absorption coefficient of water at 1640 nm is 669 m^{-1}. A 1-cm layer of water over a surface will therefore reduce its reflectance by a factor of $e^{-2 * 0.01 * 669} = 0.00015\%$ (the factor of two accounts for the two-way light attenuation). Likewise, a 1-mm water lens will reduce the reflectance to about 26%. In other words, single-band images using these wavelengths will appear dark over water and brighter over land. The various methods simply seek efficient ways to extract this information while minimizing the impacts of the observing conditions or increasing computational efficiency.

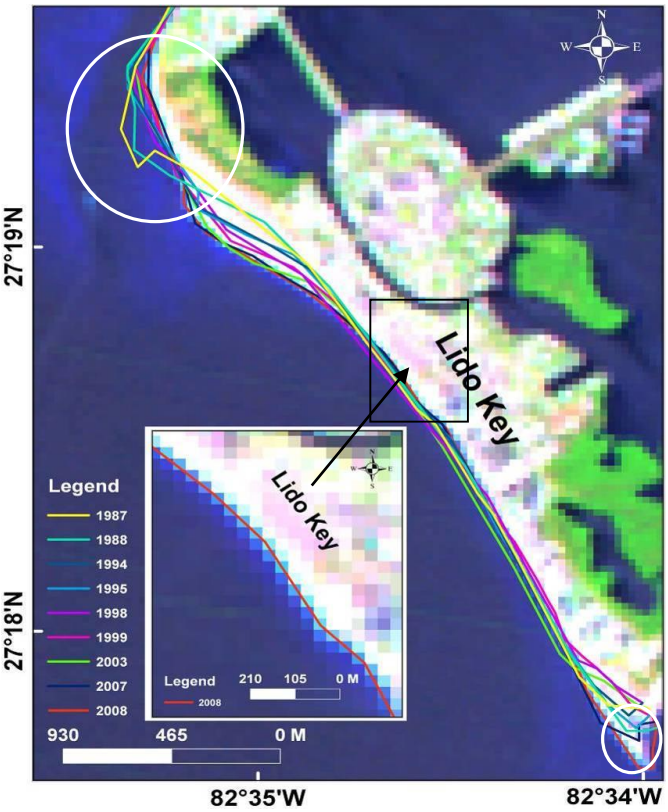

Figure 2.2.1. – Shoreline delineation from nine Landsat TM images covering central West Florida near Lido Key. Inset image shows an example of how the determined shoreline (red line) traces the land-water interface pixels. The two white circles highlight the two shoreline sections that experienced opposite shoreline changes (erosion and accretion). Figure adapted from Yu *et al*., (2011).

A recent example of using Landsat 30-m resolution data to document decadal shoreline changes along central Florida's west coast is given in Yu *et al*., (2011). The time-series images were carefully selected to be within a tidal range of ±9 cm, so the tidal influence on the shoreline delineation accuracy would be within one Landsat pixel for a shelf slope of 3‰ - 24‰. Results indicated both beach erosion and beach accretion in different places between 1987 and 2008 as a consequence of natural processes and human influence (e.g., beach nourishment). Like Landsat, high latitude revisit times for HyspIRI are closer to a few to several days, affording more opportunities to observe more rapid change along coastlines (Oey *et al*., 2007).

The HyspIRI VSWIR data cover a wide spectral range from the visible to the shortwave infrared. Together with their high spatial resolution, the data will be particularly suitable for shoreline delineation/change detection as well as for flood mapping, as the water and land pixels can be classified using the candidate methods outlined above. In addition, the same concept can be extended to the detection of ice

edges over water because of the reflectance contrast between ice and water. This capacity will enable not only the ice edge delineation and ice size estimation, but also studies of ocean biogeochemistry in adjacent waters.

Groundwater Discharge

Groundwater discharge to coastal regions impacts local ecological conditions by introducing local temperature changes, lower salinity and nutrient loads that are often high. Nutrient supply by groundwater discharge has been linked to eutrophication and has been suggested as a potential precursor to harmful algal blooms after hurricanes in Tampa Bay (Hu *et al*., 2006) and Masan Bay in South Korea (Lee and Kim, 2007), or increased bacterial concentrations in the surf zone (Boehm *et al*., 2004). Detecting locations and quantifying the contribution of groundwater discharge into coastal waters are challenging because field observations are limited. However, there are remote sensing techniques that have been proven a useful tool for monitoring groundwater discharge using temperature differences between coastal water and groundwater.

The temperature of groundwater discharges is almost constant throughout the year, and the use of thermal remote sensing to delineate groundwater discharge to the coastal regions has been reported in many places. For example, Banks *et al*., (1996) used airborne Thermal Infrared Multispectral Scanner (TIMS) images to identify the location and the spatial extent of groundwater discharge to the Gunpower River in Chesapeake Bay, and Portnoy *et al*., (1998) used the Landsat Enhanced Thematic Mapper (ETM+) TIR imagery and shoreline salinity surveys to characterize groundwater discharge to an estuary in Cape Cod. Other examples include McKenna *et al*., (2001); Miller and Ullman (2004); and Wang *et al*., (2008), who used TIR imagery to identify groundwater discharges in Delaware's Inland Bays. In addition, the Great Bay Estuary, New Hampshire, Waquiot Bay, Massachusetts, and Hawaii were also noted by Roseen *et al*., (2001) and Johnson *et al*., (2008), respectively.

Groundwater discharge locations (see Figure 2.2.2) have been identified in Delaware on the north shore of Rehoboth Bay west of the Lewes and the Rehoboth Canal, on Herring and Guinea Creeks, on the north shore of Indian River and on the north shore of Indian River Bay near Oak Orchard. The identified locations are consistent with other indicators of ground-water discharge.

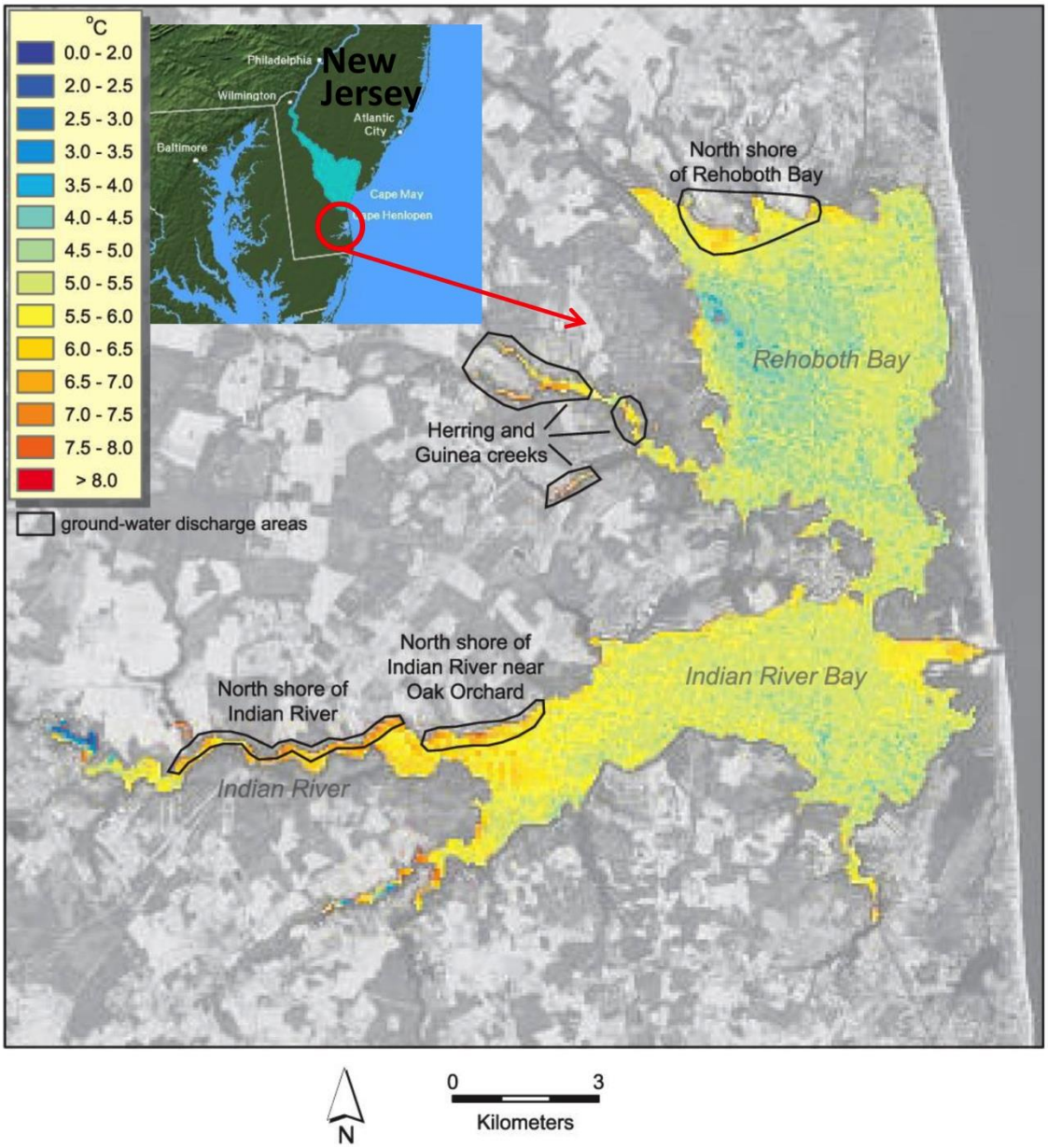

Figure 2.2.2 – Ground-water discharge areas in the Delaware Inland Bays identified using Landsat 7 imagery acquired on February 19, 2002. This figure is adopted from Wang *et al.*, (2008).

In addition to thermal effects of the groundwater on coastal ecosystems, groundwater discharge was studied using the Compact Airborne Spectrographic Imager 550 (CASI-550) sensors (Kolokoussis *et al.*, 2011). These efforts used turbidity-related water Inherent Optical Properties (IOP) to demonstrate that turbidity can be effectively identified and estimated using certain band ratios or feature-extraction methods. Since the groundwater discharge affects the water quality in the coastal regions, hyperspectral remote sensing has been used to monitor water quality related properties (Lee *et al.*, 1994; Gould and Arnone, 1997; Flink *et al.*, 2001; Kallio *et al.*, 2001; Ostlund *et al.*, 2001; Ammenberg *et al.*, 2002; Galvao *et al.*, 2003; Yang and Pan, 2007). According to

Hakvoort *et al*., (2002), estimation and mapping of water quality constituents, such as concentrations of dissolved organic matter, chlorophyll or total suspended matter from optical remote sensing techniques, have proved to be useful and successful.

Challenges

The 1640-nm band enables highly accurate classifications of water and land pixels. However, for shoreline delineation and flood mapping, there are several practical considerations for accuracy assessment. The first is the geo-location accuracy of the individual pixels on satellite images, which is often in the order of a half pixel size (Root Mean Square, or RMS, uncertainties). For example, the highest geo-location accuracy of MODIS data for a nadir view is about 150 m (Wolfe *et al*., 2002), about half of the 250-m pixel. For Landsat data, the half-pixel accuracy often requires manual geo-rectification using known ground control points (e.g., Yu *et al*., 2011). Assuming the principle is universal, the HyspIRI land and water classification uncertainties will be roughly of a half pixel. The second is the influence of tides, which can range from centimeters to meters depending on the location. To achieve the half-pixel accuracy in shoreline delineation, the changes in tides must be restricted to a range which, after accounting for the slope of the inter-tidal zone, will result in less than a half-pixel uncertainty (Yu *et al*., 2011). The third is the revisit frequency. Due to the high spatial resolution requirement, HyspIRI may revisit the same place less frequently than Landsat (19 days at the equator, less at higher latitudes). This not only creates difficulty in finding time-series data that meet the tidal change constraint for shoreline change assessment, but also makes it difficult for flooding assessment because the dry/wet conditions over land may change quickly. Therefore, for flooding events, the sensor may be tilted to assure rapid response. Overall, although there are some potential limitations for shoreline delineation and flood mapping, it is possible to overcome these difficulties with engineering advancement and algorithm improvement to achieve an RMS accuracy of a half pixel. However, it should be noted that this challenge is lessened at higher latitudes.

Hyperspectral remote sensing has been used to map optical water quality concentrations of colored dissolved organic matter, chlorophyll and total suspended matter simultaneously in the complex waters of estuarine and coastal systems. The issues of accuracy and limitations in the use of HyspIRI for groundwater discharge into the coastal regions depend on the algorithms for estimating biogeochemical constituents, as described in Section 2.4. Because HyspIRI performs better than Hyperion with respect to its SNR and its spatial, spectral and radiometric resolutions, its accuracy for estimations of water quality related properties should be better. Compared to HICO measurements, HyspIRI provides additional TIR observations, which are critical to monitoring thermal variations in the coastal regions due to groundwater, run-off and river discharges.

Mission Relevance

Numerous natural and anthropogenic causes can result in shoreline changes, for example, sea level change, hurricanes, coastal circulation, riverine discharge patterns, beach nourishment and sand dredging (Wu, 2007). Such changes may affect coastal zone resilience to storm surge and flooding, with significant impacts on ecosystem health and species diversity (Desantis *et al*., 2007). The changes may also have important socio-

economic consequences on local residency and tourism. Thus, it is important to assess shoreline changes periodically for management decision support, such as beach nourishment (e.g., location and frequency). Likewise, flooding (or drought) events from either extreme weather or poor management (e.g., damage of a levee) often lead to property loss, economic hardship and threat to people's life. In addition, rapid changes of the dry/wet conditions can change the surface exposure periods to water and sunlight, therefore influencing the local ecosystem (e.g., Kanai *et al*. 2002). Accurate estimation of the flood patterns is a first important step to help flood control, search and rescue, land use planning and ecological conservation. The unique capacity of HyspIRI enabled by its high spectral and high spatial resolutions will greatly enhance our current ability to provide accurate maps of shoreline changes and flood maps for targeted areas, and provide useful tools for managers, researchers, environmental groups and the general public for the wellbeing of coastal zones.

Groundwater discharge has been considered a potentially significant diffuse source of nutrients, dissolved substances and diffuse pollution to coastal regions (Leote *et al*., 2008). Anthropogenic materials, such as pesticides, herbicides, chemical fertilizers and petroleum products, are common groundwater pollutants. These pollutants usually enter groundwater when polluted surface water percolates down from the Earth's surface. Relatively small groundwater discharge rates can deliver comparatively large quantities of nutrients and pollutants to coastal areas. Leaking underground storage tanks are another major source of groundwater pollution. It is estimated that there are millions of underground storage tanks in the United States. Agricultural and lawn application of fertilizers also present a major diffuse source of nutrients that can enter coastal and inland waters through ground water discharge.

The difficulty of studying the diffuse sources of pollutants into estuarine and lacustrine waters has limited the regulation and management of coastal and inland water quality. The combination of the high spatial resolution hyperspectral VSWIR and thermal information from HyspIRI provides a unique opportunity to map groundwater discharge sites and their effect on surrounding biological processes. Further combining the HyspIRI remote sensed data, GIS data, and field measurements could provide an unprecedented capability for characterizing groundwater flow systems and discharge-recharge relationships.

In addition to land/water geomorphology, HyspIRI can be used in studying ice geomorphology. Global warming is altering the timing, rate and extent of formation, melting and breaking of the ice pack and ice shelves at high latitudes. As ice melts, fresh water strongly affects phytoplankton ecology. Phytoplankton form blooms within the ice and extensive ice edge blooms near ice edges (Muller-Karger, 1984; Muller-Karger *et al*., 1987a, 1987b and 1990). This phenomenon can be strongly affected by climate change (Perrette *et al*., 2011). Accordingly, it is critically important to study phytoplankton in ice pools (Lee *et al*., 2012), and changes in that environment as a result of climate change. HyspIRI is an appropriate sensor studying both thermal and biogeochemical constituents around ice edges. However, there are challenges using HyspIRI, such as, low irradiance (hence lower SNR for the sensor) and atmospheric adjacency effects. Instrument stray

light characteristics accentuated by the stark contrast of the ice edge will also require careful prelaunch testing. These problems may be partially compensated by the shorter revisit period for polar regions (closer to 4-5 days for the spectrometer, rather than 19 days at the equator) and the low sun glint at high latitudes.

2.3 Water Surface Feature Classification

Science Questions Addressed

The ability to classify water surface features using HyspIRI data will help address the following HyspIRI science question (from Table 1.2).

VQ1. What is the global spatial pattern of ecosystem and diversity distributions and how do ecosystems differ in their composition or biodiversity?

Candidate Products or Applications

Many materials and marine plants can float or aggregate on the ocean surface, leading to enhanced reflectance in the NIR and possibly other wavelengths. These primarily include macro algae of *Sargassum spp.*, macro algae of *Ulva prolifera*, cyanobacterium *Trichodesmium spp.*, emulsified oil and marine debris (plastic or other trash) (see Figure 2.3.1). Differentiating and quantifying these cover types are complicated by their enhanced reflectance in the red-NIR wavelengths, and sometimes even in the SWIR wavelengths. In particular, the atmospheric correction that assumes "black pixel" (i.e., negligible remote sensing reflectance or R_{rs}) in the NIR (Gordon, 1997) or in the SWIR (Gao *et al.*, 2000; Wang and Shi, 2007) wavelengths will fail. This poses three challenges for the detection and quantification of these surface floating materials from space-borne remote sensing: 1) How to delineate these features in an automatic fashion; 2) How to differentiate the identified features (i.e., what are they?); 3) How to quantify the identified features (e.g., biomass or volume).

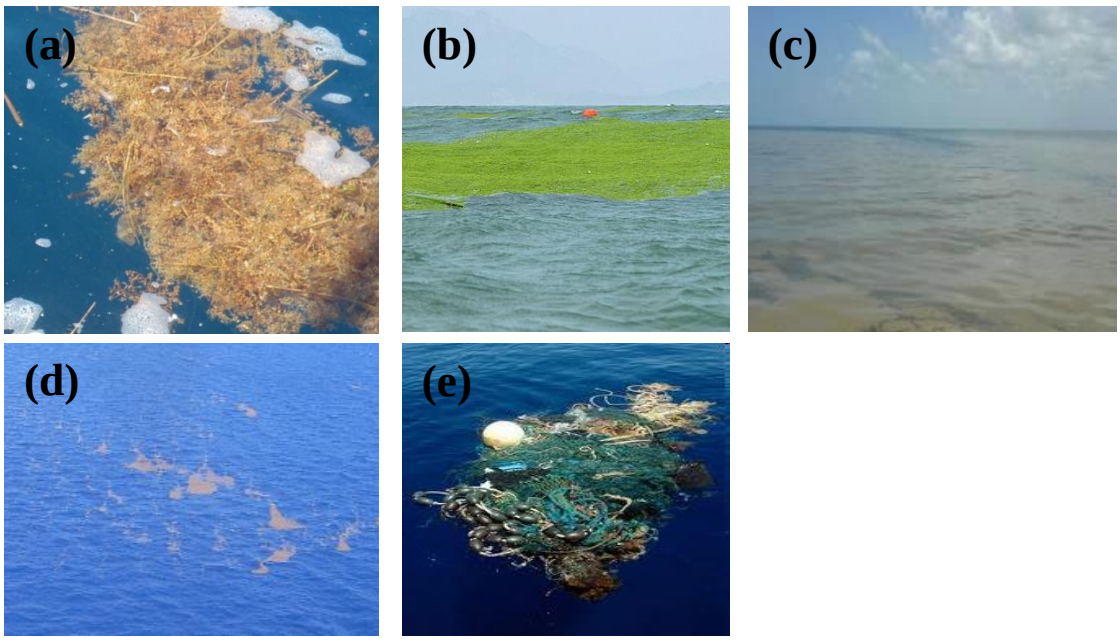

Figure 2.3.1 – Materials and marine plants floating on the ocean surface. (a) *Sargassum spp.* in the Gulf of Mexico; (b) *Ulva prolifera* bloom off Qingdao, China; (c) *Trichodesmium* mats in the Gulf of Mexico; (d) Weathered oil from the Deepwater Horizon oil spill in the Gulf of Mexico; (e) Marine garbage patch (fishing net, plastic, and other debris) in the Pacific ocean.

There have been only a few published studies to show the capabilities of current multi-band sensors in detecting some of these features. The limitations have been in the spectral, temporal, and spatial resolution. Some of these limitations will be overcome by the HyspIRI VSWIR data, covering a wide spectral range from the visible to the shortwave infrared at high spatial resolution.

Gower *et al*., (2006) is perhaps the first study that demonstrates the detection and quantification of *Sargassum* using MERIS and MODIS, based on a few assumptions. In the study, the reflectance red edge at the 709-nm MERIS band (300-m resolution) is examined, and elevated reflectance is assumed to be caused by *Sargassum* surface aggregations. This concept has been extended to MODIS data at 859-nm (250-m resolution) to detect *Sargassum* in the Gulf of Mexico and *Ulva prolifera* (a green seaweed) in the Yellow Sea and East China Sea using a floating algae index (Hu, 2009), because the 859-nm band does not saturate over bright targets. However, surface *Trichodesmium* mats also show elevated reflectance in the NIR (Subramaniam *et al*., 2001) including the MERIS 709-nm and MODIS 859-nm bands. Although the overall MERIS spectral shape has been used in Gower *et al*., (2006) to differentiate *Sargassum* from *Trichodesmium*, more direct spectral evidence is still required. Hu *et al*., (2010a) combined MODIS land bands and ocean bands to examine the spectral curvatures in the blue-green to unambiguously differentiate *Trichodesmium* from other look-alike features, based on the unique pigments in *Trichodesmium*. This concept will be extended to

HyspIRI, and similar algorithms will be developed and enhanced for the HyspIRI hyperspectral data.

The detection algorithms will be based on the different spectral shapes (not magnitudes) of the surface floating materials. Although field-based measurements are still required, some preliminary measurements are available from either refereed or gray literature. Figure 2.3.2 shows examples of their reflectance spectra collected by several groups. The spectra are demonstrated here to illustrate the difference in their spectral shapes rather than the magnitudes, and are intended to differentiate the various materials. Although they all show enhanced reflectance in the NIR, their spectral shapes in the visible are different: *Sargassum* mats have a unique reflectance decrease between 600 and 650 nm; *Ulva prolifera* show typical reflectance of green plants; *Trichodesmium* mats show unique spectral curvatures in the blue-green that can be captured by the current MODIS bands; emulsified oil show unique spectral curvatures around 1200 nm and 1700 nm; marine debris show smoothly increased reflectance across the entire spectrum as compared to nearby water.

The proof-of-concept of using multi-band satellites for the detection of the above marine organisms and materials has heavily demonstrated in the literature (Gower *et al*., 2006; Hu, 2009; Hu *et al*., 2009, 2010a&b; He *et al*., 2011; Gower and King, 2011; Hu *et al*., 2011). Given the known and distinguishable spectral characteristics of these surface floating features, detection of them using higher spatial and higher spectral resolution HyspIRI will be improved, with the possibility to quantify them in aerial coverage and mass. Specifically, the following products are possible from HyspIRI are possible:

1) Maps of delineated surface features of *Sargassum*, *Ulva prolifera*, oil slicks, and marine debris (classification),
2) Estimates of aerial coverage of the classified features (quantification),

3) Estimates of biomass of *Sargassum* and *Ulva prolifera*, surface oil volume, and mass of marine debris (quantification).

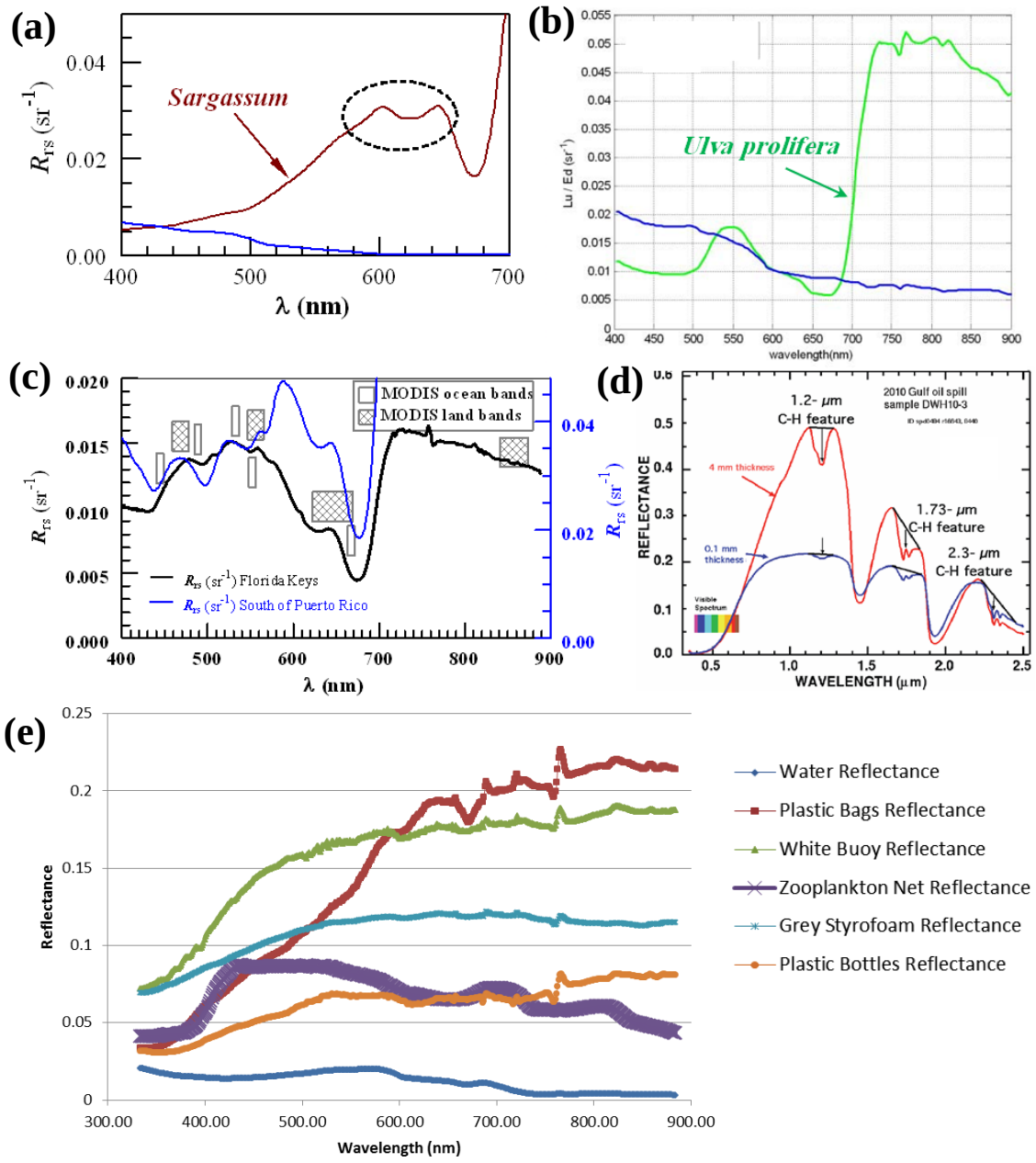

Figure 2.3.2. – Changes in reflectance spectral shapes from different materials and marine plants floating on the ocean surface. (a) *Sargassum spp.* in the Gulf of Mexico (GOM) (Hu unpublished data); (b) *Ulva prolifera* bloom off Qingdao, China (He *et al*., 2011); (c) *Trichodesmium* mats in the Florida Keys and coastal waters off Puerto Rico (Hu *et al*., 2010a); (d) Weathered oil from a lab experiment (Clark *et al*., 2010); (e) Various marine garbage (fishing net, plastic and other debris) from an experiment (data courtesy of Daniel Sensi, USF College of Marine Science).

However, despite the preliminary success of using existing multi-band data for some of these products, technical challenge still remains on the algorithm development and especially on the accuracy assessment.

Methods

Several steps are required to derive the products above, each contributing some amount of uncertainty.

First, assuming a well-calibrated (both radiometrically and spectrally) HyspIRI measurement, atmospheric correction (AC) is required to remove most of the atmospheric effects, especially those that interfere with the spectral shape classification. For feature delineation, this is perhaps not required because a feature detection algorithm can rely purely on the spatial contrast (edge detection) rather than on spectral shape. For feature classification, a crude AC is needed. To quantify the classified feature, a more accurate AC is required to obtain the surface reflectance of the feature. This can be difficult as the non-zero surface reflectance in the NIR or SWIR will cause atmospheric correction failure (e.g., Figures 2c & 2d of Gower *et al*., 2006). A nearest-neighbor atmospheric correction (Hu *et al*., 2000) may be implemented to use atmospheric properties derived from the nearby water to remove the atmospheric effects over the already-delineated feature. This approach has been used to derive surface reflectance over oil slicks (Hu *et al*., 2003) and *Trichodesmium* mats (Hu *et al*., 2010a). The uncertainties in the derived surface reflectance are primarily from the residual errors of the atmospheric correction, in the order of <0.002 (dimensionless reflectance) at 443 nm and <0.0003 at 670 nm (Gordon, 1997; Hu *et al*., 2013).

Second, the feature delineation will rely on the spatial contrast in either single-band reflectance or multi-band product (e.g., Hu, 2009. Also see Figure 2.3.3 for example). This type of image segmentation technique has been established for decades and is mature. One potential uncertainty comes from the difficulty in differentiating these features from other look-alike features, such as cloud edge or small cloud patches (note that cloud detection over sun glint or other bright targets is still a challenge). Further, ocean fronts may appear like isolated slicks under severe sun glint (the optical contrast between fronts and nearby waters is exaggerated, He *et al*., 2011). However, these potential false delineations can be removed by the following step using spectral analysis.

Third, all delineated features through the above edge detection will be examined through the spectral analysis using the spectral library established from the field or laboratory measurements (e.g., Figure 2.3.2). The accuracy of this spectral classification relies on: 1) The signal-to-noise ratio of the HyspIRI measurements; 2) Whether an image pixel has full or partial coverage mixed with water; 3) Accuracy of atmospheric correction. If the pixel of interest is covered mostly by open water, it is possibly that the spectral signatures of the various features (Figure 2.3.2) may not be detected. Hu (2009) estimated that with the SNR of MODIS, once the macroalgae forms a line of several 250-m image pixels, a thickness of 5-10 m appears to be the lower detection limit. Currently, the threshold of the feature/water mixing ratio is unknown, but this represents one major uncertainty source in generating the feature-specific distribution maps.

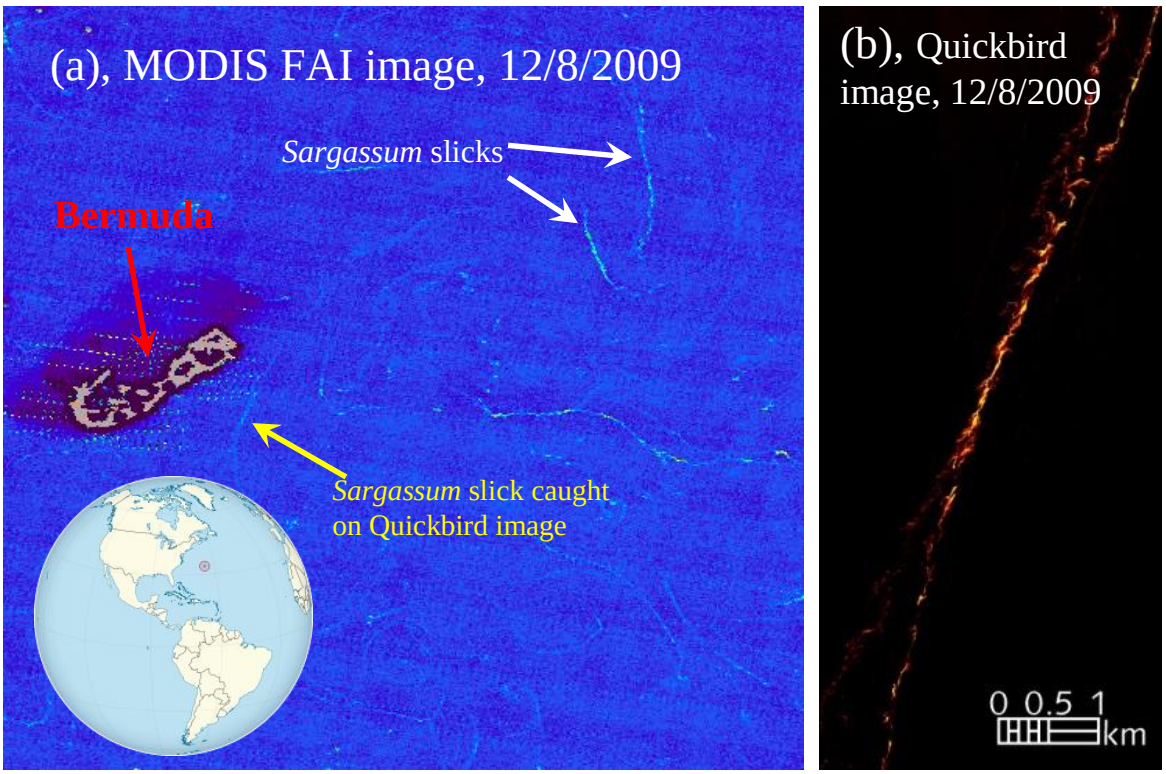

Figure 2.3.3. – (a) MODIS/Terra FAI image (250-m resolution) near Bermuda on 12/8/2009 showing surface slicks that are thought to be *Sargassum*; (b) Color-infrared WordView-2 image (2-m resolution) on the same day showing a long slick thought to be *Sargassum*, corresponding to the slick annotated with a yellow arrow in (a). The inset map shows the location of Bermuda (red circle).

Fourth, area coverage (in km^2 or acres) could be quantified from the feature-specific distribution maps. The accuracy of this step relies on how well we can determine the proportions of feature/water in a pixel of interest. If the algorithm used to detect the feature is a linear combination of spectral bands (e.g., Hu, 2009), a linear unmixing scheme can be developed (Settle and Drake 1993; Hu *et al*., 2010b). Otherwise, a field-based experiment is required to determine the unmixing algorithm. The accuracy of this step is currently unknown due to lack of field measurements, yet the unmixing uncertainty is unlikely to exceed 50%.

Finally, the most challenging task is to quantify the delineated and classified features in order to generate biomass (or oil volume or mass) distribution maps. The difficulty arises from a lack of available measurements to establish relationships between these quantities and their associated spectral reflectance (magnitudes). Gower *et al*. (2006) and Gower and King (2011) estimated *Sargassum* biomass based on several crude assumptions, yet these assumptions require field validation. Likewise, the assumption used in Hu *et al*. (2010b) on the biomass of *Ulva prolifera* per unit area also needs field validation. While measurements of *Sargassum* and *Ulva prolifera* biomass may be straightforward, determining biomass *Trichodemium* is more difficult because the presence of a boat may disturb the floating mats, resulting in inaccurate sample

collection. This is different from determining *Trichodemium* biomass suspended in the water column (Westberry *et al*., 2005). Even more difficult is the determination of oil volume (or thickness) from the field. To date, although laboratory experiments can easily determine the oil thickness under a controlled environment (e.g., Svejkovsky and Muskat, 2009; Wettle et al., 2009; Clark *et al*., 2010), there is nearly no field-based oil thickness measurement, not to mention how to relate the spectral shapes and magnitudes with the oil thickness (and possibly type. For example, fresh versus emulsified). The laboratory based works of Wettle *et al.*, (2009) and Clark *et al*., (2010) focused on, respectively, fresh and emulsified oils. How these lab-based relationships are used in the real environment is still an area of active research. In short, the uncertainties in the estimated quantifies of these features are currently unknown and will require further research. This is especially true for the delineation and quantification of marine debris, as there is currently not a single demonstration to show even the possibility of detecting marine debris from satellite optical remote sensing.

Challenges

The fundamental questions that must be addressed in order to derive surface feature products are:

1) Does the feature produce a significant signal in the satellite imagery?
2) Can the feature be spectrally differentiated from surrounding area?
3) Can the feature be further quantified (e.g., thickness, biomass, etc.)?

Edge detection and spectral analysis answer the first two questions should be positive (except for the marine debris case). The third is currently very challenging, especially for the mass (volume) estimations. This represents the most technical challenge and limitation for HyspIRI surface feature observations. However, this challenge may be addressed with targeted field measurements and analysis.

Of the listed features, marine debris is perhaps the most difficult to observe from space due to two reasons: they are typically small, and they can be submerged in water instead of floating on the surface. It would be difficult to detect them from space, even from high-spatial and high-spectral HyspIRI measurements. On the other hand, if they aggregate near ocean fronts or on beaches to form an area or slick sufficiently large for the 60-m HyspIRI pixels, it may be possible to detect and spectrally classify these features. However, because of the limited footprint and revisit frequency (every 17 days), one may need some *a priori* knowledge in order to tilt the sensor for the area of interest (e.g., after a major tsunami event).

The limitation of HyspIRI coverage and revisit frequency also applies to all other feature detection and quantification, as they are not spatially or temporally static. Even with the tilting capability, it would be difficult to trace a feature or develop a time series to document their temporal changes, especially when the ocean is well mixed under high winds. Thus, the detection and quantification will be opportunistic in nature. However, once identified from HyspIRI measurements, the features can be monitored and studied with other complementary measurements, such as targeted airborne surveys or those from

geo-stationary platforms (e.g., GEOstationary Coastal and Air Pollution Events, or GEO-CAPE; see Fishman *et al*., 2012).

Mission Relevance

Accurate and timely detection of the various ocean surface features is important for both scientific research and management decision support.

Pelagic *Sargassum* provides important habitat (food, shade, shelter from predators) to fish, shrimp, crabs and other marine organisms, including several threatened species of turtles (South Atlantic Fishery Management Council, 2002; Rooker *et al*., 2006; Witherington *et al*., 2012). Knowledge of *Sargassum* occurrence and biomass distributions help plan field surveys to study these marine organisms and their associate ecosystem. *Sargassum* may also play an important role in marine primary productivity, and thus, contributing to carbon cycling (Gower *et al*., 2006). Further, it may affect local biogeochemistry through nutrient remineralization, enhanced colored dissolved organic matter and bacteria activities (Lapointe, 1995; Zepp *et al*., 2008). *Sargassum* can also be a natural source of fertilizer for dune plants, which help to stabilize coastal dune systems from erosion (Tsoar, 2005, Anthony *et al*., 2006). Likewise, the green macroalgae, *Ulva prolifera*, also serve as important habitat for marine animals, and can be utilized as fertilizers. On the other hand, excessive *Sargassum* or other macroalgae on the beach represents a nuisance and a health hazard, and is a burden to local management since they have to be physically removed in a prompt fashion (e.g., Hu and He, 2008). Many beaches around the Gulf of Mexico (GOM) and in the southern Caribbean suffer from *Sargassum* deposition on a regular basis. Providing timely information regarding the occurrence of *Sargassum* or other types of macroalgae bloom is useful for both research and management, including implementation of harvesting policy, equipment rental for beaching cleaning and guidance on recreational fishing. Although HyspIRI is not designed to support routine monitoring, any data would inform scientific and decision-making stakeholders. Also, HyspIRI data can be used to develop techniques based on hyperspectral data to support more routine monitoring in future missions.

Nitrogen fixation by *Trichodesmium* plays a significant role in global nitrogen and carbon cycles (Capone *et al*., 1997; Gruber and Sarmiento, 1997; Karl *et al*., 1997). *Trichodesmium* blooms have also been proposed to serve as a significant nitrogen source under oligotrophic conditions for the toxic phytoplankton species *Karenia brevis* (Walsh and Steidinger, 2001), and thus could be used a precursor to forecast Harmful Algal Blooms (HABs). Timely observation of *Trichodesmium* blooms can thus improve understanding of nutrient cycling and the dynamics of *K. brevis* HABs. To date, it has been difficult to obtain timely and synoptic assessments of the distribution of *Trichodesmium* in optically complex waters, although the MODIS full spectral data at coarse resolution have been demonstrated useful (Hu *et al*., 2010a). The ability of HyspIRI to observe *Trichodesmium* blooms at higher-resolution than MODIS will provide unprecedented information on studies of nutrient and carbon cycles in coastal oceans as well as forecasting capacity for HABs monitoring.

The Deepwater Horizon oil spill sets a perfect example on the importance of timely detection and mapping of surface oil slicks (Hu *et al*., 2011). It is not only critical

in initializing and validating oil tracking models (Liu *et al*., 2011), but also important to help guide field activities (measurements and mitigation). Unfortunately, there has been a lack of quantitative measure of the surface oil volume. Such difficulty may be overcome with the HyspIRI mission provided targeted efforts in establishing appropriate algorithms in relating spectral reflectance to surface oil volume (or thickness). In the absence of major oil spill events, the detection capacity will be useful to identify small-scale spills from ships and possibly for finding new oil seeps.

Garbage patches (e.g., fishing nets) and marine debris (small plastic pieces) are hazard to fish, turtles, sea birds, coral reefs, marine mammals and even human activities (Laist, 1987; Derraik, 2002; Gregory *et al*., 2009). Although the marine debris has been found in convergence zones of the North Atlantic (Carpenter and Smith, 1972; Law *et al*., 2010) and Pacific Oceans (Venrick *et al*., 1973), where currents are driven by wind convergence, our present knowledge on marine debris is very limited (Thompson *et al*., 2004). The most abundant form of plastic marine debris at the open ocean surface consists of millimeter-sized fragments of consumer plastics with an average material density of 965 kg/m^3 (polyethylene, polypropylene and foam polystyrene) that is less than the surface sea water density of 1027 kg/m^3, so they are often found floating near the sea surface. While biological effects were unknown, many of the plastics contain considerable quantities of polychlorinated biphenyls (PCBs) as plasticizers, and that these plasticizer materials were likely lost into the surrounding seawater during weathering. In addition, they might be incorporated into marine algae and animals (Carpenter and Smith, 1972). Indeed, marine debris is now widely recognized as one of the major anthropogenic contaminants in the world's oceans (Law *et al*., 2010). Detection and quantification of marine debris will help understand their impact on the marine ecosystem as well as assist in mitigation efforts such as beaching cleaning. The remote sensing algorithms on marine debris detection, however, need to be developed before a solid application can be implemented for HyspIRI.

2.4 Water-Column Retrievals

The launch of sensors with more spectral channels and better spatial and spectral resolutions than those of CZCS, combined with progressively advanced algorithm development by the science community, has expanded the scope of ocean color applications of satellite data beyond merely mapping global oceanic biomass. Sensors with high spatial and spectral resolutions enable the retrieval of a large number of geophysical parameters from satellite-derived water-leaving radiances, such as phytoplankton concentration, concentration of dissolved organic matter, diffuse attenuation coefficient, backscattering coefficient, suspended sediment concentration, phytoplankton community structure, etc. Improvements in the spatial and spectral resolutions have enabled observations in inland, estuarine, and coastal waters in addition to open ocean waters for which the legacy sensors were designed.

The launch of a hyperspectral, high-resolution sensor will open a new era in the observation and monitoring of the ocean and, in particular, the coastal environment. Using the high spectral resolution of HyspIRI, we can expect to not only improve the accuracy of the retrieval (e.g., chl-*a* concentration, inherent optical properties), but to also

derive new products that were not retrievable using multispectral sensors (e.g., pigment composition and new land-ocean ecosystem observations). This section discusses the retrieval of various optical and bio-optical properties routinely measured by multispectral ocean-color sensors, and the improvements that could be achieved with data from hyperspectral sensors such as HyspIRI over coastal and inland waters.

Science Questions Addressed

The water-column data products provided by HyspIRI will help answer the following science questions.

VQ1. What is the global spatial pattern of ecosystem and diversity distributions and how do ecosystems differ in their composition or biodiversity?

VQ2. What are the seasonal expressions and cycles for terrestrial and aquatic ecosystems, functional groups, and diagnostic species? How are these being altered by changes in climate, land use, and disturbance?

VQ3. How are the biogeochemical cycles that sustain life on Earth being altered/disrupted by natural and human-induced environmental change? How do these changes affect the composition and health of ecosystems and what are the feedbacks with other components of the Earth system?

VQ4. How are disturbance regimes changing and how do these changes affect the ecosystem processes that support life on Earth?

CQ1. How do inland, coastal, and open ocean aquatic ecosystems change due to local and regional thermal climate, land-use change, and other factors?

CQ4. How do species, functional type, and biodiversity composition within ecosystems influence the energy, water and biogeochemical cycles under varying climatic conditions?

Candidate Products or Applications

One of the primary differences among algorithms for biophysical parameter retrieval lies in the choice of wavelengths used for the retrieval. The choice of wavelengths used in a retrieval algorithm is a critical factor because the goal is to capture and take advantage of the unique spectral signature of the bio-optical product of interest. Hyperspectral data offer more choices of wavelengths, and consequently, an improved capability to capture spectral signatures of the bio-optical products of interest. This section addresses the use of various types of algorithms for retrieving various bio-optical parameters of the water column from R_{rs}, measurements and the expected improvement in their performance with the use of hyperspectral data. The approaches for the development of these algorithms can be classified into two broad categories: empirical and analytical. Empirical algorithms are fundamentally data-driven and include band ratios (Gordon *et al.*, 1983; O'Reilly *et al.*, 1998), band differences (Hu *et al.*, 2012b), Principal Component Analysis (PCA) (Sathyendranath *et al.*, 1994; Craig *et al.*, 2012) and Artificial Neural Networks (ANN) (Schiller and Doerffer, 1999; Ioannou *et al.*, 2011), with implicit or explicit empirical expressions that relate R_{rs} to the biophysical product of interest. The analytical algorithms are theoretically driven, and include

techniques based on spectral inversion (Roesler and Perry, 1995; Hoge and Lyon, 1996; Lee *et al*., 2002), spectral optimization (Lee *et al*., 1999), and look-up-tables Carder *et al*., 1991; Mobley *et al*., 2005). These algorithms encompass a wide range of complex approaches, but are generally derived from the following basic radiative transfer equation that relates R_{rs} to the optical properties of water (Gordon *et al*., 1975):

$$R_{rs}(\lambda) = \frac{b_b(\lambda)}{a(\lambda) + b_b(\lambda)}, \quad (3)$$

Where $a(\lambda)$ and $b_b(\lambda)$ are the bulk absorption and backscattering coefficients of water and its constituents, respectively, and G(λ) is a scaling factor that accounts for geometrical conditions, bidirectional effects and the state of the air-water interface.

Many algorithms are based on a combination of empirical and analytical approaches. For example, empirical algorithms such as ANN use datasets that are developed based on the radiative transfer model. Some algorithms based on the analytical radiative transfer model are empirically parameterized using datasets collected *in situ* (Dall′ Olmo and Gitelson, 2005). Such algorithms are often referred to as semi-empirical or semi-analytical algorithms.

A discussion of the merits of each algorithm for each product is beyond the scope of this document. The following is a brief discussion on how HyspIRI might improve retrieval accuracies. Further work is required to quantitatively estimate the quality of these products and their applicability to specific science questions.

Inherent Optical Properties

The optical properties of water are conventionally divided into two classes: (1) Inherent Optical Properties (IOPs); and, (2) Apparent Optical Properties (AOPs). The inherent optical properties depend only on the medium (i.e., water) and are independent of the ambient light field within the medium, while the apparent optical properties depend on the medium as well as the geometric structure of the ambient light field within the medium.

Absorption Coefficient

Total absorption and backscattering are the two main drivers of the magnitude and shape of the reflectance signal; they are crucial parameters for the characterization and inversion of the water-leaving radiance. A number of algorithms have been developed to derive either the total absorption coefficient or the individual absorption coefficients of the primary absorptive components, namely, pure seawater (a_w), phytoplankton (a_{ph}), and yellow substances (a_y) (IOCCG, 2006). The retrieval of the absorption coefficient is performed at a given set of wavelengths or over the entire visible spectrum. The absorptions by detritus and yellow substances are often combined into a single component due to the similarity of their spectral shapes. Semi-empirical and analytical algorithms will see an immediate gain from the increased number of wavelengths at which the absorption coefficient could be retrieved. For example, the Quasi-Analytical

Algorithm (QAA) developed by Lee *et al*., (2002) would be able to provide the total absorption and phytoplankton absorption coefficients at all visible wavelengths of HyspIRI (Lee *et al*., 2005). Subsequent decomposition into absorptions by individual components would therefore be more accurate, as the number of wavelengths available to characterize the absorption would significantly outnumber the number of individual components.

Figure 2.4.1 shows the absorption coefficients of various marine components in the visible and near-infrared regions. The measured reflectance spectrum is roughly inversely proportional to the total absorption spectrum, and hence, is marked by spectral features due to absorption by water-column constituents. The high spectral resolution of HyspIRI can resolve details that cannot be resolved by multispectral sensors — details such as the secondary peaks of absorption by phytoplankton (e.g., at 640 nm for chl-$c_{1,2}$).

In general, optimization methods derive a limited number of parameters, such as $a_{ph}(443)$, $a_{y}(443)$ and $b_{bp}(443)$, as dictated by the number of wavelengths at which R_{rs} is available. Access to hyperspectral information would increase the number of retrievable parameters (e.g., slope of spectral dependence of yellow substances) by exploiting different parts of the spectra depending on the parameter of interest. Using hyperspectral information, one can expect to distinguish between the contributions from detritus and yellow substances to the total absorption coefficient. ANN analyses would benefit from the supplementary information contained in hyperspectral data (over what is contained in multispectral data), resulting in a better characterization of the magnitude and shape of the total absorption coefficient, and consequently, a better decomposition of the total absorption signal into the individual components. For example, Schofield *et al*., (2004) showed that hyperspectral data of the total absorption coefficient could be de-convolved into absorptions by three groups of phytoplankton representative pigments (chl-*a*-*c*, phycobilin, and chl-*a*-*b*), yellow substances and detritus. Their method assumed predetermined spectral shapes for the absorption by the three phytoplankton populations, and allowed some variation in the spectral slopes of absorptions by gelbstoff and detritus. An optimization scheme was used to derive the contribution of each component to the total absorption by minimizing the squared difference between the reconstructed spectra and the measured spectra. This type of approach, ideally suited for hyperspectral data, helps infer valuable information about coastal ecosystem processes and the fate of biogeochemical components in the coastal shelf.

Backscattering Coefficient

Total backscattering coefficient is often described as the sum of the backscattering coefficients of pure seawater and particulates. The particulate backscattering includes backscattering by living (phytoplankton, viruses and bacteria) and non-living (mineral) particles. Although ignored in current algorithms, it has been shown that scattering, and therefore backscattering, by pure seawater is affected by water temperature and salinity (Zhang and Hu, 2010). The presence of a thermal infrared sensor in addition to the VSWIR sensor would enable testing and possibly correcting for the effect of variations in the temperature and result in improved retrieval of the backscattering coefficient of pure seawater. Two aspects of the particle backscattering coefficients provide useful information on the marine constituents: the magnitude and the

spectral dependence, the former being related to the concentration of particles and the latter to the size distribution of the particles. In open ocean waters, where phytoplankton is the main driver of the optical variability, a value of one for the slope of the spectral dependence (described as a power law) is commonly accepted. In coastal areas, this assumption becomes invalid and the slope of the spectral dependence can vary from −1 to 3 in extreme cases (Loisel *et al*., 2006; Martinez-Vicente *et al*., 2010). Algorithms for retrieving backscattering coefficients (some algorithms retrieve both absorption and scattering coefficients) would gain in accuracy for the same reasons, as described earlier for the retrieval of the absorption coefficients. Improved accuracy in the retrieval of the spectral slope of the backscattering coefficient would yield, in theory, improved information on particle size distribution (Loisel *et al*., 2006; Kostadinov *et al*., 2009), a key parameter for studying biogeochemical cycles. The magnitude of the slope of the spectral dependence changes across the visible and NIR regions because of particulate absorption (Doxaran *et al*., 2009). Using hyperspectral data, we can develop methods that would account for this change in the magnitude of the slope of the backscattering coefficient in the visible and near infrared regions. Doxaran *et al*., (2009) proposed a model based on hyperspectral measurements to account for absorption by particles in the near infrared region when retrieving the backscattering coefficient, which could only be applied to data collected by a hyperspectral sensor such as HyspIRI.

Apparent Optical Properties

Diffuse Attenuation Coefficient

The diffuse attenuation coefficient (K_d) is typically calculated to estimate the penetration of downwelling light in the water column. This coefficient is important for studying biological processes and water turbidity. One of the earliest methods to derive the diffuse attenuation coefficient from remotely sensed data was based on a ratio of water-leaving radiances, developed by Austin and Petzold (1981). They showed that K_d(490) could be derived using a simple linear regression of the ratio of water-leaving radiances at two wavebands centered at 443 and 550 nm. Later, Mueller and Trees (1997) replaced the waveband at 443 nm with one at 490 nm and the waveband at 550 nm with one at 555 nm to improve the retrieval of K_d(490); their algorithm was selected to retrieve the standard K_d (490) product for the Sea-viewing Wide Field-of-view Sensor (SeaWiFS). The higher number of wavebands available with HyspIRI would give more opportunities to test different combinations of wavelengths, and undoubtedly improve the accuracy with which K_d(490) could be retrieved. Moreover, a simple linear regression or a more complex formulation (Loisel *et al*., 2006) of band ratios against K_d(490), or algorithms based on more than two wavelengths (Fichot *et al*., 2008; Jamet *et al*., 2012), could be used to improve the retrieval of K_d (490) in coastal waters.

Given the number of wavebands available on HyspIRI, the diffuse attenuation coefficients could also be derived at other wavelengths besides 490 nm using simple mathematical formulations. Fichot *et al*., (2008) proposed a method based on principal component analysis to derive K_d at 320, 340, 380, 412, 443, and 490 nm, using data from the multispectral bands of SeaWiFS. Similarly, Jamet *et al*., (2012) used an ANN-based algorithm to compute K_d(490) in coastal waters using multispectral remote sensing reflectance. The use of hyperspectral data would certainly improve the retrieval of the

diffuse attenuation coefficient for statistically based approaches, provided that the training dataset is large enough and encompasses a variety of optical environments, such as those encountered in coastal waters. The algorithm from Fichot *et al.*, (2008) would certainly gain in accuracy from R_{rs} collected in the ultraviolet (UV) region (HyspIRI will collect radiances starting at 380 nm), as the primary goal for that algorithm is to derive K_d in the UV and short visible wavelengths. Applications that depend on photochemistry (e.g., photodegradation of yellow substances) would benefit significantly from the measurements in the UV region.

A limitation of empirical or semi-empirical algorithms is that they omit or ignore the impact of sun elevation on the retrieval of K_d. K_d is an apparent optical property that can vary by ~30% between when the sun is at the zenith and when it is 60° off zenith. Consequently, empirical band ratio algorithms overestimate K_d when the sun is close to the zenith and underestimate K_d when the sun is close to the horizon. The semi-analytical approach based on IOPs (Lee *et al.*, 2005) overcomes this limitation by explicitly including the solar angle in the calculation of K_d, and it is found that this algorithm works fine for both oceanic and coastal waters (Zhao *et al.*, 2013; Cunningham *et al.*, 2013). In particular, this algorithm is applicable to both multispectral and hyperspectral data, which would be extremely useful for a HyspIRI-type sensor.

In summary, irrespective of the method used (i.e., simple regression or advanced statistics), the use of hyperspectral data would allow the derivation of the diffuse attenuation coefficient with better accuracy than what is achievable using multispectral data.

Optically Active Constituents

Colored Dissolved Organic Matter (CDOM)

In coastal waters that receive river runoff, colored dissolved organic matter (CDOM) or Gelbstoff, can represent a large fraction of the organic material present in the water column. CDOM plays an important role in the biogeochemical cycles within the ecosystem through re-mineralization by photochemistry, and by altering the light available for photosynthesis by phytoplankton and the subsequent biological production. With a high spatial resolution, HyspIRI would enable an accurate mapping of coastal waters that are under the influence of CDOM. The hyperspectral information would make it possible to test new multi-band algorithms and improve upon existing methods.

A number of empirical, analytical and semi-analytical algorithms have been developed to retrieve CDOM concentration from remotely sensed data. Band ratios, such as $R_{rs}(443)/R_{rs}(510)$ (D'Sa and Miller 2003), $R_{rs}(490)/R_{rs}(555)$ (Mannino *et al.*, 2008), $R_{rs}(510)/R_{rs}(670)$ (Del Castillo and Miller, 2008), and $R_{rs}(570)/R_{rs}(655)$ (Ficek *et al.*, 2011), are the most common type of empirical algorithm. Morel and Gentili (2009) used the relationship between the reflectance ratios $R_{rs}(412)/R_{rs}(443)$ and $R_{rs}(490)/R_{rs}(555)$ to isolate the effects of CDOM on measured reflectance, and subsequently retrieve the concentration of CDOM. Bélanger *et al.*, (2008) used a polynomial expression to derive the ratio of CDOM absorption to the total absorption at 412 nm as a function of $R_{rs}(555)$, $R_{rs}(412)/R_{rs}(555)$ and $R_{rs}(490)/R_{rs}(555)$. These band ratios are based on the spectral

channels of multispectral sensors such as MODIS and SeaWiFS, and were mostly developed for Case-I, open ocean waters. They generally perform poorly in optically complex coastal waters because of overlapping absorptions by chl-*a* and CDOM and the difficulty in separating their effects at the blue wavelengths used in the band ratios. The use of HyspIRI's narrow bands in the short wavelengths (starting from 380 nm) will enable better separation of the optical effects of chl-*a* and CDOM, which absorbs UV light. It also provides more options for band combinations to use in empirical and semi-empirical algorithms.

The semi-analytical algorithm QAA retrieves the combined absorption of CDOM and detritus, i.e., a_{dg}. Using above-water hyperspectral reflectance measured using a field spectrometer, Zhu *et al*., (2011) developed an enhanced version of QAA, called QAA-E, which can separate the absorption coefficient of CDOM from a_{dg} by using the relationship between the absorption coefficient of either non-algal particles or total particles, and the particulate back-scattering coefficient. Zhu and Yu (2013) further improved QAA-E by using hyperspectral data from Hyperion to optimize essential parameters and functions used in QAA for turbid coastal waters. Zhu and Yu (2013) were limited by their inability to use $R_{rs}(410)$ from Hyperion, because of the low SNR of Hyperion, and the consequent difficulty in calibrating the spectral channel centered at 410 nm. HyspIRI, with its high SNR, will not have such limitation.

HyspIRI would also improve the retrieval of the absorption coefficient of CDOM using spectral inversion schemes. Algorithms such as the Garver-Siegel-Maritorena (GSM) model, which in its original version uses six wavelengths, would theoretically yield more accurate results when applied to 30 or more wavelengths. Fichot *et al*., (2013) showed that the concentration of terrigenous dissolved organic matter (tDOM) could be unambiguously derived from the slope of their absorption spectra between 275 and 295 nm (inferred from reflectances at longer wavelengths), which was extrapolated from MODIS reflectance in the visible region. Their method would benefit from the use of hyperspectral data because an increase in the number of available wavelengths could strengthen the underlying spectral relationships on which their method is based.

Suspended Matter

Suspended Particulate Matter (SPM) or Total Suspended Matter (TSM) is a critical parameter for studying water quality, coastal erosion, availability of light to submerged aquatic vegetation and transport of sediments and pollutants in water bodies (e.g., Bergamaschi *et al*., 2012). The nature and concentration of TSM in water are highly related to the bulk optical properties of the water (e.g., Chen *et al*., 1991; Astoreca *et al*., 2012). Phytoplankton may form a significant fraction of TSM. Together with inorganic particles, they play a significant role in coastal waters. Approaches based on the relationships between IOPs and TSM would benefit from the use of hyperspectral data. First, we can expect the accuracy of the retrieved TSM to increase if the IOPs are retrieved with better accuracy. Numerous studies (Doxaran *et al*., 2009, 2012; Ritchie *et al*., 1976; Sterckx *et al*., 2007) have demonstrated the usefulness of near infrared and infrared bands to assess TSM concentration in turbid coastal waters, estuaries and rivers, as long as spatial resolution criteria are sufficiently met. For example, using hyperspectral data from the Advance Hyperspectral Sensor (AHS), Sterckx *et al*., (2007) showed that TSM was related to the logarithm-linear relationship of the difference between the reflectances at 833 and 1004 nm (r^2 = 0.83; RMSE = 15.53 mg/L) for TSM concentrations up to 350 mg/L. Their approach used the insensitivity of the band at 1004 nm to TSM concentration to remove contaminations from cirrus clouds and adjacency effects. Doxaran *et al*., (2012) also found a significant relationship between TSM and the ratio of R_{rs}(780) to R_{rs}(560). Linear regression of the derived TSM concentration against the measured TSM concentration, showed an r^2 of 0.98 with a slope of 0.94, and an RMSE of 6.1 mg/L. These two examples of simple algorithms illustrate the need for hyperspectral observations when dealing with turbid waters. The visible part of the spectrum can be exploited for moderate-to-high levels of TSM (less than 50 mg/m^3). However, as the concentration of TSM increases, reflectance in the near infrared and infrared bands are necessary to obtain reliable retrievals of the TSM concentration. HyspIRI would be a valuable asset for retrieving TSM concentration in turbid and very turbid waters, and would allow testing of different combinations of reflectances in the visible and near infrared regions to not only estimate the concentration of TSM, but also remove adverse environmental effects on remotely sensed data, such as adjacency effects, contamination from high altitude clouds and sun glint.

Chlorophyll-a Retrieval

The concentration of chl-*a* in water is a strong indicator of the trophic status of a water body (Falkowski and Raven, 1997; Schalles *et al*., 1998). Continuous monitoring of the biophysical status of a water body requires regular estimation of its primary productivity and phytoplankton biomass, usually indicated in the form of chl-*a* concentration. With its ubiquity in surface waters and ease of measurement in a laboratory setting, chl-*a* concentration is a convenient and reliable indicator of water quality, and is used routinely for monitoring marine and lacustrine waters. Remote sensing of ocean color for water quality analysis has been historically focused on estimating chl-*a* concentration in open ocean waters (IOCCG, 1999). Various algorithms have been developed for estimating chl-*a* concentration in open ocean, coastal, estuarine and inland waters using remotely sensed data. In the open ocean, phytoplankton dominates the optical properties of water, and algorithms based on simple ratios of reflectance in the blue and green spectral regions have been commonly used to retrieve

accurate estimates of chl-*a* concentration from satellite data (Gordon *et al*., 1983; O'Reilly *et al*., 1998). In most inland, estuarine and coastal waters, however, CDOM and SPM occur in high abundance besides phytoplankton, resulting in complex optical properties. Often, the bottom also contributes to water-leaving radiance from shallow coastal waters. These conditions render the simple blue-green algorithms unreliable for obtaining accurate estimates of chl-*a* concentration in optically complex coastal waters. For such waters, algorithms based on reflectances in the red and near-infrared (NIR) regions (Gitelson 1992; Dall'Olmo and Gitelson 2005) are preferred, due to the decreased effects of CDOM and SPM at these spectral regions.

Matthews (2011) and Odermatt *et al*., (2012) have provided reviews of many recently developed chl-*a* algorithms. Most of the algorithms were developed for application to multispectral data, and have produced chl-*a* estimates with varying degrees of accuracy for open ocean, coastal, estuarine and inland waters, limited primarily by the inability to resolve from multispectral data the complex, overlapping spectral features from various constituents in turbid productive waters. The hyperspectral data from HyspIRI would enable the resolution of fine spectral features due to various phytoplankton pigments in addition to chl-*a*, leading to more accurate estimates of chl-*a* concentration, and assisting in understanding the composition of the phytoplankton community in inland, estuarine and coastal waters.

The two-band NIR-red model (Gitelson, 1992),

$$\text{Chl-}a \propto \left[R_{\lambda_1}^{-1} \times R_{\lambda_2} \right] \tag{4}$$

and the three-band NIR model (Dall'Olmo and Gitelson, 2005),

$$\text{Chl-}a \propto \left[\left(R_{\lambda_1}^{-1} - R_{\lambda_2}^{-1} \right) \times R_{\lambda_3} \right] \tag{5}$$

where R_λ is the remote sensing reflectance at the spectral channel centered at λ nm, have been shown to yield accurate estimates of chl-*a* concentration in optically deep inland and coastal waters in North America, Asia and Europe (Gilerson *et al*., 2010; Gitelson *et al*., 2011; Gurlin *et al*., 2011; Moses *et al*., 2012a), with the spectral band positions of the models fixed at MERIS' spectral channels centered at 665 nm, 708 nm, and 753 nm. These MERIS-based NIR-red algorithms have yielded chl-*a* estimates with consistently high accuracies on the order of 90% or more for waters with a wide range of chl-*a* concentrations.

The hyperspectral data from HyspIRI would provide increased flexibility in the choice of spectral bands for these models, and could potentially lead to different band combinations. Such an adaptive algorithm could provide more accurate estimates of chl-*a* concentration than what has been achieved using the spectral bands of MERIS. For instance, MERIS does not have a spectral band centered between 708 nm and 753 nm; therefore, λ_3 for the three-band model has to be set at 753 nm. However, the spectral band centered at 753 nm is susceptible to significant effects due to instrument noise and

imperfect atmospheric correction, which significantly affects the performance of the three-band model (Moses *et al*., 2009b). The hyperspectral data from HyspIRI would enable the use of a shorter wavelength for λ_3, which could improve the performance of the three-band NIR-red model.

HyspIRI's hyperspectral data would also enable the use of algorithms based on sophisticated, numerically driven approaches such as the Levenberg Marquardt multivariate optimization for estimating water quality parameters (Pozdyanok *et al*., 2005; Moses *et al*., 2012b). This is a non-linear least squares approach that uses a forward model, such as Hydrolight, to generate modeled reflectance, and estimates biophysical parameters by iteratively minimizing a user-supplied cost function, such as the squared difference between the measured and modeled reflectances. In fact, this method can simultaneously retrieve multiple biophysical parameters besides chl-*a* concentration. A method such as this requires hyperspectral data with high SNR, such as what would be provided by HyspIRI, as it considers a broad spectral range, and relates reflectance features within the range to optically active constituents in water. Noisy data would cause the method to misinterpret noise features as actual spectral features, and produce inaccurate estimates of biophysical parameters.

For optically shallow waters, algorithms such as those based on spectral inversion techniques (Lee *et al*., 1998, 1999) or Look-Up-Tables (Mobley *et al*., 2005) have been used to minimize the effect of reflectance from the bottom and retrieve the chl-*a* concentration in water. The use of hyperspectral data will help improve the isolation of contributions from the bottom, and lead to more accurate retrievals of chl-*a* concentration.

Davis *et al*., (2007) used data from Hyperion and several airborne hyperspectral sensors to evaluate the spatial resolution required to study coastal waters, with a specific focus on detecting algal bloom patches. They concluded that a spatial resolution less than 100 m is required to adequately capture the spatial dynamics of heterogeneous coastal waters. With a spatial resolution of 60 m, HyspIRI would be capable of adequately capturing spatial variability in coastal waters. HyspIRI's temporal revisit cycle of several observations per week at latitudes higher than 60° for the visible and short wave infrared spectrometer, will help monitor algal blooms in inland, estuarine and coastal waters at those latitudes, but not at the equator where the revisit time is about 19 days.

Phytoplankton Functional Types (PFT)

The HyspIRI mission will provide the scientific community with hyperspectral observations that will lead to a more robust chl-*a* product, and the opportunity to detect various accessory pigments that can be utilized to identify biogeochemically important Phytoplankton Functional Types (PFT). Understanding the spatial and temporal distribution of PFTs will allow the scientific community to improve its knowledge of biologically mediated fluxes of elements that contribute to the carbon cycle (Falkowski *et al*., 2004). Information on biodiversity provides a valuable quantitative database for structuring sophisticated predictive models that include taxonomic phytoplankton community information, such as size spectra, probability distributions of certain taxa and upper trophic level estimations, such as fisheries productivity (Chesson and Case, 1986; DeAngelis and Waterhouse, 1987; Chase *et al*., 2013). Determining the spatial variability and concentrations of various PFTs is critical to improving primary productivity estimates and understanding the feedbacks of climate change (Moisan *et al*., 2011). Hyperspectral techniques, which can enhance the discernment of subtle features in hyperspectral data, could also enable the detection of marker pigments.

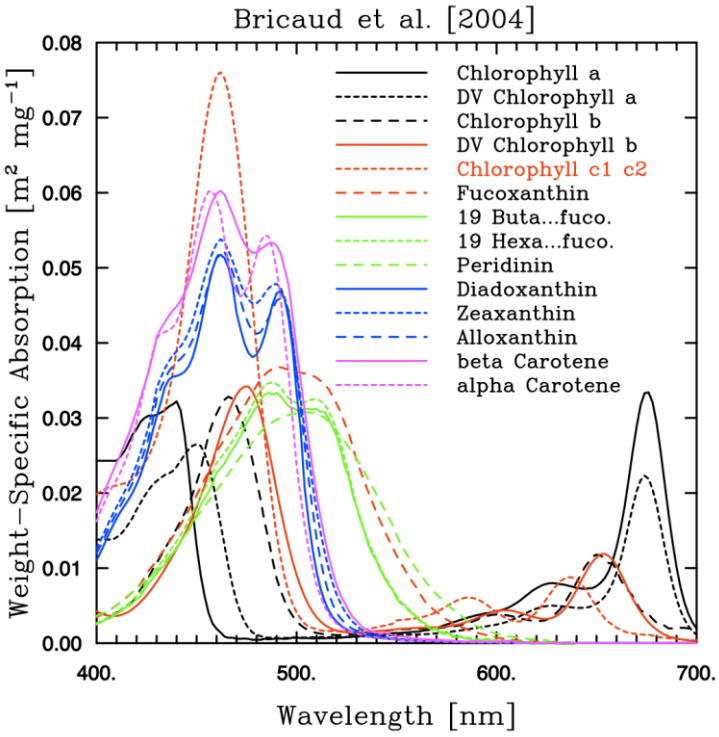

Figure 2.4.1 – Weight-specific in vitro absorption spectra of various pigments, $a_i^*(\lambda)$, derived from measuring the absorption spectra of individual pigments in solvent and shifting the maxima of the spectra according to Bidigare *et al*., (1990). Data obtained courtesy of Annick Bricaud (See Bricaud *et al*., 2004). Note, that only 14 of the total 18 pigments encountered in this study have pigment-specific relationships available from laboratory studies (Moisan *et al*., 2011).

To spectrally detect marker pigments, the total absorption is first retrieved from the measured reflectance using an algorithm (e.g., based on inversion of a water-column radiative transfer model), and then the total absorption is separated into absorption by individual endmembers. High-resolution reflectance spectra will facilitate the retrieval of total absorption at high resolution. This can lead to better discrimination between relative concentrations of photosynthetic and photo-protective pigments, which serve as taxonomic marker pigments, and provide a proxy for the physiological function of the phytoplankton community.

Figure 2.4.1 shows the *in vivo* absorption spectra of the photo-protective and photosynthetic pigments in solution. The weight-specific absorption coefficients were derived by measuring the absorption spectra of individual pigments in solvent and shifting the maxima of the solvent according to the method described by Bidigare *et al*., (1990). The spectra on Figure 2.4.1 were generated using data published by Bricaud *et al*., (2004). Not all pigments shown are easily discernible, but certain key marker pigments (or groups of pigments) can be distinguished and used to identify functional types present in the water column. Chl-*a*, chl-*b* and chl-*c* are characterized by sharp absorption bands, whereas the carotenoids have a broader absorption spectrum. Carotenoids can be further divided into several photosynthetic pigments (fucoxanthin, peridinin, 19'-hexanoyloxyfucoxanthin and 19'-butanoyloxyfucoxanthin), whose maximum absorption occurs around 490–500 nm, and non-photosynthetic pigments (zeaxanthin, diadinoxanthin, alloxanthin, and β-carotene), which have two absorption peaks around 460 and 500 nm. Methods based on phytoplankton absorption have been used successfully to obtain information using the unique spectral signatures of pigments, such as chl-*b*, chl-*c*, photosynthetic and nonphotosynthetic carotenoids (Hoepffner and Sathyendranath, 1993; Bricaud *et al*., 2007), and fucoxanthin (Chazottes *et al*., 2007).

Historically, algorithm development for detecting PFTs has been based on IOPs and AOPs and their relationship to marker pigments for phytoplankton taxa or groups within a community. Development of algorithms for detecting PFTs in the coastal ocean has been a challenge due to the optical complexity caused by sediment re-suspension, coastal runoff and bottom reflectance. However, successful modeling of absorption has led to the development of mathematical approaches to estimate photo-protective and photosynthetic pigments that vary with cell size, carbon content, and pigment packaging effects (Balch et al. 1991; Subramanian et al. 1999). Recently, algorithms have been developed to distinguish phytoplankton groups such as *Phaeocystis* and diatoms (Sathyendranath *et al*., 2004; Moisan *et al*., 2011). A number of approaches based on phytoplankton absorption to retrieve pigment composition (e.g., Schofield *et al*., 2004; Whitmire *et al*., 2010) or phytoplankton size distribution e.g., (Devred *et al*., 2006, 2011; Ciotti *et al*., 2006; Hirata *et al*., 2008) would show great improvements when applied to HyspIRI data. Applications such as PHYSAT (PHYtoplankton groups from SATellites, Alvain *et al*., 2004) and PhytoDOAS (Phytoplankton Differential Optical Absorption Spectroscopy; Bracher *et al*., 2009; Sadeghi *et al*., 2012) use spectrally resolved reflectance to interpret changes in community structure, and reduce the noise due to the presence of yellow substances or suspended minerals, and are well suited for coastal observations. Lubac *et al*., (2008) demonstrated the advantage of using a hyperspectral sensor over a multispectral sensor to detect *Phaeocystis globosa* spp. in turbid coastal waters based on the second derivative of $R_{rs}(\lambda)$. Millie *et al*., (1997) used fourth order spectral derivatives to quantitatively detect the red tide dinoflagellate *Gymnodinium breve* in the Sarasota Bay in Florida. Methods based on high-order spectral derivatives require hyperspectral data.

Algorithms for detecting PFTs have also been developed based on the incorporation of ecological and geographic knowledge of ocean color, bio-optical

characteristics and remotely sensed physical parameters, such as Sea Surface Temperature (SST), Photosynthetically Active Radiation (PAR) and sun-induced fluorescence (Raitsos *et al*., 2008). The incorporation of ecological and geographical knowledge with ocean color, bio-optical characteristics and remotely sensed physical parameters is a powerful approach for capturing variability due to environmental conditions. For instance, it is known that some species, such as *Alexandrium* spp., require favorable environmental conditions to germinate (Anderson *et al*., 2012). The simultaneous measurements of visible (phytoplankton) and infrared (SST) radiation by HyspIRI will enable such an approach.

Fluorescence

Sun-induced fluorescence by phytoplankton, modeled as a Gaussian curve centered around 683 nm, can be used to infer phytoplankton concentration (Behrenfeld *et al*., 2009; Gower *et al*., 1999; Huot *et al*., 2005, 2007). Approaches that use fluorescence to derive phytoplankton concentration have been promoted for ocean color applications in coastal areas, because the portion of the spectrum that they exploit is only moderately impacted by other marine constituents besides phytoplankton. Ocean color sensors like MERIS and MODIS carry specific wavebands to record the fluorescence emission embedded in the reflectance signal. The reflectance signal in the near infrared also carries information on the absorption and elastic scattering.

A simple model to derive the magnitude of fluorescence, referred to as the Fluorescence Line Height (FLH), was developed to deduce the contribution from elastic scattering to the total reflectance signal. This approach is based on a reflectance baseline formed linearly between the reflectances at two wavelengths, where the fluorescence is negligible (e.g., 667 and 748 nm for MODIS; Abbott *et al*., 1999; 665 and 709 nm for MERIS), which is then subtracted from the total reflectance signal at the sensor's "fluorescence" band (678 nm for MODIS and 681 nm for MERIS) to yield the FLH. For MERIS, the same approach was developed to take account of the shift in the reflectance peak to longer wavelengths for highly productive waters to derive a Maximum Chlorophyll Index (MCI, Gower *et al*., 2008). Blondeau-Patissier *et al*. (2014) used FLH, MCI, and chl-*a* concentration, estimated using a neural network algorithm to characterize algal bloom dynamics, and distinguish surface blooms dominated by chl-*a* from those due to cyanobacterium *Trichodesmium* spp. in the Great Barrier Reef and Van Diemen Gulf regions in Northern Australia. Although these approaches are relatively insensitive to perturbations of CDOM (Hu *et al*., 2005; McKee *et al*., 2007), FLH suffers from interference from particulate scattering in highly turbid waters (McKee *et al*., 2007). Therefore, more sophisticated approaches have been used to derive the fluorescence signal based on the radiative transfer theory (Huot *et al*., 2005). The use of hyperspectral data will allow for a better characterization of the fluorescence signature in the reflectance data, especially when choosing the baseline wavelengths and the peak wavelength. Mischaracterization of the baseline may lead to negative estimation of the FLH. Shifts in the location of the wavelength of peak reflectance will affect the ability of a multispectral sensor to accurately quantify the fluorescence signal. The availability of more bands could lead to more advanced schemes of inversion of the reflectance signal.

In addition to providing information on chl-*a* concentration, FLH also provides a

powerful tool to assess the physiological state of the phytoplankton community (Falkowski and Kiefer, 2005; Behrenfeld *et al*., 2009). FLH is an excellent indicator of factors that control phytoplankton primary productivity, such as pigment concentration, non-photochemical quenching, and pigment packaging effects. Both laboratory and field studies have demonstrated that these physiological indicators change on rapid time scales and represent new avenues for understanding primary productivity and carbon flow globally (Cleveland *et al*., 1987; Moisan *et al*., 1998). The fluorescence quantum yield (Φf) may vary by an order of magnitude in marine environments, especially in the coastal ocean, due to variations in the taxonomic composition of phytoplankton, nutrient availability, temperature and light (Berhrenfeld *et al*., 2009). Changes in Φf and FLH may emphasize linkages between phytoplankton physiology and environmental variability, which was a key point in the 2007 Decadal Survey. With accurate characterization of FLH in the coastal regions, HyspIRI will provide unprecedented coverage of changing phytoplankton community response to coastal issues, such as eutrophication, ecosystem health and changing nutrient ratios (Westberry and Siegel, 2003).

Coastal Fronts and Plumes

The combination of hyperspectral and thermal imagery provides an opportunity to improve the detection and mapping of coastal fronts and plumes at high spatial resolution, leading to a unique data product with useful applications. Coastal plumes produced by the continuous discharge of rivers and estuaries are common features in shelf and coastal waters, and contain harmful runoff from land. They influence various aspects of the coastal environment, from circulation patterns to biogeochemical processes, causing eutrophication, turbidity and spread of harmful pollutants (Mestres *et al*., 2007; Riegl *et al*., 2009). The complex behavior of coastal plumes is determined by various factors, including river discharge characteristics, topography/bathymetry and wind and tidal effects (Stumpf *et al*., 1993; Wiseman and Garvin, 1995; Blanton *et al*., 1997). Estuarine and ocean fronts result when denser water underrides lighter water, giving rise to an inclined interface and a strong convergence at the surface, which can concentrate phytoplankton and pollutants such as oil slicks.

To detect and map coastal fronts and plumes, remote sensors exploit differences in their turbidity, color, temperature and salinity from the background water (Muller-Karger *et al*., 1988; Odriozola *et al*., 2007). Due to their high turbidity and color gradients, most estuarine fronts and coastal plumes can be detected by satellites, such as SeaWiFS, MODIS, and Landsat TM (Purkis and Klemas, 2011). The lower salinity and temperature of some shelf features, such as the Amazon, Orinoco, Mississippi, La Plata River and many other river plumes, have been mapped using various ocean color sensors. Open ocean fronts, such as the Iceland-Faroes front, often have strong temperature gradients, while coastal upwelling fronts can be detected by their colder temperatures and colors due to high chl-*a* concentration. With its relatively high spatial resolution, hyperspectral VSWIR channels and TIR channels, HyspIRI will improve our ability to identify and analyze coastal plumes and oceanic fronts. Combining HyspIRI's high-resolution data with Synthetic Aperture Radar (SAR) and multispectral imagery from other satellites should provide the temporal and spatial resolution required for imaging

the location, extent, composition and dynamics of coastal plumes, fronts and oil slicks.

The high spectral resolution of HyspIRI will enable us to estimate the concentrations of biogeochemical constituents in plumes and fronts (Chang *et al*., 2002; Brando and Dekker, 2003). The biogeochemical constituents vary according to their origin, which can be river runoff or wind-induced upwelling. Schroeder *et al*., (2012) used an enhanced version of the Linear Matrix Inversion algorithm (Hoge and Lyon, 1996) to map fresh water plumes in the Great Barrier Reef lagoon using MODIS images. They retrieved chl-*a*, non-algal particulate matter, and CDOM simultaneously from MODIS reflectances, and used CDOM as a surrogate for salinity to map the extent of freshwater. As stated previously, hyperspectral data will greatly improve the performance of such spectral inversion techniques. HyspIRI data can also help us to analyze water quality, nutrient loads and changes in fisheries due to natural and human-induced stress on marine ecosystems at fine spatial scales.

Challenges

There are a few aspects that should be considered regarding the characteristics of the HyspIRI mission and its applicability to remote retrievals of the water column parameters discussed in this section. Sun glint presents a problem in the tropics and subtropics that has to be addressed to exploit the full potential of HyspIRI. Examination of MODIS scenes indicated that a 4° westward tilt at an 11:00 a.m. ascending equatorial crossing, could result in a maximum glint signal that is between 20% and 100% of the magnitude of the surface reflectance at 488 nm (Hochberg *et al*., 2011). In operational processing of ocean color products, sun glint is often flagged by applying thresholds for water-leaving radiance. Such flags can be used to mask a large portion of an image. For HyspIRI, this would result in a substantial loss of opportunities to observe the water column at low latitudes. However, new algorithms, such as POLYMER (Steinmetz *et al*., 2011), which processes the atmospheric and oceanic signals simultaneously through optimization schemes, have proven efficient at removing sun glint. Given HyspIRI's high spectral resolution and spectral coverage extending into the SWIR region, improved performances of algorithms such as POLYMER is expected, provided that the initial conditions (i.e., spectral dependence of marine and atmospheric components) have been properly addressed. Figure 2.4.2 illustrates the correction of sun glint by the POLYMER algorithm.

The 19-day equatorial revisit cycle (shorter at higher latitudes) of the HyspIRI mission is inadequate to monitor or map short-term events, such as the development and movement of harmful algal blooms or enhanced production following a storm event (Babin *et al*., 2004). Nevertheless, the revisit time would be adequate to map coastal in-water constituents and their optical properties for long term monitoring (on seasonal or annual scales). Detailed snapshots of inland, estuarine and coastal waters, though acquired infrequently, can be used in conjunction with data from multispectral sensors that provide almost daily global coverage to provide a better understanding of the temporal evolution of aquatic ecosystem processes. Moreover, as described in previous sections, the detailed snapshots can also lead to the development of improved techniques for retrieving bio-optical products. The primary general application of HyspIRI would be to look at persistent, long-term water quality issues and relate them to spatial processes

(e.g., nutrient or sediment discharge hotspots along the coasts). HyspIRI might also provide information on seasonal succession of species in estuaries and inland waters, or snapshots of responses to episodic events. At high latitudes, the revisit time reduces to only a few days, thereby improving the temporal resolution greatly. Provided the signal strength is sufficiently strong, HyspIRI might be able to coarsely observe phytoplankton bloom dynamics in polar systems.

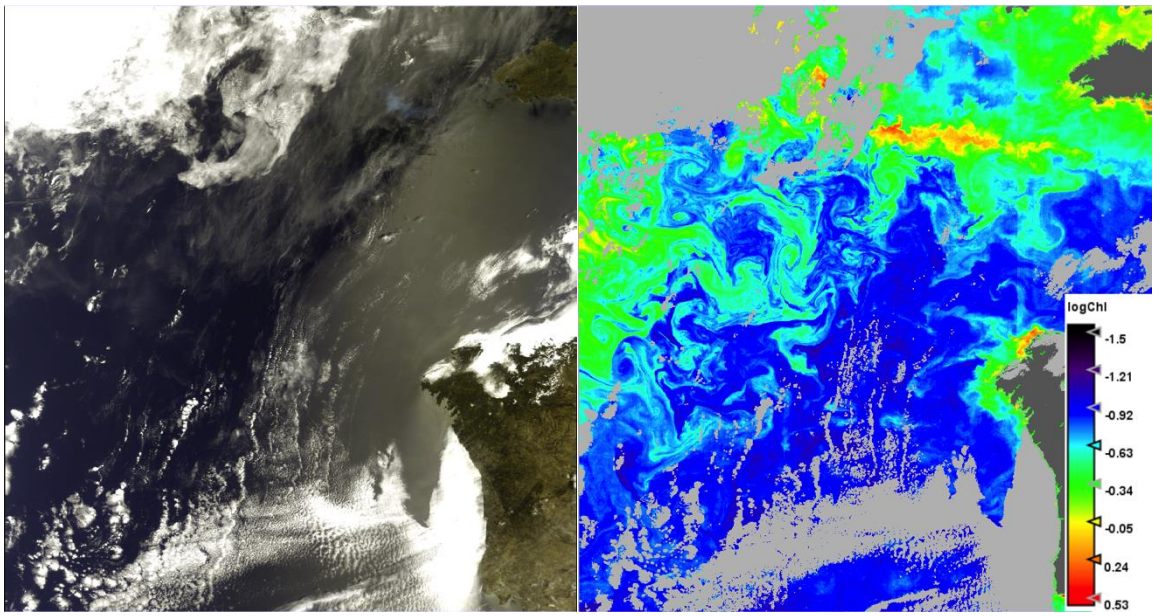

Figure 2.4.3 – MERIS false color image acquired off the coast of Portugal on 21 June 2005 (left), and chl-*a* concentration derived by the POLYMER algorithm (right). The algorithm was able to retrieve chl-*a* concentration in the presence of thin clouds and sun glint (Courtesy of F. Steinmetz).

The final accuracy of the biophysical products retrieved from satellite data depends on a number of factors, such as the ability of the particular bio-optical model to correctly relate variations in the biophysical parameter of interest to the measured reflectance without being sensitive to effects caused by variations in other optically active constituents in the water, the accuracy of atmospheric correction, the reliability of radiometric calibration and the inherent noise in the sensor. Regardless of the improvements that can be achieved in the rest of the factors, the total noise in the sensor, as commonly indicated by the SNR, sets a constraint on the minimum error that would be invariably present in the retrieved biophysical product. A high SNR is essential for the ability to detect fine spectral features of low magnitude, as would be required to discriminate among PFTs, or estimate the absorption coefficient of phytoplankton. Fisher (1985) has shown that the number of independent quantities retrieved from remote sensing reflectance would significantly decrease when the noise increases. Moreover, spectral inversion techniques that rely on accurate absolute reflectance require high SNR.

The projected SNR of HyspIRI (Gao, 2010) is better than that of Hyperion (Hu *et al*., 2012a), comparable to that of HICO (Moses *et al*., 2012b; Lucke *et al*., 2011), and is considered reasonably adequate for accurately retrieving hyperspectral reflectance from

the water surface, and consequently, the aquatic biophysical parameters described here. Finally, hyperspectral algorithms will require a large *in situ* dataset for development and validation activities, such as the SeaWiFS Bio-optical Archive and Storage System (SeaBASS) and the NASA bio-Optical Marine Algorithm Dataset (NOMAD) (Werdell *et al*., 2002, 2005). The aggregation of such a dataset would require tremendous effort from the ocean color/hyperspectral community, especially in coastal areas, which are known to be under-documented even for multispectral applications. In addition, to derive PFTs, a library of pigments and spectra of specific IOPs will be required to validate the existing algorithms (e.g., to provide endmembers for unmixing the absorption spectra), and explore potential candidates for identification. An effort is underway to collect data from the community, and develop a spectral library to support the HyspIRI mission. However, further plans to expand this effort will need to be put in place within the next few years to assure that sufficient specific absorption spectra are collected and processed for use with algorithms, perhaps in preparation for a broader HyspIRI validation program.

Mission Relevance

Currently, there are no civilian spaceborne hyperspectral instruments designed to provide continuous, regular global coverage of coastal and inland waters at high spatial and spectral resolution. However, the upcoming HyspIRI mission will offer these capabilities. In this section, we have provided a brief summary of the characteristics of HyspIRI, and discussed the valuable benefits from the use of HyspIRI for retrieving biophysical parameters of the coastal water column. HyspIRI data can be used to develop new techniques or improve existing techniques to retrieve aquatic data products at a level of spatial and spectral detail and accuracy that is not achievable with multispectral data. The increased spectral resolution in the visible region will allow for more accurate retrievals for water quality assessment using data products, such as the diffuse attenuation coefficient (an indicator of turbidity), chl-*a* concentration (an indicator of eutrophication), primary production (an indicator of the functions of an ecosystem), backscattering coefficient and TSM concentration (indicators of the nature and size distribution of particles and sediment transport), and PFTs (indicators of harmful algal blooms and the state of the ecosystem). HyspIRI's hyperspectral data with high SNR would be well suited for sophisticated retrieval algorithms, such as those based on spectral inversion, spectral derivatives, ANN, Look-Up Tables (LUT), and the Levenberg-Marquardt non-linear least squares minimization method, which can be used to retrieve multiple biophysical parameters of the water column simultaneously.

As the increased complexity of the ecosystem is resolved, the HyspIRI mission will provide highly resolved spatial measurements of the Carbon Cycle as it relates to seasonal, annual and decadal time scales. A few studies have already illustrated the use of spaceborne hyperspectral data for studying the coastal aquatic environment. Hyperion initially showed potential for coastal aquatic studies (Nikolakopoulos, 2006). However, problems due to the radiometric instability of the sensor and low SNR have made Hyperion unreliable for accurate, quantitative analysis of aquatic ecosystems (NRC, 2007). HICO has been shown to provide accurate estimates of the concentrations of optically active components in coastal waters (Gitelson *et al*., 2011; Braga *et al*., 2013; Moses *et al*., 2014). HICO is a demonstration mission on the International Space Station (ISS), with on-demand image acquisition. The orbital constraints on the ISS platform

prevent HICO from providing either regular or global coverage. Except for HICO, there is no spaceborne hyperspectral sensor designed specifically for coastal waters currently in operation or scheduled to be launched in the near future. With an SNR that is comparable to that of HICO's, HyspIRI's regular high-resolution snapshots can be used for seasonal monitoring of global coastal waters.

2.5 Bathymetry

Science Questions Addressed

Bathymetry derived from HyspIRI data will help answer the following science questions:

VQ4. How are disturbance regimes changing and how do these changes affect the ecosystem processes that support life on Earth?

CQ1. How do inland, coastal, and open ocean aquatic ecosystems change due to local and regional thermal climate, land-use change, and other factors?

Candidate Product or Application

Knowledge of ocean bathymetry is important for both scientific studies, as well as management plannings. Because of the enormously large area of the global oceans and limited coverage provided by ship surveys, bathymetric data in fine detail are still lacking for many parts of the oceans. One approach to fill this data void is through the measurement of water color, and then derive the depth of sea bottom through analyzing the spectral shape of this water color, a scheme that was pioneered by Polcyn *et al*., about 40 years ago (Polcyn *et al*., 1970). Basically, it takes advantage of the fact that photons hitting the shallow sea bottom and reflecting back to the surface modify the appearance of ocean color. To reliably retrieve bottom properties from this spectral analysis requires adequate signal from the bottom, or the water column has to be optically shallow. In other words, the water needs to be transparent enough and the sea bottom cannot be too deep. However, because both water and bottom properties vary spatially, retrieval of bottom depth from the analysis of this spectrum is not straightforward.

Methods

Earlier methods to estimate bathymetry from ocean color were limited to approaches (Polcyn *et al*., 1970; Lyzenga, 1981; Philpot, 1989) that require a few known depths to develop an empirical relationship, which then allows researchers to convert multiband color images to a bathymetric map. The resulting empirical relationship are generally sensor and site specific (Dierssen *et al*., 2003; Stumpf *et al*., 2003) and not transferable to other images or areas. Further, the approach is not applicable for regions difficult to reach, due to lack of *in situ* calibration data.

To overcome such a limitation, physics-based approaches have been developed in the past decade (Lee *et al*., 1999; Klonowski *et al*., 2007; Brando *et al*., 2009; Dekker *et al*., 2011). Basically, a model based on radiative transfer theory is developed to analytically describe the spectral variation of shallow-water color, normally measured by its remote-sensing reflectance (R_{rs}, sr^{-1}), the ratio of water-leaving radiance to downwelling irradiance incident on the sea surface. Unlike the empirical approaches

focusing on the retrieval of depth from water color (Lyzenga, 1981; Philpot, 1989; Dierssen *et al*., 2003; Stumpf *et al*., 2003), such analytical approaches retrieve both water and bottom properties simultaneously. The following is a brief summary of such an analytical inversion system.

For optically shallow waters, R_{rs} not only depends on the absorption and scattering properties of dissolved and suspended materials in the water column, but also on the depth and reflectivity of the bottom. R_{rs} is also influenced by contributions from inelastic scattering, such as fluorescence and Raman emission (Marshall and Smith, 1990; Lee *et al*., 1998), but they are generally negligible for optically shallow waters. The spectral R_{rs} can be conceptually summarized as

$$R_{rs}(\lambda) = f[a(\lambda), b_b(\lambda), \rho(\lambda), H], \quad (6)$$

where $a(\lambda)$ is the absorption coefficient, $b_b(\lambda)$ is the backscattering coefficient, $\rho(\lambda)$ is the benthic spectral reflectance, and H is the bottom depth. Explicit description or approximation of R_{rs} was further developed through numerical simulations (Lee *et al*., 1998; Albert and Mobley, 2003).

Equation 6 can be applied to $R_{rs}(\lambda)$ measured by a sensor with n spectral bands, creating n equations, with H being constant with λ. The other four variables, however, are wavelength dependent, thus the variable H cannot not be generally analytically determined. In order to retrieve H from R_{rs} with confidence, spectral models regarding the optical properties and bottom reflectivity have to be established.

Lee *et al*., (1999) reduced the three spectra ($a(\lambda)$, $b_b(\lambda)$, and $\rho(\lambda)$) to four scalar variables through bio-optically modeling and by employing two contrast bottom classes (grass and sand), and the solution is achieved by minimizing the difference between the modeled and measured R_{rs} spectra, or the so-called spectral optimization or minimization. This scheme was modified recently by Adler-Golden *et al*., (2003), with constant water optical properties within a scene, three substratum types for coral reef environments (Goodman and Ustin, 2007; Klonowski *et al*., 2007) and determination of optical and bottom spectral shapes in the solution phase (Brando *et al*., 2012).

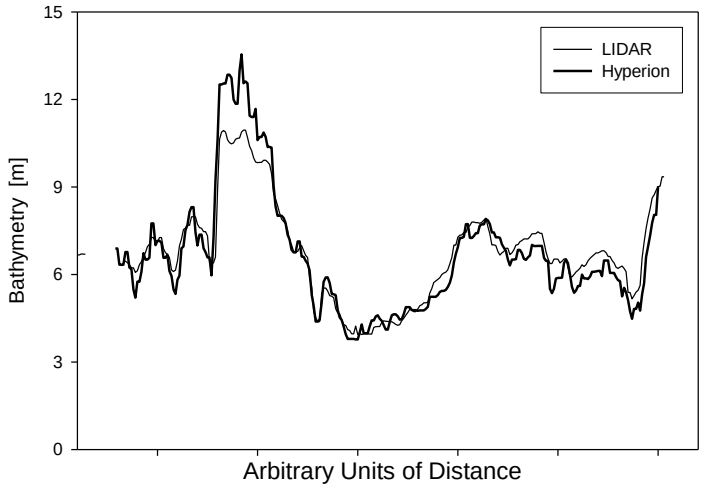

Figure 2.5.1 – Comparison of Bathymetry from Satellite Hyperspectral Data and Airborne LIDAR (from Lee *et al*., 2007b).

An approach that is in principle the same as the above is the look-up-table scheme (Mobley *et al*., 2005), where a library of spectra corresponding to different combinations of depth, bottom type and water properties was developed (Mobley *et al*., 2005; Louchard *et al*., 2003; Lesser and Mobley, 2007), and solutions were achieved by finding the R_{rs} spectrum that best matches the measured R_{rs} spectrum.

Figure 2.5.1 demonstrates that using hyperspectral data from the Hyperion instrument, bathymetric measurements can be made that are comparable to relatively accurate airborne LIDAR data. HyspIRI is expected to have better radiometric calibration and SNR compared to Hyperion and improved results are expected.

2.6 Benthic Cover Classification and Mapping

Submerged aquatic habitats present a particularly challenging environment for remote sensing, owing in large part to the confounding effects of the overlying water column and water surface. In this situation, it is the benthic surface (e.g., the substrate type and habitat composition) that is the primary subject of interest, and any analysis of water properties and bathymetry, as discussed previously, is instead shifted into a supporting role. The challenge, and thereby the objective, of this analysis is thus to differentiate the contributions of the benthos, water column and air-water interface in order to ultimately resolve habitat and substrate characteristics. Given the complexity of light interactions in this environment, even in tropical locations with exceptionally clear water, it has been shown that imaging spectroscopy is more robust, and provides greater accuracy than what can typically be achieved using traditional multispectral sensors (Botha *et al*., 2013). With that in mind, we discuss the relevant application areas and associated capabilities that HyspIRI addresses, with respect to the field of benthic cover classification and mapping. Discussion is apportioned into two main categories, biotic and abiotic, followed by a summary of the relevant limitations and applications.

Amongst the various submerged biotic habitat types, coral reefs have received the most attention from the remote sensing community, and as discussed below, there is significant ecological importance and sound physical reasoning for this attention. However, this is not the only habitat type where large-scale assessment and monitoring efforts benefit from imaging spectroscopy capabilities. Other relevant habitats include submerged aquatic vegetation, mollusk beds and benthic algae, which each also have their own unique environmental, economic and societal importance.

Science Questions Addressed

HyspIRI data can be used to detect and delineate a variety of benthic cover classes, which will help answer the following science questions.

VQ1. What is the global spatial pattern of ecosystem and diversity distributions and how do ecosystems differ in their composition or biodiversity?

VQ3. How are the biogeochemical cycles that sustain life on Earth being altered/disrupted by natural and human-induced environmental change? How do these

changes affect the composition and health of ecosystems and what are the feedbacks with other components of the Earth system?

VQ6. What are the land surface soil/rock, snow/ice and shallow-water benthic compositions?

CQ1. How do inland, coastal, and open ocean aquatic ecosystems change due to local and regional thermal climate, land-use change, and other factors?

Candidate Products or Applications – biotic cover maps

Coral Reefs

Coral reefs are complex marine ecosystems distributed throughout the world's tropical ocean in territorial waters of more than 100 countries (Salvat, 1992). Reefs directly occupy an estimated area of 250,000–600,000 km^2 (Smith, 1978; Kleypas, 1997; Spalding and Grenfell, 1997). These values correspond approximately to 0.05–0.15% of the global ocean area, respectively, and about 5–15% of the shallow sea areas within 0–30 m depth. Differences between areal estimates reflect the use of different estimation methodologies, as well as variations in reef definition (Buddemeier and Smith, 1999).

Coral reefs have existed over millennia as geologic features, but their construction is biogenic, composed of the skeletons of hermatypic (reef-building) organisms (Achituv and Dubinsky, 1990). The most conspicuous organisms in reef formation are scleractinian corals, which have high calcification rates, and produce most of the calcium carbonate (aragonite) that makes up the reef framework. Other important reef calcifiers are various calcareous algae: crustose red coralline algae cement the softer, more porous coral skeletons, creating a more wave-resistant structure, and the calcareous green alga, *Halimeda*, can account for large fractions (up to 80%) of reef sand deposits (Berner 1990). The association of these organisms produces a living structure that grows and maintains itself near sea level.

Because coral and algae are responsible for reef construction and maintenance, their environmental limits determine the distribution of reefs (Kleypas *et al*., 1999). The abiotic parameters most affecting the distributions of coral and algae are temperature, light, salinity, nutrients, carbonate saturation state and water motion (Smith and Buddemeier, 1992), while the most important biotic parameter is grazing (Berner 1990). The specific influences of these parameters on reef-building organisms are interconnected and complex, and they are a major focus of ongoing reef research.

Major coral reef ecosystem processes include those linking the physical environment to the reef community (Hatcher, 1997). Reefs are noted for their high rates of ecosystem gross primary production and respiration (Odum and Odum, 1955; Kinsey, 1985). At the ecosystem spatial scale and at seasonal time scales, respiration generally equals production so that ecosystem net production is near zero (Kinsey, 1983; Kinsey, 1985). The same is not necessarily true for shorter time periods (days to weeks), smaller sub-reef areas, or even some entire reef systems (Falter *et al*., 2001; Falter *et al*., 2011).

In addition to the reef-building organisms, coral reefs host a diversity of life that rivals that of tropical rain forests, with the number of species potentially reaching the millions (Small *et al*., 1998; Bellwood and Hughes, 2001). This biodiversity and the general abundance of life on reefs, provide a vital resource for human populations around the world, supporting, among other activities, artisanal, commercial and sport fisheries and ecotourism (Moberg and Folke, 1999). It has been estimated that direct and indirect use of reefs contributes more than US$1 billion annually to the economy of the Philippines (White *et al*., 2000), and nearly US$7 billion USD annually to the economy of four southeastern Florida counties (Johns *et al*., 2001). While the accuracies of these dollar amounts are debatable, it is certain that coral reefs and their biodiversity are important to the cultural and economic lives of millions of people around the world.

It is incontrovertibly clear that many reefs are in various stages of decline, often attributed to local and regional anthropogenic factors. Hundreds (if not thousands) of research papers have documented human impacts to reefs at the local scale. These are well summarized in several review papers and volumes (e.g., Salvat, 1992; Smith and Buddemeier, 1992; Ginsburg, 1994; Connell, 1997; Carpenter *et al*. 2008). Local and regional human impacts include, but are certainly not limited to, destructive fishing practices, mining calcium carbonate, anchor damage, oil spills and land-use practices leading to terrestrial sediment deposition, with subsequent resuspension that decreases water transparency vital for reef photosynthesis. [Contrary to popular belief, human-sourced nutrient loading is not a major impact on coral reefs. See Szmant (2002) and Atkinson (2011).] The common result of all these impacts has been an ecological shift from coral- to algal-dominated reef benthic community structures. Accompanying this shift has been a similar decline in diversity of reef flora and fauna (Pandolfi *et al*., 2003; Jones *et al*., 2004).

Already stressed by human activities at local and regional scales, reef ecosystems are under increased threat by global climate change (Smith and Buddemeier, 1992; Hoegh-Guldberg *et al*., 2007; IPCC, 2007). The convolved influences of rising sea surface temperature and increasing ocean acidification are predicted to imminently cause a global shift in reef benthic community structure from coral-rich to coral-poor, with an accompanying loss of ecosystem services and economic value. However, current assessments of global reef conditions are based on simple extrapolation from the very sparse available data (e.g., Wilkinson, 2008) gathered using traditional methods: quadrats, transects, or semi-quantitative towed-diver surveys. Remote sensing is the only approach that can provide a truly synoptic evaluation of reef health.

The main indicators of reef health are benthic cover, productivity and calcification. Only very broad trends are known regarding the spatial distributions of these parameters. Reef geomorphology is a function of antecedent topography and physical forcings (e.g., waves, currents, light), and different geomorphic zones often exhibit characteristic biological communities (Stoddart, 1969). Natural, balanced coral reefs are mosaics of coral, algae and sand. When corals die, their skeletons are invaded by fleshy algae and boring organisms. Healthy reefs usually increase coral coverage during recovery from disturbance, with corals often returning to the pre-disturbance level

(Connell, 1997). On degraded reefs, there is little or no recovery of corals. With the loss of reef-builders, the carbonate structure erodes, ultimately becoming a flat bottom with shifting rubble and sand.

In short, reef "health" is reducible to the quantitative measure of the distribution of coral, algae and sand (i.e., benthic cover). The amounts and spatial arrangements of these benthic types are important for understanding coral reef processes, which in turn are fundamental to coral reef health. Satellite spectral imaging is perfectly suited to the task of mapping coral reef bottom-types.

Productivity and calcification also follow geomorphology, with maximal rates generally occurring in zones of high wave and current energy (Kinsey, 1983). The few observations are considerably uniform across latitudes, leading to the hypothesis of "standard" performance: reef patches with 100% coverage of 100% of a given benthic type exhibit modal rates of productivity and calcification, regardless of location around the world (Kinsey, 1983; Kinsey, 1985). This fortuitous relationship has been the basis for a few case studies that utilize remote sensing to map benthic cover, then apply the modal rates to extrapolate to the ecosystem scale (Atkinson and Grigg, 1984; Andréfouët and Payri, 2001; Brock *et al*., 2006; Moses *et al*., 2009).

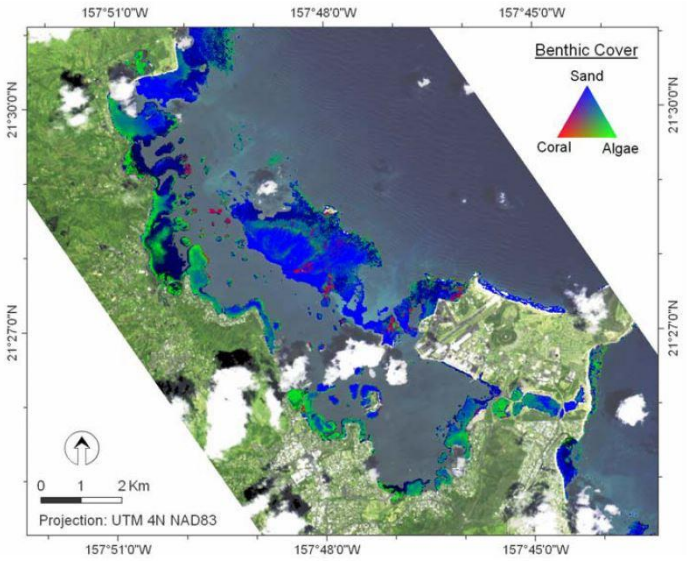

Figure 2.6.1 – Spectral unmixing example of Kaneohe Bay, Hawaii using AVIRIS (16 m spatial resolution), illustrating sub-pixel composition of sand, coral and algae (Goodman and Ustin, 2007).

Kuchler *et al*., (1988); Green *et al*., (1996); Mumby *et al*., (2004); Andréfouët *et al*., (2005); Hochberg (2011); and, Goodman *et al*., (2013) provide good comprehensive reviews of the history of coral reef remote sensing. The following is a very brief overview: From the 1970s through the1990s, imagery from high-resolution (30 - 80 m) multispectral sensors, including the Landsat Multispectral Scanner (MSS), Thematic Mapper (TM), Enhanced Thematic Mapper Plus (ETM+); the SPOT High Resolution Visible (HRV); and the Terra Advanced Spaceborne Thermal Emission and Reflect-ion Radiometer (ASTER), was used to effectively map reef geomorphology. Because different geomorphologic zones are associated with characteristic benthic communities, some investigations extrapolated map themes to depict biotope type. The advent of high-resolution airborne spectral imaging (e.g., AVIRIS, HyMap, CASI) in the 1990s led to direct mapping of reef biological communities. This was further demonstrated by space-borne spectral imagers (e.g., EO-1

Hyperion, HICO). In the early 2000s, very-high-resolution multispectral imagery (e.g., IKONOS®, Quickbird®) became widely available to the public, and this sparked a wider interest among coral reef researchers into using remote sensing products in their studies. Through the history of coral reef remote sensing, the only attempt at developing a consistent, global product has been the Millennium Coral Reef Mapping Project, which used Landsat-TM and -ETM+ imagery as basemaps for manual digitization of reef geomorphology (IMaRS-USF and IRD, 2005; IMaRS-USF, 2005; UNEP-WCMC, WorldFish Centre, WRI and TNC, 2010).

HyspIRI's spatial and spectral resolutions afford the potential to develop the first global map of benthic community structure and thus reef health, showing the distributions of coral, algae and sand for the reefs of the world. As a spectral imager, HyspIRI has the spectral resolution to discriminate between these three fundamental bottom-types with very high accuracy (Hochberg and Atkinson, 2003). It has also been shown that higher spectral resolution equates to improved capacity for classifying coral reefs to increased water depths (Botha *et al*., 2013). With a ground sample distance of 60 m, HyspIRI pixels would not have the ability to spatially resolve homogeneous patches of the bottom-types. But, this is not a strict requirement, as spectral unmixing provides a mechanism to identify sub-pixel composition (e.g., Figure 2.6.1; Goodman and Ustin, 2007). Certainly, HyspIRI is capable of spatially delineating reef geomorphology.

Benthic community structure products can form the basis for higher-level derived products, namely primary productivity and calcification using modal rates. An alternative approach would be to use HyspIRI imagery to model light absorption and light-use efficiency of the benthos (Hochberg and Atkinson, 2008), as is routinely done in terrestrial remote sensing studies (e.g., Running *et al*., 2004). Important ancillary products include water depth and water optical properties.

Kelp

Giant kelp (*Macrocystis pyrifera)* forests are among the most productive systems on earth, and provide food and habitat for a diverse assemblage of ecologically and economically important species, including algae, invertebrates, fish and marine mammals whose consumptive and non-consumptive uses produce at least $250 million in revenue per year (Dayton and Tegner, 1984; Mann, 2000; Leet *et al.,* 2001). The high growth rate of giant kelp is coupled with a relatively short lifespan, leading to standing biomass turnover six to seven times per year (Reed *et al*., 2008) and thus necessitating high demands for nutrients such as carbon and nitrogen. Nutrient delivery to giant kelp forests changes in mechanism and magnitude throughout the year, with upwelling processes, internal waves, terrestrial storm runoff and biological regeneration all being important nitrogen inputs (McPhee-Shaw *et al*., 2007; Hepburn and Hurd, 2005).

Factors such as grazing, anthropogenic impacts and wave action contribute greatly to biomass reduction (Reed *et al*., 2011). El Niño events cause a decrease in upwelling, which leads to warmer sea surface temperatures, low nutrient concentrations and increased storm and wave activity, which greatly reduces giant kelp density and declines in kelp forest associated fishes (McGowan *et al*., 1998). Kelp responds quickly to changes in environmental conditions, and so the physiological condition of giant kelp

displays great seasonal and inter-annual variability, such as extremely high growth rates (up to 0.5 m d^{-1}) during optimal conditions, surface frond deterioration during periods of low nitrate availability and regional crashes associated with changes in the Pacific Decadal Oscillation (Zimmerman and Kremer, 1984).

Recent work by Cavanaugh *et al*., (2011) has established the method of using multispectral remotely sensed images from the Landsat TM sensor to estimate giant kelp biomass. This work has led to a superb time series of kelp biomass in the Santa Barbara Channel at a spatial and temporal resolution that would be impossible using field observation alone, and provided information for numerous studies on subjects such as net primary production, food webs and population synchrony (Reed *et al*., 2011; Byrnes *et al*., 2011; Cavanaugh *et al*., 2013). This work is continuing along the California and Baja California Peninsula using the Landsat ETM+ sensor and will soon incorporate the recently launched Landsat Operational Land Imager (OLI).

Currently, work is under way to better understand the relationship between giant kelp reflectance and various growth and productivity metrics. A time series of laboratory measured spectral properties of surface blades from kelp forests along the California coast is being related to photosynthetic pigment and tissue elemental concentrations and ratios. The temporal variation of kelp reflectance in these forests will be related to growth and productivity measures to ultimately establish reflectance indices for "photosynthetic condition." These indices will be adjusted for hyperspectral data from AVIRIS, which is currently imaging kelp forests 3x $year^{-1}$ in the Santa Barbara Channel through the HyspIRI Preparatory Airborne Campaign.

HyspIRI can provide products that not only show the spatial distributions of giant kelp forests through time, but also provide information on the changes of pigment concentrations and ratios as light and nutrient levels change. As stated above, giant kelp exists in areas of coastal upwelling, which vary seasonally and interannually, leading to nutrient levels that differ by greater than an order of magnitude. Once appropriate reflectance indices for pigments and other photosynthetic metrics are established, HyspIRI will be able track the changes of these measures over large spatial scales for this important foundational species.

Submerged Aquatic Vegetation

Seagrasses cover extensive coastal areas and are widely distributed, from the temperate northern to the temperate southern oceans, including all the tropical coasts in the world (Short *et al*., 2007). Although there are few species of seagrasses (about 60 species), the geographic distribution of a single species can cover thousands of kilometers (Short *et al*., 2007).

Seagrass classification and maps have been successfully retrieved from hyperspectral aerial imagery and multispectral satellite data (e.g. Andréfouët *et al*., 2004; Phinn *et al*., 2008) making use of differences in reflectance associated with seagrass species and their biomass. Hyperspectral information, such as the proposed by the HyspIRI mission, will enhance the seagrass habitat detection and mapping (Figure 2.6.2).

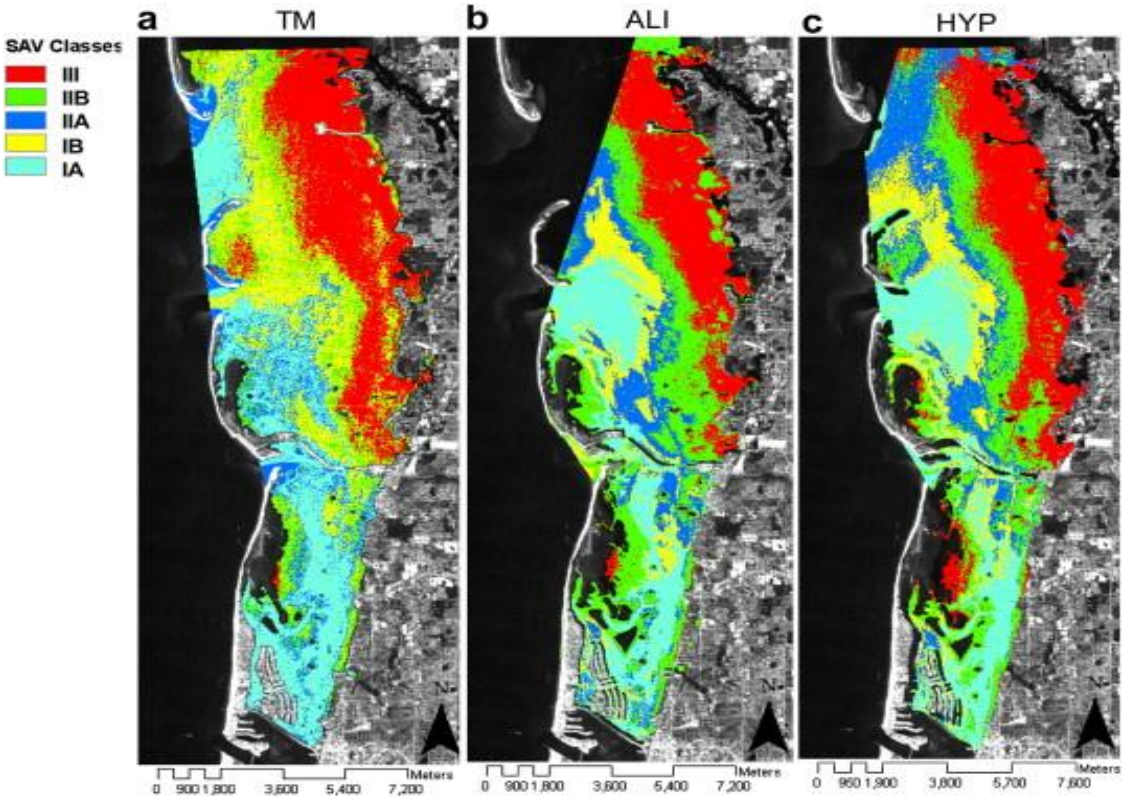

Figure 2.6.2 – Comparison of Submerged Aquatic Vegetation (SAV) mapping in Pinellas County, FL using three different sensor systems: Landsat TM and EO-1 Advanced Land Imager (ALI) and Hyperion. Results indicated highest accuracy was achieved using Hyperion. SAV classes depict percent habitat cover: III ≥75%, IIB 50–74%, IIA 25–49%, IB 1–24%, and IA <1%. (Pu *et al*., 2012)

Candidate Products or Applications – abiotic cover maps

The detection of changes in the distribution of abiotic material, as well as variations in water properties, can have profound implications for the condition and health of submerged habitats. These relationships contribute biological and ecological significance to the assessment of non-living benthic components (such as sand and sediment), and also dictate a level of synergy between benthic habitat analysis and many other aquatic applications, particularly those associated with water-column retrievals and sea surface temperature. As a result, the capabilities HyspIRI provides for assessing benthic composition, and the capabilities it offers for deriving various water properties, both contribute to understanding the environment that surrounds benthic habitats.

Sand and Sediment

The ability to differentiate biotic from abiotic benthic components, such as distinguishing sand from coral and algae, is relatively straightforward when the spatial resolution of the imaging sensor is less than or equal to the scale of habitat distribution. However, when the spatial resolution of the imaging sensor is greater than that of the scale at which habitat components vary, differentiating these components benefits

significantly from the use of spectral unmixing techniques. For example, whereas sand is easily distinguished from seagrass due to substantial differences in their relative magnitudes of reflectance, without the necessary spectral information and ability to use unmixing, image classification is hindered along habitat margins and areas of substantial heterogeneity (e.g., areas of mixed sand and seagrass). This becomes particularly relevant at the spatial resolution of HyspIRI, where unmixing plays a pivotal role in assessing sub-pixel habitat composition. The significance this has to submerged aquatic habitats is that it contributes to our ability to establish baselines and assess changes in sand and sediment distribution that in turn can be used to evaluate habitat loss after storm events or other disturbances.

Water-Column and Benthic Habitats

As discussed in previous sections, there are a number of applications and products related to water-column retrievals, such as optical properties and water constituents, which can be derived from HyspIRI imagery. When these capabilities are extended to also include associated environmental stressors and climatic events, such as algal blooms, terrestrial runoff and sediment resuspension, certain situations and particular conditions can also be indicative of impacts to benthic habitats.

Water Surface Temperature

Remote sensing of water surface temperature, particularly as it relates to coral health and coral bleaching, is an established field, with a strong scientific foundation and a robust lineage of operational products. For example, consider some of the many tools offered through NOAA's Coral Reef Watch program, such as the HotSpot, Degree Heating Week and Bleaching Alert products. While effective for regional and global assessments, such analyses are produced at scales measured in kilometers (Figure 2.6.3), and thus do not resolve spatial details within close proximity to most reefs. The 60 m resolution TIR imagery to be obtained for shallow aquatic habitats by the HyspIRI program will provide valuable insight into localized spatial dynamics of sea surface temperature. This, in turn, provides a foundation for investigating reef-scale biological and ecological relationships associated with coral bleaching, as well as studying coral adaptation to changing environmental conditions.

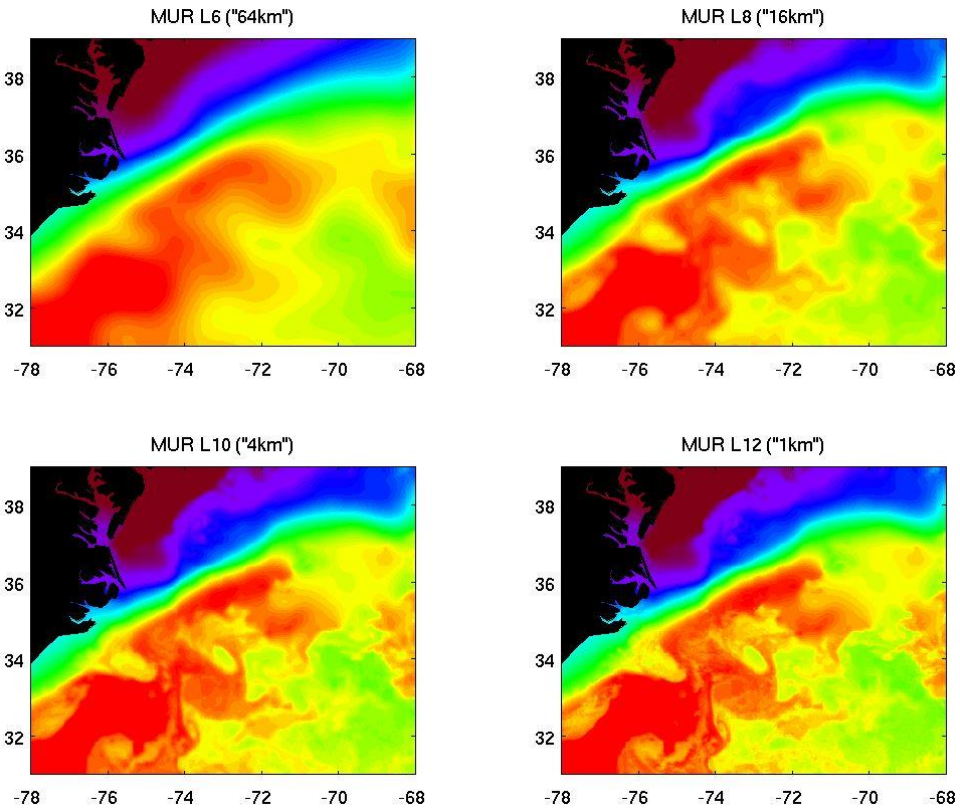

Figure 2.6.3 – Comparison of different spatial resolution output from the Multi-scale Ultra-high Resolution (MUR) SST analysis, with increasing detail evident at higher resolutions (courtesy Physical Oceanography Distributed Active Archive Center, JPL). HyspIRI will provide even higher resolution (60 m), and hence greater detail, for shallow water areas, and similar resolution (1 km) for the global oceans.

3. Discussion

The previous sections develop a conceptual list of data products for the HyspIRI mission to support aquatic remote sensing of coastal and inland waters. These data products were based on mission capabilities, characteristics and expected performance. The topic of coastal and inland water remote sensing is very broad. Thus, this report focuses on aquatic data products to help keep the scope of this document manageable. The HyspIRI mission requirements already include the global production of surface reflectance and temperature. Atmospheric correction and surface temperature algorithms, which are critical to aquatic remote sensing, are covered in other mission documents. Hence, these algorithms and their products were not evaluated in this report. In addition, terrestrial products (e.g., land use/land cover, dune vegetation, beach replenishment) were not considered. It is recognized that coastal studies are inherently interdisciplinary across aquatic and terrestrial disciplines, but products supporting the latter are expected to already be evaluated by other components of the mission. The coastal and inland water data products that were identified by the HASG covered six major environmental and ecological areas for scientific research and applications, including remote sensing of wetlands, shoreline processes, the water surface, the water column, bathymetry and benthic cover types. Accordingly, each product was evaluated for feasibility, given the HyspIRI mission characteristics, and whether it was unique and relevant to the HyspIRI science objectives.

For each of the six major environmental and ecological areas of aquatic data products, several key example data products have been identified (see Table 3.1). These were assigned priority ranking based on three major factors. The first was the uniqueness to the HyspIRI mission, specifically, the global hyperspectral VSWIR spectrometer or TIR band measurements that it will produce. In certain cases, products could be identified as not being easily generated on global scales via any other orbiting remote sensing asset planned by the US government. Second, the urgency for such data products in the support of scientific research and application was weighed. In particular, the involved assessing how well products contribute to the HyspIRI science questions or were tied to objectives identifiend by the 2007 Decadal Survey. In addition, the importance or urgency to science research and applications was also considered, even if not clearly defined by the mission science questions or Decadal Survey. Finally, the feasibility or ease of implementation, and the chances that accurate results would be obtained was considered. Combining these three criteria, a subjective priority was assigned to key candidate products and applications.

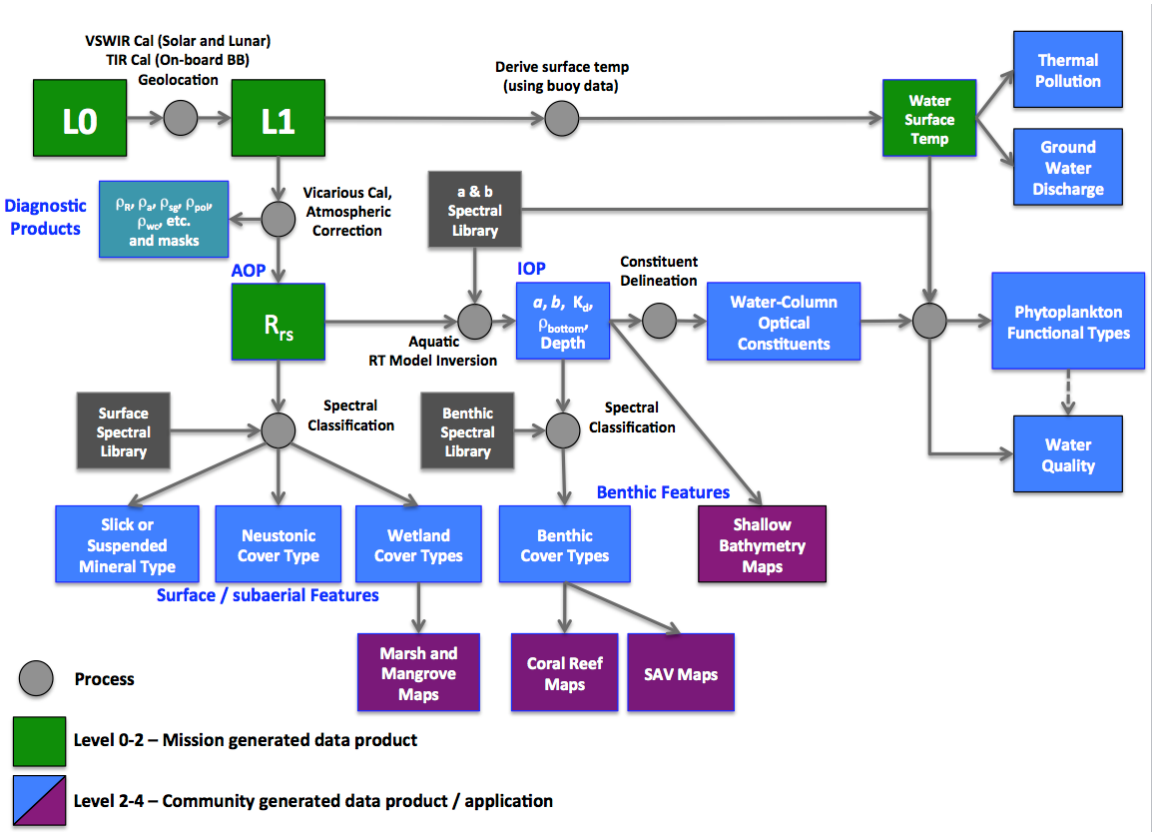

Figure 3.1 – Diagram of Candidate Aquatic Data Product Generation. Raw and calibrated data products (Level-0 and Level-1, respectively, depicted with light gray boxes) are inputs to Level-2 algorithms. Resulting Level-2 products are generated by the mission (green boxes). Various Level-2 satellite swath products (blue), and Level-3 or Level-4 maps products (purple), are subsequently generated by the community.

1. Wetlands — In general, wetland remote sensing represents one of the strongest areas amongst identified data products. This is largely because of a generally higher signal-to-noise available to generate these products more accurately, especially at longer wavelengths. The most important of these products are the delineation of wetlands from other terrestrial and aquatic surface cover types. High spatial, hyperspectral data from HyspIRI is expected to be uniquely useful for the creation of new baseline global maps of wetland distribution. Hyperspectral data may also provide information that can discriminate between different types of wetlands (e.g., saltmarshes, mangroves). Determining species composition would also be extremely useful, but classification schemes at this level have not been demonstrated on a global scale. As coastal marshes tend to form monospecific canopies that zonate in response to changes in the stress gradient (e.g., changes in drainage or salinity), mapping the location of individual species could provide important information regarding the marsh characteristics, and the HyspIRI mission could lay the groundwork for understanding how those characteristics are changing globally. Identification of canopies at the species level using field data has been done successfully. However, applying hyperspectral techniques to aerial data and multispectral satellite data has had mixed results. Although it is hoped that HyspIRI

hyperspectral capability could demonstrate coastal wetland species discrimination, we currently consider this vital and unique product to be experimental at the global scale.

Determining the fraction of vegetation cover or the fraction of open water within a pixel, are physical measurements that directly describe the physical condition of the surface. These fractions can theoretically be derived using spectral unmixing algorithms, which would be ideally supported by the HyspIRI spectrometer. Assessing, and where possible, minimizing their uncertainty is an additional challenge, which would require some error analysis and ground validation. Because HyspIRI currently does not have a validation program, these (and other) physical measurements are recommended being given a slightly lower priority. However, because a relatively coarse 60-meter spatial resolution is needed to globally map wetlands, it is important to recover some structural information that would better inform the user of conditions in the wetland.

Other complementary, multi-band wetland products were also considered for the HyspIRI mission. Although these additional products are not unique to the HyspIRI mission, they are still compelling because they could be used contemporaneously with other HyspIRI data products in research studies. For instance, as an early study, the results of a new hyperspectral algorithm to estimate a particular vegetation parameter could be compared to quantities inferred from a multi-band index (e.g., Vegetation Indices (VI) or NDWI, which are based on very feasible multi-band algorithms). Given that hyperspectral bands could be combined to further reduce noise, HyspIRI could very likely provide very good quality data for such indices. Similarly, thermal bands can be combined with VSWIR spectroscopy to obtain canopy temperature and soil moisture, which could perhaps feed into energy budget, evapotranspiration and hydrological models. These measurements would complement contemporaneous wetland delineation data products, which are more uniquely tied the HyspIRI mission capabilities.

2. Coastline and Ice Margins — Most data products related to land/water geomorphology are not uniquely or particularly well supported by the HyspIRI instrument. Under typical conditions, multi-band algorithms could delineate land and water to identify shorelines. In addition, this would probably be better accomplished using an instrument with higher spatial resolution, such as Landsat 8 or 9. However, for some shallow water or turbid conditions, the hyperspectral data might be necessary to better discriminate emergent from submerged landscape. In such cases, HyspIRI could become a superior tool to multi-band instruments for mapping coastlines (e.g., after a severe storm disturbance). Combining this with the thermal band could further enhance the discrimination. In addition, using contemporaneous thermal imagery with VSWIR spectroscopy over coastal waters could identify diffuse sources of nutrient loading (e.g., from ground water discharge) and the biological response in the affected waters. This unique capability of HyspIRI could shed new light regarding how nutrients from diffuse sources are delivered to coastal and inland waters, a process that is currently not well understood. Similarly, the combination of VSWIR and thermal measurements could be used to observe changes in polar water conditions along the ice edge, which is strongly affected by climate change. However, separating the VSWIR spectrometer and thermal

band instrument onto separate orbiting platforms, as has been suggested, would degrade the quality of this compelling observational opportunity.

3. Water Surface Features — HyspIRI can provide useful information regarding materials, biotic and abiotic, that are floating on the water surface. The primary products would be material identification, coverage density and mass estimates for various types of surface cover, as discussed in Section 2.2. Water surface features tend to be transient in nature, being subject to currents and wind conditions. Therefore, observations will be somewhat limited by the temporal measurement frequency of HyspIRI. However, the hyperspectral data can serendipitously be used to identify the composition of floating material when observed by the VSWIR spectrometer. Imaging the spatial distribution of floating material could provide some insight into the original, and some aspects of small-scale dynamics of these surface formations. Likewise, the availability of hyperspectral data could support spectral unmixing algorithms, which could provide further information regarding the nature of the surface features. Understanding how biotic materials on the surface (e.g., trichodesmium mats) affect the spectral signal at coarser spatial resolutions could also benefit understanding of data from traditional ocean color instruments at coarser resolutions. How well hyperspectral algorithms can identify and quantify surface features will likely to depend on the ability to detect a signal from the material observed. Some materials, such as masses of floating plastics, may be problematic, while other surface materials may be more readily measured. Therefore, some priority can be assigned to certain types of surface materials. In addition, observating the effects of disasters, such as oil spills or the debris following a tsunami, can be given increased priority in real-time acquisitions. The mission Level-1 requirements provide for steering the VSWIR instrument to take repeated looks only a few days apart. However, such observations are expected to be rare, and likely will not include slicks of algal or microbial mats, unless the event is particularly significant and presents a danger to coastal residents or economy.

4. Water Column — Retrieval of optical constituents in the water column is perhaps the most challenging measurement for the HyspIRI mission. This is because of the relatively weak signal from such substances and the dynamic nature of water conditions. However, the HyspIRI VSWIR spectrometer, if sufficiently calibrated, has a signal-to-noise ratio similar to HICO, and is expected to be able to retrieve the typically higher concentrations of phytoplankton pigments, and optically active dissolved and suspended material in coastal and inland waters. The temporal resolution of HyspIRI would limit what dynamics can be observed, but spatial distributions of river plumes and algal blooms can still provide information on underlying dynamic processes. Identification of pigments could tag certain spectral functional types of phytoplankton for algal blooms that are observed. As these features are transient, HyspIRI can only support mapping of the most persistent of patterns for Level-3 or 4 data products. Nonetheless, the data could still be useful to coastal and inland communities when available, providing episodic information regarding events such as harmful algal blooms or degradation of inland water quality. In fact, only one or two images per season should be sufficient to indicate general water quality for many small and medium-sized lakes for water resource

managers. Also, having some idea of what is in the water column could help acquire information regarding the benthic community beneath.

The key products for the water column would be generated in a hierarchical fashion. Hyperspectral surface reflectance, R_{rs}, and water surface temperature are the Level-2 products generated by the mission. The community would then be responsible for generating any other AOP quantities, such as K_d, and IOP quantities from hyperspectral reflectance, including hyperspectral absorption and backscatter. Other geophysical quantities, such as concentrations of CDOM, TSM or Total Suspended Sediment (TSS), and pigment concentrations would be generated based on IOP products (and possibly AOP products). A key phytoplankton pigment of interest will be chlorophyll *a* concentration (chl-*a*), but several others are identified in Section 2.4. The presence of indicator pigments can be used to differentiate phytoplankton functional types in a Level-2 hyperspectral image. Combined with thermal data, functional types could possibly be further discriminated. In addition, the reflectance data could be used to measure the chlorophyll fluorescence line height, providing a window into phytoplankton photosynthesis, and hence, possibly primary production.

5. Bathymetry — HyspIRI can also be used to perform shallow water bathymetry. This has been done using multi-band instruments with some success. Improvement has been achieved with hyperspectral data. Therefore, HyspIRI offers an opportunity to determine the depth of shallow coastal waters and lakes anywhere on the globe. This would provide bathymetry in regions that are too expensive or dangerous to measure *in situ*. The quality of this product depends on optical depth and the bottom reflectivity, not just bottom depth. Turbid water or very deep water would be problematic. As turbidity can be a transient condition, repeated attempts to measure depth should improve the data product over time. Thus, HyspIRI can provide bathymetry maps that may increase in accuracy over the course of the mission. Therefore, this is another important product that can be supported by the HyspIRI mission.

6. Benthic Community — Maps of benthic cover are also an important product that can be provided by HyspIRI. Like wetlands, coral reefs and SAV beds are largely stationary features, and well suited for being mapped. Thus, the mission's temporal resolution is less of an issue. The bottom reflectance can be obtained through modeling the contribution of the water column to the Level-2 reflectance data. Classification algorithms are employed to discriminate between abiotic cover, such as sand, mud and and rocks, as well as biotic cover, including algae, coral reefs, shell beds and reefs, and SAVs. Further analysis can help discriminate these types of abiotic and biotic cover. Kelp forests, which often rise to the surface, can also be identified and mapped. In some cases, specific types may be further classified, including bleached verses normal corals. Relative quantities of cover types within 60-meter pixels may also be determined through spectral unmixing algorithms. Combining these maps with maps of persistent patterns in surface temperature, may also support baseline studies of how climate change affects benthic ecologies.

Table 3.1 - Products and Prioritization. Summarized are key data products or applications for Sections 2.1 through 2.6 of this report. For each data product or application, a priority is assigned from 1 to 4 (1 being the highest priority), which is based on the relevance to the HyspIRI mission, the urgent and compelling nature and the feasibility of each proposed product.

Category	Data Product	Priority
1. Wetlands	**Wetland Delineation and Type**	**1**
	Fraction of Vegetation Cover (subpixel)	**2**
	Fraction of Water Cover (subpixel)	**2**
	Fraction of Exposed Soil (subpixel)	**2**
	Sub-aerial Biomass	**3**
	Species Map	**3**
	Vegetation and Water Indices	**3**
	Evaporation Rates	**3**
	Soil Water Content	**3**
	Substrate Type	**4**
	Substrate Grain Size	**4**
	Substrate Bearing Strength	**4**
2. Coastlines / Ice Margins	Groundwater Discharge and Eco Response	**2**
	Ice Margin Phytoplankton Pigments	**2**
	Floods and Coastlines Maps (Episodic)	**3**
3. Water Surface Features	**Water Surface Temperature***	**1**
	Floating Material Type Map	**2**
	Floating Material Density	**2**
	Total Mass	**3**
4. Water Column	Apparent Optical Properties	
	-Remote Sensing Reflectance (R_{rs})*	**1**
	-Diffuse Attenuation Coefficient (K_d)	**3**
	Inherent Optical Properties	
	-Absorption (a)	**3**
	-Particle Backscatter (b_p)	**3**
	Fluorescence Line Height	**2**
	TSM	**3**
	TSS	**3**
	CDOM	**3**
	Chlorophyll *a* concentration	**3**
	Pigment Concentrations	**3**
	Phytoplankton Functional Type	**3**
5. Bathymetry	**Depth**	**1**
6. Benthos	**Benthic Cover Type (Coral, Algae, SAV, etc.)**	**1**
	Species Maps	**3**

*** - Project Supported Data Products**

4. Conclusions and Recommendations

A salient strength of HyspIRI for coastal and inland water applications is its high resolution — both spatial and spectral. The inclusion of contemporaneous thermal observations with the VSWIR spectroscopy at high spatial resolution opens new avenues to study coastal and inland waters, including the coupling of physical and ecological processes. Issues of scale and interactions between complex biophysical dynamics and ecosystem response could provide input into modeling studies for important biogeochemical constituents. Studies of scale could lead to better algorithms or enhanced understanding of the uncertainties encountered in coarser-resolution ocean color instruments. The three-year HyspIRI mission could establish techniques that are transferrable to future missions that would provide potentially near-real time operational support for inland and coastal water resource management. Further work toward determining the extent and quality of HyspIRI-derived bio-optical products, taking into account the instrument and mission characteristics, is recommended, and would need to be chiefly carried out by the research community, as the mission is not scoped to produce any scientific products beyond surface reflectance and temperature. The HASG hopes to continue to encourage community researchers who are interested in the development and use of these products to put forward their analyses and views regarding the quality of HyspIRI-derived aquatic data products, and provide the forum for an on-going dialogue.

With this in mind, the HASG discussed and compiled a list of candidate data products and applications. These were further assigned priorities to help inform future mission planning for NASA, and community development of data products and algorithms. However, these priority assignments should serve only as general guidance. In addition, the list of candidate products and applications described in this report should not be considered exhaustive. Future proposals can and should be expected to introduce new ideas that employ the VSWIR spectrometer, the thermal band instrument, or both in observations of coastal and inland waters. However, the current candidate list should provide a sketch of the types of efforts that are likely to be of interest to the coastal and inland aquatic remote sensing communities.

Two main challenges will face the coastal and inland aquatic remote sensing community in developing the data products described in this report. First, community-owned Level-2, 3, or 4 algorithms must be shown to generate products on synoptic scales using HyspIRI Level-1 or Level-2 surface reflectance or temperature data. Second, it must also be shown that these community-generated data products will be of sufficient quality to achieve science objectives, especially those that are aligned with answering the mission science questions. To address these two challenges, recommendations are provided in the last section of this report. But, these recommendations are also not exhaustive. A collaborative dialogue will need to be continued between community algorithm developers, researchers in the field, mission engineering teams, and project and program management. To facilitate this, some earlier algorithm development should be supported by NASA. In addition, other efforts (e.g., PACE) and other resources can be

leveraged when possible. The HASG can serve as a forum to facilitate this discussion throughout the algorithm development phase of the mission.

To that end, it is recommended that HyspIRI community efforts be synergized with other efforts in the greater coastal and inland remote sensing community. A community-wide dialogue could also be facilitated through the HASG, by providing a forum for development efforts supporting other hyperspectral or coastal and inland water remote sensing. In addition, it is important that the HASG leadership inform mission project and program management of community developments, interests and recommendation. Finally, the HASG could facilitate a dialogue with the mission engineering team to develop a complete understanding of instrument characteristics, calibration, and project-owned Level-2 algorithm function and characteristics. It is expected that this exchange could be collaborative, but moderated by project management, as necessary. It is also assumed that any adjustments for instrument behavior, calibration, or Level-2 algorithm characteristics will be implemented and maintained in community-developed algorithms, unless directed otherwise by project management.

Some initial discussion has begun within the HASG regarding the first challenge of a lack of basic generality for coastal and inland water data products. In most cases in the literature, it was found that many of the existing algorithms needed to be tailored for application on a scene-by-scene basis. Thus, studies so far have involved only a limited set of data. More development is needed to demonstrate and support generation of data products capable of support global or large-scale studies. There are opportunities that may help address this issue. Currently, the HyspIRI Preparatory Airborne Campaign is providing some data over aquatic regions along the coast of California, both from aerial and *in situ* instruments. Similar efforts have been undertaken with the PRISM airborne spectrometer over coastal waters. In addition, HICO data are now being operationally generated and distributed via the Ocean Biology Processing Group (OBPG). Finally, a new PACE science team is being formed to look at hyperspectral atmospheric correction over water and retrieval of water column inherent optical properties. These resources and associated efforts may help build operational capabilities for generation of global data sets. However, given the diverse array of Level-2, 3, and 4 products, and their unique characteristics and challenges, further research will be needed to fully realize global coastal and inland water remote sensing data support for all selected Level-2, 3 and 4 data products and their applications. Therefore, in addition to leveraging off various existing resources and efforts, it is recommended that mission program management consider allotment of some initial resources to support some HyspIRI-specific aquatic algorithm development efforts.

A number of other issues relate to the second major challenge. Level-1 products must be sufficiently calibrated, and any instrument artifacts that would otherwise undermine data quality must be minimized. This could be addressed by developing a full understanding of instrument characteristics, such as radiometric and spectral response, polarization response and noise characteristics. In addition, Level-2 VSWIR spectral remote sensing surface reflectance requires a robust atmospheric correction.

Atmospheric correction over water is a significant but necessary challenge for aquatic remote sensing, especially in coastal and inland waters, where assumptions made for deep-water applications do not hold, and where terrestrial aerosols and trace gas absorption can become more complex and harder to address. In addition, correction for specular glint in coastal and inland waters at 60-meters resolution, spatial scales where surface wind fields cannot be employed to model surface roughness, must leverage off of spectral information to discriminate contribution from the water/air interface and from the atmospheric. Thus, glint correction will likely need to be integrated into the atmospheric correction. The coastal and inland water remote sensing community, needs to carefully consider all these issues while algorithms are being developed. Part of that evaluation might be to perform sensitivity analyses for community-developed algorithms to determine the potential impact of instrument artifacts, noise, calibration uncertainty, atmospheric effects and glint to data product quality. Such a step would help algorithm and data product developers understand the input quality requirements, and also lay the groundwork for data product accuracy or uncertainty estimates.

In addition, the current Level-1 mission requirements state that retrievals over open water will have 60-meter spatial resolution, wherever the depth does not exceed 50 meters. For water with greater depths, the spatial resolution switches to 1000 meters. However, to be sure that coastal data products achieve the coverage required to answer mission science questions, a new mask for maintaining the 60-meter resolution may need to be developed. Project management has expressed interest in supporting such a mask, provided that it does not significant increase the mission data volume, and that it is simple to implement. Therefore, it is a task for the community to develop a new mask that achieves optimal coverage, without significantly increasing the data volume. This will be an on-going topic in upcoming HASG forums.

Finally, as previously mentioned, many of the aquatic data products are, by their nature, highly sensitive to uncertainty in the steps taken to obtain Level-2 surface reflectance data (e.g., calibration, adjusting for subtle instrument behavior and atmospheric correction). The complex interdependency between data products and the reliance on project generated input, suggests community-supported product generation and distribution must be linked to a calibration/processing team that is familiar with the instrument characteristics and performance, the required algorithms to generate Level-1 and 2 surface reflectance and temperature products, and the interrelationships between products. This model has worked well for NASA ocean color remote sensing to support biological oceanographic research. It is thus recommended that such a team be supported for the HyspIRI data product community. This capability could possibly be built on existing resources cost-effectively (e.g., those of the OBPG). However, such a calibration/processing team would also require an expanded interdisciplinary skill set because of the unique and diverse characteristics of coastal and inland aquatic environments. Even an existing team, such as the OBPG, would need to supplement its current expertise to move to coastal and inland water applications. This could be done by permanently adding experts to the team, by having coastal and inland water community members rotate positions on the calibration/processing team, or by the HASG maintaining close communication links between community and calibration/processing

teams. The last option, in particular, is the most cost effective and, in the case of the OBPG, the easiest to facilitate as both the HASG and OBPG management are based at the same NASA center.

References

Abbott, M., & Letelier, R. (1999). Algorithm Theoretical Basis Document - Chlorophyll Fluorescence (MODIS Product Number 20). *NASA*, (20), 1–42.

Achituv, Y., & Dubinsky, Z. (1990). Evolution and zoogeography of coral reefs. In: Dubinsky, Z. (Ed). *Ecosystems of the World 25: Coral Reefs.* Elsevier, Amsterdam, The Netherlands, 1-9.

Adam, E., Mutanga, O., & Rugege, D. (2010). Multispectral and hyperspectral remote sensing for identification and mapping of wetland vegetation: a review. *Wetlands Ecology and Management*, *18*(3), 281–296. doi:10.1007/s11273-009-9169-z

Adler-Golden, S., Acharya, P., Berk, A., Matthew, M., & Gorodetzky, D. (2005). Remote Bathymetry of the Littoral Zone From AVIRIS, LASH, and Quickbird Imagery. *IEEE Transactions on Geoscience and Remote Sensing*, *43*(2), 337–347. doi:10.1109/TGRS.2004.841246

Albert, A., & Mobley, C. (2003). An analytical model for subsurface irradiance and remote sensing reflectance in deep and shallow case-2 waters. *Optics Express*, *11*(22), 2873–2890. doi:10.1364/OE.11.002873

Alongi, D. M. (2002). Present state and future of the world's mangrove forests. *Environmental Conservation*, *29*(03), 331–349. doi:10.1017/S0376892902000231

Alvain, S., Moulin, C., & Dandonneau, Y. (2005). Remote sensing of phytoplankton groups in Case 1 waters from global SeaWiFS imagery. *Deep Sea Research Part 1*, *52*, 1989–2004.

Ammenberg, P., Flink, P., Lindell, T., Pierson, D., & Strombeck, N. (2002). Bio-optical modelling combined with remote sensing to assess water quality. *International Journal of Remote Sensing*, *23*(8), 1621–1638. doi:10.1080/01431160110071860

Anderson, L. O., Malhi, Y., Aragão, L. E. O. C., Ladle, R., Arai, E., Barbier, N., & Phillips, O. (2010). Remote sensing detection of droughts in Amazonian forest canopies. *The New Phytologist*, *187*(3), 733–750. doi:10.1111/j.1469-8137.2010.03355.x

Anderson, D. M., Alpermann, T. J., Cembella, A. D., Collos, Y., Masseret, E., Montresor, M. (2012). The globally distributed genus *Alexandrium*: multifaceted roles inmarine ecosystems and impacts on human health. *Harmful Algae*, *14*, 10–35.

Andréfouët, S., & Payri, C. (2001). Scaling-up carbon and carbonate metabolism of coral reefs using in-situ data and remote sensing. *Coral Reefs*, *19*, 259–269. doi:10.1007/s003380000117

Andréfouët, S., Zubia, M., & Payri, C. (2004). Mapping and biomass estimation of the invasive brown algae *Turbinaria ornata* (Turner) J. Agardh and Sargassum mangarevense (Grunow) Setchell on heterogeneous Tahitian coral reefs using 4-meter resolution IKONOS satellite data. *Coral Reefs*, 23(1), 26-38. doi: 10.1007/s00338-003-0367-5

Andréfouët, S., Hochberg, E. J., Chevillon, C., Müller-Karger, F. E., Brock, J. C., & Hu, C. (2005). Multi-scale remote sensing of coral reefs. In: Miller, R. L., Castillo, C. E. D., &

McKee, B.A. (Eds). *Remote sensing of coastal aquatic environments: technologies, techniques and applications.* Springer, Dordrecht, The Netherlands, 299-317.

Anthony, E. J., Vanhee, S., & Ruz, M.-H. (2006). Short-term beach–dune sand budgets on the north sea coast of France: Sand supply from shoreface to dunes, and the role of wind and fetch. *Geomorphology*, *81*(3-4), 316–329. doi:10.1016/j.geomorph.2006.04.022

Arai, E., Shimabukuro, Y. E., Pereira, G., & Vijaykumar, N. L. (2011). A multi-resolution multi-temporal technique for detecting and mapping deforestation in the Brazilian Amazon rainforest. *Remote Sensing*, *3*(12), 1943–1956. doi:10.3390/rs3091943

Armenakis, C., Leduc, F., Cyr, I., Savopol, F., & Cavayas, F. (2003). A comparative analysis of scanned maps and imagery for mapping applications. *ISPRS Journal of Photogrammetry and Remote Sensing*, *57*(5-6), 304–314. doi:10.1016/S0924-2716(02)00160-0

Astoreca, R., Doxaran, D., Ruddick, K., Rousseau, V., Lancelot, C. (2012). Influence of suspended particle concentration, composition and size on the variability of inherent optical properties of the Southern North Sea *Continental Shelf Research, 35,* 117-128. doi : 10.1016/j.csr.2012.01.007

Artigas, F. J., & Yang, J. S. (2005). Hyperspectral remote sensing of marsh species and plant vigour gradient in the New Jersey Meadowlands. *International Journal of Remote Sensing*, *26*(23), 5209–5220. doi:10.1080/01431160500218952

Artigas, F. J., & Yang, J. S. (2006). Spectral discrimination of marsh vegetation types in the New Jersey Meadowlands, USA. *Wetlands*, *26*(1), 271–277. doi:10.1672/0277-5212(2006)26[271:SDOMVT]2.0.CO;2

Atkinson, M. J., & Grigg, R. W. (1984). Model of a coral reef ecosystem. *Coral Reefs*, *3*(1), 13–22. doi:10.1007/BF00306136

Atkinson, M. J. (2011). Biogeochemistry of nutrients. In: Dubinsky, Z., & Stambler, N. (Eds). *Coral reefs: an ecosystem in transition.* Springer, Dordrecht, The Netherlands, 199-206.

Austin, R.W., & Petzold, T. (1981). The determination of the diffuse attenuation coefficient of sea water using the Coastal Zone Color Scanner. In: Gower, J.R. (Eds). *Oceanography from Space*. Plenum Press, New York, USA, 239–256.

Babin, S. M. (2004). Satellite evidence of hurricane-induced phytoplankton blooms in an oceanic desert. *Journal of Geophysical Research*, *109*(C3), C03043. doi:10.1029/2003JC001938

Bachmann, C. M., Nichols, C. R., Montes, M. J., et al. (2010). Retrieval of substrate bearing strength from hyperspectral imagery during the Virginia Coast Reserve (VCR'07) multi-sensor campaign. *Marine Geodesy, 33,* 101-116.

Bachmann, C. M., Gray, D., Abelev, A., Philpot, W., et al. (2012). Linking goniometer measurements to hyperspectral and multisensory imagery for retrieval of beach properties and coastal characterization. *SPIE Proceedings*, Vol. 8390, 9 p.

Bachmann, C. M., Philpot, W., Abelev, A., & Korwan, D. (2014). Phase angle dependence of sand density observable in hyperspectral reflectance. *Remote Sensing of Environment, 150,* 53-65. doi:10.1016/j.rse.2014.03.024

Banks, W. S. L., Paylor, R. L., & Hughes, W. B. (1996). Using thermal-infrared imagery to delineate ground-water discharged. *Ground Water, 34*(3), 434–443. doi:10.1111/j.1745-6584.1996.tb02024.x

Barbier, E. B., Hacker, S. D., Kennedy, C., Koch, E. W., Stier, A. C., & Silliman, B. R. (2011). The value of estuarine and coastal ecosystem services. *Ecological Monographs, 81*(2), 169–193. doi:10.1890/10-1510.1

Bayram, B., Acar, U., Seker, D., & Ari, A. (2008). A novel algorithm for coastline fitting through a case study over the Bosphorus. *Journal of Coastal Research, 244*(4), 983–991. doi:10.2112/07-0825.1

Behrenfeld, M. J., Westberry, T. K., Boss, E. S., O'Malley, R. T., Siegel, D. A., Wiggert, J. D., et al. (2009). Satellite-detected fluorescence reveals global physiology of ocean phytoplankton. *Biogeosciences, 6*(5), 779–794. doi:10.5194/bg-6-779-2009

Bélanger, S., Babin, M., & Larouche, P. (2008). An empirical ocean color algorithm for estimating the contribution of chromophoric dissolved organic matter to total light absorption in optically complex waters. *Journal of Geophysical Research, 113*(C4), C04027. doi:10.1029/2007JC004436

Bellwood, D. R., & Hughes, T. P. (2001). Regional-scale assembly rules and biodiversity of coral reefs. *Science, 292*(5521), 1532–1535. doi:10.1126/science.1058635

Bendjoudi, H., Weng, P., Guérin, R., & Pastre, J. (2002). Riparian wetlands of the middle reach of the Seine river (France): historical development, investigation and present hydrologic functioning. A case study. *Journal of Hydrology, 263*(1-4), 131–155. doi:10.1016/S0022-1694(02)00056-2

Bergamaschi, B. A., Fleck, J. A., Downing, B. D., Boss, E., Pellerin, B. A., Ganju, N. K., Schoellhamer, D. H., Byington, A. A., Heim, W. A., Stephenson, M., & Fujii, R. (2012). Mercury dynamics in a San Francisco estuary tidal wetland: Assessing dynamics using *in situ* measurements. *Estuaries and Coasts, 35*,1036-1048. doi: 10.1007/s12237-012-9501-3.

Berner, T. (1990). Coral-reef algae. In: Dubinsky, Z. (Ed). *Ecosystems of the World 25: Coral Reefs.* Elsevier, Amsterdam, 253-264.

Bidigare, R. R., Latasa, M., Johnson, Z., Barber, R. T., Trees, C. C., & Balch, W. M., (1997). Observation of a *Synechococcus*-dominated cyclonic eddy in open-oceanic waters of the Arabian Sea. *Proceedings of SPIE Ocean Optics XIII, 2963,* 260–265.

Blanton, J., Amft, J., & Tisue, T. (1997). Response of a small-scale bottom-attached estuarine plume to wind and tidal dissipation. *Journal of Coastal Research, 13*(2), 349–362.

Blasco, F., Aizpuru, M., & Gers, C. (2001). Depletion of the mangroves of Continental Asia. *Wetlands Ecology and Management, 9,* 245-256.

Blasco, F., Aizpuru, M., & Din Ndongo, D. (2005). Mangroves, remote sensing. In: *Encyclopedia of Coastal Science.* Schwartz, M. L. (Ed). Springer, Dordrecht, The Netherlands, 614 - 617.

Blondeau-Patissier, D., Schroeder, T., Brando, V.E., Maier, S.W., Dekker, A.G., & Phinn, S. (2014). ESA-MERIS 10-Year mission reveals contrasting phytoplankton bloom dynamics in two tropical regions of northern Australia. *Remote Sensing*, *6*(4), 2963-2988.

Boehm, A. B., Shellenbarger, G. G., & Paytan, A. (2004). Groundwater discharge: potential association with fecal indicator bacteria in the surf zone. *Environmental Science & Technology*, *38*(13), 3558–3566. doi:10.1021/es035385a

Botha, E., Brando, V., Anstee, J., Dekker, A. G., & Sagar, S. (2013). Increased spectral resolution enhances coral detection under varying water conditions. *Remote Sensing of Environment*, *131*, 247–261.

Bracher, A., Vountas, M., Dinter, T., Burrows, J.P., Röttgers, R., Peeken, I. (2009). Quantitative observation of cyanobacteria and diatoms from space using PhytoDOAS on SCIAMACHY data. *Biogeosciences, 6*, 751-764.

Braga, F., Giardino, C., Bassani, C., Matta, E., Candiani, G., Strombeck, N., Adamo, M., & Bresciani, M. (2013). Assessing water quality in the northern Adriatic Sea from HICO data. *Remote Sensing Letters, 4*(10).

Brando, V.E., & Dekker, A. G. (2003). Satellite hyperspectral remote sensing for estimating estuarine and coastal water quality. *IEEE Transactions on Geoscience and Remote Sensing*, *41*(6), 1378–1387. doi:10.1109/TGRS.2003.812907

Brando, V. E., Anstee, J. M., Wettle, M., Dekker, A. G., Phinn, S. R., & Roelfsema, C. (2009). A physics based retrieval and quality assessment of bathymetry from suboptimal hyperspectral data. *Remote Sensing of Environment*, *113*(4), 755–770. doi:10.1016/j.rse.2008.12.003

Brando, V. E, Dekker, A. G., Park, Y. J., & Schroeder, T. (2012). Adaptive semianalytical inversion of ocean color radiometry in optically complex waters. *Applied Optics*, *51*(15), 2808–2833. doi:10.1364/AO.51.002808

Bricaud, A., Claustre, H., Ras, J., & Oubelkheir, K. (2004). Natural variability of phytoplanktonic absorption in oceanic waters: Influence of the size structure of algal population. *Journal of Geophysical Ressearch, 109*, C11010. doi:10.1029/2004JC002419.

Bricaud, A., Mejia, C., Blondeau-Patissier, D., Claustre, H., Crepon, M., & Thiria, S. (2007). Retrieval of pigment concentrations and size structure of algal populations from their absorption spectra using multilayered perceptrons. *Applied Optics, 46*(8), 1251-1260.

Brock, J., Yates, K., Halley, R., Kuffner, I., Wright, C., & Hatcher, B. (2006). Northern Florida reef tract benthic metabolism scaled by remote sensing. *Marine Ecology Progress Series*, *312*, 123–139. doi:10.3354/meps312123

Buddemeier, R. W., & Smith, S. V. (1999). Coral adaptation and acclimatization: A most ingenious paradox. *American Zoologist*, *39*(1), 1–9. doi:10.1093/icb/39.1.1

Byers, S. E., & Chmura, G.L. (2012). Observations on shallow subsurface hydrology at Bay of Fundy macrotidal salt marshes. *Journal of Coastal Research, in press*. doi: 10.2112/JCOASTRES-D-12-00167.1

Byrd, K. B., O'Connell, J. L., Di Tommaso, S., & Kelly, M. (2014). Evaluation of sensor types and environmental controls on mapping biomass of coastal marsh emergent vegetation. *Remote Sensing of Environment, 149*, 166-180.

Byrnes, J., Reed, D., Cardinale, B., Cavanaugh, K., Holbrook, S., & Schmitt, R. (2011). Climate driven increases in storm frequency simplify kelp forest food webs. *Global Change Biology, 17*(8), 2513–2524. doi:10.1111/j.1365-2486.2011.02409.x

Capone, D. G., Zehr, J. P., Paerl, H. W., Bergman, B., & Carpenter, E.J. (1997). *Trichodesmium*, a globally significant marine cyanobacterium. *Science*, *276*(5316), 1221–1229. doi:10.1126/science.276.5316.1221

Carder, K. L., Hawes, S. K., Baker, K. A., Smith, R. C., Steward, R. G., & Mitchell, B. G. (1991). Reflectance model for quantifying chlorophyll *a* in the presence of productivity degradation products. *Journal of Geophysical Research*, *96*(C11), 20599–20611. doi:10.1029/91JC02117

Carlson, T. (2007). An overview of the "Triangle Method" for estimating surface evapotranspiration and soil moisture from satellite imagery. *Sensors*, *7*(8), 1612–1629. doi:10.3390/s7081612

Carpenter, E. J., & Smith, K. L. (1972). Plastics on the Sargasso Sea surface. *Science*, *175*(4027), 1240–1241. doi:10.1126/science.175.4027.1240

Carpenter, K. E., Abrar, M., Aeby, G., Aronson, R. B., Banks, S., Bruckner, A., Chiriboga, A., *et al*. (2008). One-third of reef-building corals face elevated extinction risk from climate change and local impacts. *Science*, *321*(5888), 560–563. doi:10.1126/science.1159196

Cavanaugh, K. C., Siegel, D. A., Reed, D. C., & Dennison, P. (2011). Environmental controls of giant-kelp biomass in the Santa Barbara Channel, California. *Marine Ecology Progress Series*, *429*, 1–17. doi:10.3354/meps09141

Cavanaugh, K. C., Kendall, B. E., Siegel, D. A., Reed, D. C., Alberto, F., & Assis, J. (2013). Synchrony in dynamics of giant kelp forests is driven by both local recruitment and regional environmental controls. *Ecology*, *94*(2), 499–509. doi:10.1890/12-0268.1

Chang, G. C., Dickey, T. D., Schofield, O. M., Weidemann, A. D., Boss, E., Pegau, W. S., Moline, M. A., & Glenn, S. M. (2002). Nearshore physical processes and bio-optical properties in the New York Bight. *Journal of Geophysical Research, 107*(C9), 3133.

Chase, A., Boss, E., Zaneveld, R., Bricaud, A., Claustre, H., Ras, J., Dall'Olmo, G., & Westberry, T. K. (2013). Decomposition of *in situ* particulate absorption spectra, *Methods in Oceanography*. *7*, 110-124.

Chazottes, A., Crepon, M., Bricaud, A., Ras, J., & Thiria, S. (2007). Statistical analysis of absorption spectra of phytoplankton and of pigment concentrations observed during three POMME cruises using a neural network clustering method. *Applied Optics*, *46*(18), 3790−3799.

Chen, J.-H., Kan, C.-E., Tan, C.-H., & Shih, S.-F. (2002). Use of spectral information for wetland evapotranspiration assessment. *Agricultural Water Management*, *55*(3), 239–248. doi:10.1016/S0378-3774(01)00143-3

Chen, Y., Huang, C., Ticehurst, C., Merrin, L., & Thew, P. (2013). An evaluation of MODIS daily and 8-day composite products for floodplain and wetland inundation mapping. *Wetlands, in press.*

Chen, Z., Hanson, J. D., & Curran, P. J. (1991). The form of the relationship between suspended sediment concentration and the spectral reflectance: its implications for the use of Daedalus 1268 data, *International Journal of Remote Sensing*. *12*(1), 215−222.

Chesson, P. L., & Case, T. J. (1986). Nonequilibrium community theories: chance, variability, history, and coexistence. In: Diamond J. & Case T. (Eds). *Community Ecology*. Harper and Row, New York, USA, pp. 229-239.

Chopra, R., Verma, V. K., & Sharma, P. K. (2001). Mapping, monitoring and conservation of Harike wetland ecosystem, Punjab, India, through remote sensing. *International Journal of Remote Sensing*, *22*(1), 89–98. doi:10.1080/014311601750038866

Christian, B., & Krishnayya, N. (2009). Classification of tropical trees growing in a sanctuary using Hyperion (EO-1) and SAM algorithm. *Current Science*, *96*(12), 1601–1607.

Church, J. A., & White, N. J. (2006). A 20th century acceleration in global sea-level rise. *Geophysical Research Letters*, *33*(1), L01602. doi:10.1029/2005GL024826

Ciotti, A.M. & Bricaud A. (2006). Retrievals of a size parameter for phytoplankton and spectral light absorption by Colored Detrital Matter from water-leaving radiances at SeaWiFS channels in a continental shelf region off Brazil. *Limnology and Oceanography Methods*, *4*, 237–253.

Clark, R. N., Swayze, G. A., Leifer, I., Livo, K. E., Lundeen, S., Eastwood, M., Green, R. O., Kokaly, R., Hoefen, T., Sarture, C., McCubbin, I., Roberts, D., Steele, D., Ryan, T., Dominguez, R., Pearson, N., and the Airborne Visible/Infrared Imaging Spectrometer (AVIRIS) Team. (2010) A method for qualitative mapping of thick oil spills using imaging spectroscopy. Open-File Report 2010-1101, U.S. Geological Survey.

Cleveland, J., & Perry, M. (1987). Quantum yield, relative specific absorption and fluorescence in nitrogen limited, Chaetoceros gracilis. *Marine Biology*, *497*, 489–497.

Connell, J. H. (1997). Disturbance and recovery of coral assemblages. *Coral Reefs*, *16*, S101–S113. doi:10.1007/s003380050246

Cracknell, A. P. (1999). Remote sensing techniques in estuaries and coastal zones an update. *International Journal of Remote Sensing*, *20*(3), 485–496. doi:10.1080/014311699213280

Craig, S. E., Jones, C. T., Li, W. K. W., Lazin, G., Horne, E., Caverhill, C., & Cullen, J. J. (2012). Deriving optical metrics of coastal phytoplankton biomass from ocean colour. *Remote Sensing of Environment*, *119*, 72–83. doi:10.1016/j.rse.2011.12.007

Cunningham A., Ramage L., & McKee D. (2013). Relationships between inherent optical properties and the depth of penetration of solar radiation in optically complex coastal waters. *Journal of Geophysical Research: Oceans*, *118*(5), 2169-9291, doi:10.1002/jgrc.20182

Dall'Olmo, G., & Gitelson, A. A. (2005). Effect of bio-optical parameter variability on the remote estimation of chlorophyll-a concentration in turbid productive waters: experimental results. *Applied Optics*, *44*(3), 412–422. doi:10.1364/AO.44.000412

Dahl, T. E. (2011). Status and trends of wetlands in the conterminous United States 2004 to 2009. U.S. Department of the Interior, U.S. Fish and Wildlife Service, Fisheries and Habitat Conservation.

Davis, C.O., Kavanaugh, M., Letelier, R., Bissett, W. P., & Kohler, D. (2007), Spatial and spectral resolution considerations for imaging coastal waters. *Proceedings of the SPIE, 6680*, 1-12.

Dayton, P. K., & Tegner, M. J. (1984). Catastrophic storms, El Niño, and patch stability in a Southern California kelp community. *Science*, *224*(4646), 283–285. doi:10.1126/science.224.4646.283

DeAngelis, D. & Waterhouse, J. C. (1987). Equilibrium and nonequilibrium concepts in ecological models. *Ecological Monographs, 57*, 1–21.

Del Castillo, C. E., & Miller, R. L. (2008). On the use of ocean color remote sensing to measure the transport of dissolved organic carbon by the Mississippi River plume. *Remote Sensing of Environment*. *112*, 836–844.

Dekker, A. G., Phinn, S. R., Anstee, J., Bissett, P., Brando, V. E., Casey, B., Fearns, P., et al. (2011). Intercomparison of shallow water bathymetry, hydro-optics, and benthos mapping techniques in Australian and Caribbean coastal environments. *Limnology and Oceanography: Methods*, *9*, 396–425. doi:10.4319/lom.2011.9.396

Dekker, A.G. & Hestir, E. L. (2012). Evaluating the Feasibility of Systematic Inland Water Quality Monitoring with Satellite Remote Sensing, CSIRO: Water for a Healthy Country National Research Flagship, Australia, ISBN 978 0 643 10849 3

Derraik, J. G. B. (2002). The pollution of the marine environment by plastic debris: a review. *Marine Pollution Bulletin*, *44*(9), 842–852. doi:10.1016/S0025-326X(02)00220-5,

Desantis, L. R. G., Bhotika, S., Williams, K., & Putz, F. E. (2007). Sea-level rise and drought interactions accelerate forest decline on the Gulf Coast of Florida, USA. *Global Change Biology*, *13*(11), 2349–2360. doi:10.1111/j.1365-2486.2007.01440.x

Devred E., Sathyendranath S., Stuart V., Maass H., Ulloa O. & Platt T. (2006). Bio-Optics of the ocean: a two-component model of absorption by phytoplankton, *Journal of Geophysical Research, 111,* C03011. doi :10.1029/2005jc002880

Devred E., Sathyendranath S., Stuart S. & Platt, T. (2011). Absorption-derived phytoplankton cell size: application to satellite ocean-colour data in the Northwest Atlantic, *Remote Sensing of Environment, 115*, 2255-2266.

Dierssen, H., Zimmerman, R., Leathers, R. A., Downes, T. V., & Davis, C. O. (2003). Ocean color remote sensing of seagrass and bathymetry in the Bahamas Banks by high-resolution airborne imagery. *Limnology and Oceanography*, *48*(1), 444–455.

Domenikiotis, C., Loukas, A., & Dalezios, N. R. (2003). The use of NOAA/AVHRR satellite data for monitoring and assessment of forest fires and floods. *Natural Hazards and Earth System Science*, *3*, 115–128. doi:10.5194/nhess-3-115-2003

D'Sa, E. J., & Miller, R. L. (2003). Bio-optical properties in waters influenced by the Mississippi River during low flow conditions. *Remote Sensing of Environment*, *84*, 538–549.

Doxaran D., Ruddick K. McKee D., Gentili B., Tailliez D., Chami M., & Babin M. (2009). Spectral variations of light scattering by marine particles in coastal waters, from the visible to the near infrared. *Limnology and Oceanography*, *54*, 1257-1271.

Doxaran, D., Ehn, J., Bélanger, S., Matsuoka, a., Hooker, S., & Babin, M. (2012). Optical characterisation of suspended particles in the Mackenzie River plume (Canadian Arctic Ocean) and implications for ocean colour remote sensing. *Biogeosciences*, *9*(8), 3213–3229. doi:10.5194/bg-9-3213-2012

Falkowski, P. G., & Kiefer, D.A. (1985). Chlorophyll *a* fluorescence in phytoplankton: Relationship to photosynthesis and biomass. *Journal of Plankton Research, 7*(5), 715–731. doi:10.1093/plankt/7.5.715

Falkowski, P. G. & Raven, J. A. (1997). *Aquatic photosynthesis*. Blackwell Scientific Publishers, Oxford, U.K., 375 p.

Falkowski, P. G., Katz, M. E., Knoll, A. H., Quigg, A., Raven J. A., & Schofield O. (2004). The evolution of modern eukaryotic phytoplankton. *Science, 305,* 354-360.

Falter, J. L., Atkinson, M. J., & Langdon, C. (2001). Production-respiration relationships at different timescales within the Biosphere 2 coral reef biome. *Limnology and Oceanography*, *46*(7), 1653–1660. doi:10.4319/lo.2001.46.7.1653

Falter, J. L., Atkinson, M. J., Schar, D. W., Lowe, R. J., & Monismith, S. G. (2010). Short-term coherency between gross primary production and community respiration in an algal-dominated reef flat. *Coral Reefs*, *30*(1), 53–58. doi:10.1007/s00338-010-0671-9

Feng, L., Hu, C., Chen, X., Cai, X., Tian, L., & Gan, W. (2012). Assessment of inundation changes of Poyang Lake using MODIS observations between 2000 and 2010. *Remote Sensing of Environment, 121,* 80–92. doi:10.1016/j.rse.2012.01.014

Ficek, D., Zapadka, T., & Dera, J. (2011). Remote sensing reflectance of Pomeranian lakes and the Baltic. *Oceanologia*, *53*, 959–970.

Fichot, C. G., Sathyendranath, S., & Miller, W. (2008). SeaUV and SeaUVC: Algorithms for the retrieval of UV/Visible diffuse attenuation coefficients from ocean color. *Remote Sensing of Environment, 112*, 1584–1602. doi:10.1016/j.rse.2007.08.009

Fichot, C. G., Kaiser, K., Hooker, S. B., Amon, R. M. W., Babin, M., Bélanger, S., et al. (2013). Pan-Arctic distributions of continental runoff in the Arctic Ocean. *Scientific Reports*, *3*, 1053. doi:10.1038/srep01053

Filippi, A. M., & Jensen, J. R. (2006). Fuzzy learning vector quantization for hyperspectral coastal vegetation classification, *Remote Sensing of Environment, 100*(4), 512–530. doi:10.1016/j.rse.2005.11.007

Fischer, J. (1985). On the information content of multispectral radiance measurements over an ocean. *International Journal of Remote Sensing*, *6*(5), 773-786. doi: 10.1080/01431168508948498

Fishman, J., Iraci, L. T., Al-Saadi, J., Chance, K., Chavez, F., Chin, M., Coble, P., et al. (2012). The United States' next generation of atmospheric composition and coastal ecosystem measurements: NASA's Geostationary Coastal and Air Pollution Events (GEO-CAPE) Mission. *Bulletin of the American Meteorological Society*, *93*(10), 1547–1566. doi:10.1175/BAMS-D-11-00201.1

Flink, P., Lindell, L. T., & Östlund, C. (2001). Statistical analysis of hyperspectral data from two Swedish lakes. *Science of The Total Environment*, *268*(1-3), 155–169. doi:10.1016/S0048-9697(00)00686-0

Galvao, L. S., Pereira Filho, W., Abdon, M. M., Novo, E. M. M. L., Silva, J. S. V., & Ponzoni, F. J. (2003). Spectral reflectance characterization of shallow lakes from the Brazilian Pantanal wetlands with field and airborne hyperspectral data. *International Journal of Remote Sensing*, *24*(21), 4093–4112. doi:10.1080/0143116031000070382

Gao, J. (1998). A hybrid method toward accurate mapping of mangroves in a marginal habitat from SPOT multispectral data. *International Journal of Remote Sensing*, *19*(10), 1887–1899. doi:10.1080/014311698215045

Gao, B-C., Montes, M.J., Ahmad, Z., Davis, C.O. (2000). Atmospheric correction algorithm for hyperspectral remote sensing of ocean color from space. *Applied Optics*, *39*(6), 887-896.

Gao, B-C. (2010). HyspIRI visible to short wavelength infrared (VSWIR) water leaving reflectance algorithm theoretical basis document (ATBD). (Online) http://hyspiri.jpl.nasa.gov/

Ghilain, N., Arboleda, A., Sepulcre-Canto, G., Batelaan, O., Ardo, J., & Gellens-Meulenberghs, F. (2011). Improving evapotranspiration in land surface models using biophysical parameters derived from MSG/SEVIRI satellite. *Hydrologic Earth Systems Science*, *16*(8), 2567-2583.

Ghrefat, H. A., Goodell, P. C., Hubbard, B.E., Langford, R.P., & Aldouri, R.E. (2007). Modeling grain size variations of aeolian gypsum deposits at White Sands, New Mexico, using AVIRIS imagery. *Geomorphology*, *88*, 57-68.

Gilerson, A. A, Gitelson, A. A., Zhou, J., Gurlin, D., Moses, W., Ioannou, I., & Ahmed, S. A. (2010). Algorithms for remote estimation of chlorophyll-*a* in coastal and inland waters using red and near infrared bands. *Optics Express*, *18*(23), 24109–24125. doi:10.1364/OE.18.024109

Gilmore, M. S., Wilson, E. H., Barrett, N., Civco, D. L., Prisloe, S., Hurd, J. D., & Chadwick, C. (2008). Integrating multi-temporal spectral and structural information to map wetland vegetation in a lower Connecticut River tidal marsh. *Remote Sensing of Environment*, *112*(11), 4048–4060. doi:10.1016/j.rse.2008.05.020

Gilmore, M. S., Civco, D. L., Wilson, E. H., Barrett, N., Prisloe, S., Hurd, J. D., & Chadwick, C. (2010). Remote sensing and *in situ* measurements for delineation and assessment of coastal marshes and their constituent species. In: *Remote Sensing of Coastal Environment*. Wang, J. (Ed). CRC Press, Boca Raton, Florida.

Ginsburg, R. N. (Ed). (1994). Colloquium on global aspects of coral reefs: health, hazards and history. Rosenstiel School of Marine and Atmospheric Sciences, University of Miami, Miami.

Gitelson, A. A. (1992). The peak near 700 nm on radiance spectra of algae and water: relationships of its magnitude and position with chlorophyll concentration. *International Journal of Remote Sensing*, *13*(17), 3367–3373. doi:10.1080/01431169208904125

Gitelson, A. A., Gao, B.-C., Li, R.-R., Berdnikov, S., & Saprygin, V. (2011). Estimation of chlorophyll-*a* concentration in productive turbid waters using a Hyperspectral Imager for the Coastal Ocean—the Azov Sea case study. *Environmental Research Letters*, *6*(2), 024023. doi:10.1088/1748-9326/6/2/024023

Goodman, J. A., & Ustin, S. L. (2007). Classification of benthic composition in a coral reef environment using spectral unmixing. *Journal of Applied Remote Sensing*, *1*(1), 011501-011501. doi:10.1117/1.2815907

Goodman, J. A., Purkis, S. J., & Phinn, S. R. (Eds). (2013). *Coral Reef Remote Sensing: A Guide for Mapping, Monitoring and Management*. Springer, Dordrecht, The Netherlands, 436p.

Gordon, H. R., Brown, O. B., & Jacobs, M. M. (1975). Computed relationships between the inherent and apparent optical properties of a flat homogeneous ocean. *Applied Optics*, *14*(2), 417–427. doi:10.1364/AO.14.000417

Gordon, H. R., Clark, D. K., Brown, J. W., Brown, O. B., Evans, R. H., & Broenkow, W. W. (1983). Phytoplankton pigment concentrations in the Middle Atlantic Bight: comparison of ship determinations and CZCS estimates. *Applied Optics*, *22*(1), 20–36. doi:10.1364/AO.22.000020

Gordon, H. R. (1997). Atmospheric correction of ocean color imagery in the Earth Observing System era. *Journal of Geophysical Research*, *102*(D14), 17081–17106. doi:10.1029/96JD02443

Gould, R. W., & Arnone, R. A. (1997). Remote sensing estimates of inherent optical properties in a coastal environment. *Remote Sensing of Environment*, *61*(2), 290–301. doi:10.1016/S0034-4257(97)89496-5

Gower, J. F. R., Doeffer R., & Borstad, G. (1999). Interpretation of the 685 nm peak in waterleaving radiance spectra in terms of fluorescence, absorption and scattering, and its observation by MERIS. *International Journal of Remote Sensing*, *20*, 1771-1786. doi:10.1080/014311699212470

Gower, J. F. R, Hu, C., Borstad, G., & King, S. (2006). Ocean color satellites show extensive lines of floating *Sargassum* in the Gulf of Mexico. *IEEE Transactions on Geoscience and Remote Sensing*, *44*(12), 3619–3625. doi:10.1109/TGRS.2006.882258

Gower, J. F. R., King, S. A., & Goncalves, P. (2008). Global monitoring of plankton blooms using MERIS MCI. *International Journal of Remote Sensing*, *29*(21), 6209–6216. doi:10.1080/01431160802178110

Gower, J. F. R., & King, S. A. (2011). Distribution of floating *Sargassum* in the Gulf of Mexico and the Atlantic Ocean mapped using MERIS. *International Journal of Remote Sensing*, *32*(7), 1917–1929. doi:10.1080/01431161003639660

Green, E. P., Mumby, P. J., Edwards, A. J., & Clark, C. D. (1996). A review of remote sensing for the assessment and management of tropical coastal resources. *Coastal Management*, *24*(1), 1–40. doi:10.1080/08920759609362279

Gregory, M. R. (2009). Environmental implications of plastic debris in marine settings--entanglement, ingestion, smothering, hangers-on, hitch-hiking and alien invasions. *Philosophical Transactions of the Royal Society of London*, *364*(1526), 2013–2025. doi:10.1098/rstb.2008.0265

Gruber, N., & Sarmiento, J. L. (1997). Global patterns of marine nitrogen fixation and denitrification. *Global Biogeochemical Cycles*, *11*(2), 235–266. doi:10.1029/97GB00077

Gunawardena, M., & Rowan, J. S. (2005). Economic valuation of a mangrove ecosystem threatened by shrimp aquaculture in Sri Lanka. *Environmental Management*, *36*(4), 535–550. doi:10.1007/s00267-003-0286-9

Gurlin, D., Gitelson, A. A., & Moses, W. J. (2011). Remote estimation of chl-*a* concentration in turbid productive waters — Return to a simple two-band NIR-red model? *Remote Sensing of Environment*, *115*(12), 3479–3490. doi:10.1016/j.rse.2011.08.011

Hakvoort, H., De Haan, J., Jordans, R., Vos, R., Peters, S., & Rijkeboer, M. (2002). Towards airborne remote sensing of water quality in The Netherlands—validation and error analysis. *ISPRS Journal of Photogrammetry and Remote Sensing*, *57*(3), 171–183. doi:10.1016/S0924-2716(02)00120-X

Hatcher, B. G. (1997). Coral reef ecosystems: how much greater is the whole than the sum of the parts? *Coral Reefs*, *16*, S77–S91. doi:10.1007/s003380050244

He, M.-X., Lui, F., Yu, D., & Hu, C. (2011). Monitoring green tides in Chinese marginal seas. In: Morales, J., Stuart, V., Platt, T., & Sathyendranath, S. (Eds). *Handbook of satellite remote sensing image interpretation: applications for marine living resources conservation and management.* EU PRESPO & IOCCG. Dartmouth, Canada, 111-124.

Hepburn, C., & Hurd, C. (2005). Conditional mutualism between the giant kelp *Macrocystis pyrifera* and colonial epifauna. *Marine Ecology Progress Series*, *302*, 37–48. doi:10.3354/meps302037

Hestir, E. L., Khanna, S., Andrew, M. E., Santos, M. J., Viers, J. H., Greenberg, J. A., Rajapakse, S. S., et al. (2008). Identification of invasive vegetation using hyperspectral remote sensing in the California Delta ecosystem. *Remote Sensing of Environment*, *112*(11), 4034–4047. doi:10.1016/j.rse.2008.01.022

Heumann, B. W. (2011). Satellite remote sensing of mangrove forests: Recent advances and future opportunities. *Progress in Physical Geography*, *35*(1), 87–108. doi:10.1177/0309133310385371

Hirano, A., Madden, M., & Welch, R. (2003). Hyperspectral image data for mapping wetland vegetation. *Wetlands*, *23*(2), 436–448. doi:10.1672/18-20

Hirata, T., Aiken, J., Hardman-Mountford, N., Smyth T. J., & Barlow, R. (2008). An absorption model to determine phytoplankton size classes from satellite ocean colour, *Remote Sensing of Environment, 112*, 3153–3159.

Hochberg, E. J., & Atkinson, M. J. (2003). Capabilities of remote sensors to classify coral, algae, and sand as pure and mixed spectra. *Remote Sensing of Environment*, *85*(2), 174–189. doi:10.1016/S0034-4257(02)00202-X

Hochberg, E. J., & Atkinson, M. J. (2008). Coral reef benthic productivity based on optical absorptance and light-use efficiency. *Coral Reefs, 27*(1), 49–59. doi:10.1007/s00338-007-0289-8

Hochberg, E. J. (2011). Remote sensing of coral reef processes. In: Dubinsky, Z., & Stambler, N. (Eds). *Coral reefs: an ecosystem in transition.* Springer, Dordrecht, The Netherlands, 25-35.

Hochberg, E. J., Mobley, C. D., Park, Y., Goodman, J., Turpie, K. R., Gao, B., et al. (2011). HyspIRI sunglint subgroup: Glint characterization, determination of impacts on science, and potential mitigation approaches [Presented Slides]. Paper presented at 2011 HyspIRI Science Workshop - NASA Decadal Survey Mission. Washington, DC.

Hoegh-Guldberg, O., Mumby, P. J., Hooten, A. J., Steneck, R. S., Greenfield, P., Gomez, E., Harvell, C. D., et al. (2007). Coral reefs under rapid climate change and ocean acidification. *Science, 318*(5857), 1737–1742. doi:10.1126/science.1152509

Hoeppfner, N., & Sathyendranath, S. (1993). Determination of the major groups of phytoplankton pigments from the absorption spectra of total particulate matter. *Journal of Geophysical Research, 98*, 22789–22803.

Hoge, F. E., & Lyon, P. E. (1996). Satellite retrieval of inherent optical properties by linear matrix inversion of oceanic radiance models: An analysis of model and radiance measurement errors. *Journal of Geophysical Research*, *101*(C7), 16631. doi:10.1029/96JC01414

Hu, C., Carder, K. L., & Müller-Karger, F. E. (2000). Atmospheric Correction of SeaWiFS Imagery over Turbid Coastal Waters. *Remote Sensing of Environment, 74*(2), 195–206. doi:10.1016/S0034-4257(00)00080-8

Hu, C., Müller-Karger, F. E., Taylor, C. (Judd), Myhre, D., Murch, B., Odriozola, A. L., & Godoy, G. (2003). MODIS detects oil spills in Lake Maracaibo, Venezuela. *Eos, Transactions American Geophysical Union*, *84*(33), 313-319. doi:10.1029/2003EO330002

Hu, C., Müller-Karger, F., Taylor, C., Carder, K., Kelble, C., Johns, E., & Heil, C. (2005). Red tide detection and tracing using MODIS fluorescence data: A regional example in SW Florida coastal waters. *Remote Sensing of Environment*, *97*(3), 311–321. doi:10.1016/j.rse.2005.05.013

Hu, C., Müller-Karger, F. E., & Swarzenski, P. W. (2006). Hurricanes, submarine groundwater discharge, and Florida's red tides. *Geophysical Research Letters*, *33*(11), L11601. doi:10.1029/2005GL025449

Hu, C., & He, M. (2008). Origin and offshore extent of floating algae in Olympic sailing area. *Eos, Transactions American Geophysical Union, 89*(33), 2006–2009. doi:10.1063/1.881278.Barth

Hu, C. A novel ocean color index to detect floating algae in the global oceans. (2009). *Remote Sensing of Environment, 113*(10), 2118–2129. doi:10.1016/j.rse.2009.05.012

Hu, C., Li, X., Pichel, W. G., & Müller-Karger, F. E. (2009). Detection of natural oil slicks in the NW Gulf of Mexico using MODIS imagery. *Geophysical Research Letters*, *36*(1), L01604. doi:10.1029/2008GL036119

Hu, C., Cannizzaro, J., Carder, K. L., Müller-Karger, F. E., & Hardy, R. (2010a). Remote detection of *Trichodesmium* blooms in optically complex coastal waters: Examples with MODIS full-spectral data. *Remote Sensing of Environment*, *114*(9), 2048–2058. doi:10.1016/j.rse.2010.04.011

Hu, C., Li, D., Chen, C., Ge, J., Müller-Karger, F. E., Liu, J., Yu, F., et al. (2010b). On the recurrent *Ulva prolifera* blooms in the Yellow Sea and East China Sea. *Journal of Geophysical Research*, *115*(C5), C05017. doi:10.1029/2009JC005561

Hu, C., Weisberg, R. H., Liu, Y., Zheng, L., Daly, K. L., English, D. C., Zhao, J., et al. (2011). Did the northeastern Gulf of Mexico become greener after the Deepwater Horizon oil spill? *Geophysical Research Letters*, *38*(9), L09601. doi:10.1029/2011GL047184

Hu, C., Feng, L., Lee, Z., Davis, C. O., Mannino, A., McClain, C. R., & Franz, B. A. (2012a). Dynamic range and sensitivity requirements of satellite ocean color sensors: learning from the past. *Applied Optics*, *51*(25), 6045–6062. doi:10.1364/AO.51.006045

Hu, C., Lee, Z., & Franz, B. (2012b). Chlorophyll *a* algorithms for oligotrophic oceans: A novel approach based on three-band reflectance difference. *Journal of Geophysical Research*, *117*(C1), C01011. doi:10.1029/2011JC007395

Hu, C., Feng, L., & Lee, Z. (2013). Uncertainties of SeaWiFS and MODIS remote sensing reflectance: Implications from clear water measurements. *Remote Sensing of Environment*, *133*, 168–182. doi:10.1016/j.rse.2013.02.012

Huot, Y., Brown, C. A., & Cullen, J. J. (2005). Retrieval of phytoplankton biomass from simultaneous inversion of reflectance, the diffuse attenuation coefficient, and sun-induced fluorescence in coastal waters. *Journal of Geophysical Research, 112*, C06013. doi:10.10292006JC003794

Huot, Y., Babin, M., Bruyant, F., Grob, C., Twardowski, M. S., & Claustre, H. (2007). Does chlorophyll *a* provide the best index of phytoplankton biomass for primary productivity studies? *Biogeosciences, 4*, 853-868.

IMaRS-USF and IRD (2005). Millennium Coral Reef Mapping Project (validated maps). UNEP World Conservation Monitoring Centre. Cambridge (UK), http://data.unep-wcmc.org/datasets/13

IMaRS-USF (2005). Millennium Coral Reef Mapping Project (unvalidated maps are unendorsed by IRD, and were further interpreted by UNEP-WCMC). UNEP World Conservation Monitoring Centre. Cambridge (UK), http://data.unep-wcmc.org/datasets/13

IPCC (2007). Cross-chapter case study. In: Parry, M. L., Canziani, O. F., Palutikof, J. P., van der Linden, P. J., & Hanson, C.E. (Eds). *Climate change 2007: impacts, adaptation and vulnerability contribution of working group II to the fourth assessment report of the Intergovernmental Panel on Climate Change.* Cambridge University Press, Cambridge, UK, 843-868.

IOCCG. (1998). Minimum requirements for an operational ccean-colour sensor. In: Morel, A. (Ed). *Reports of the International Ocean-Colour. Coordinating Group No.1*, IOCCG, Dartmouth, Canada.

IOCCG. (1999). Status and plans for satellite ocean-colour missions: Considerations for complimentary missions. In: Yoder, J. A. (Ed). *Reports of the International Ocean-Colour Coordinating Group, No. 2*, IOCCG, Dartmouth, Canada.

IOCCG (2006). Remote sensing of inherent optical properties: Fundamentals, tests of algorithms, and applications. Dartmouth, Canada: IOCCG.

Ioannou, I., Gilerson, A., Gross, B., Moshary, F., & Ahmed, S. (2011). Neural network approach to retrieve the inherent optical properties of the ocean from observations of MODIS. *Applied Optics*, *50*(19), 3168–3186. doi:10.1364/AO.50.003168

Jackson, R. (1985). Evaluating evapotranspiration at local and regional scales. *Proceedings of the IEEE*, *73*(6), 1086–1096. doi:10.1109/PROC.1985.13239

Jain, S. K., Singh, R. D., Jain, M. K., & Lohani, A. K. (2005). Delineation of flood-prone areas using remote sensing techniques. *Water Resources Management*, *19*(4), 333–347. doi:10.1007/s11269-005-3281-5

Jamet, C., Loisel, H., & Dessailly, D. (2012). Retrieval of the spectral diffuse attenuation coefficient Kd(λ) in open and coastal ocean waters using a neural network inversion. *Journal of Geophysical Research*, *117*(C10), C10023. doi:10.1029/2012JC008076

Jensen, J. R., Hodgson, M. E., Christensen, E., Mackey, H. E., Tinney, L. R., & Sharitz R. (1986). Remote-sensing inland wetlands - a multispectral approach. *Photogrammetric Engineering and Remote Sensing 52*(1), 87-100.

Jensen, J. R., Coombs, C., Porter, D., Jones, B., Schill, S., & White, D. (1998). Extraction of smooth cordgrass (spartina alterniflora) biomass and leaf area index parameters from high resolution imagery. *Geocarto International*, *13*(4), 25–34. doi:10.1080/10106049809354661

Jensen, R., Mausel, P., Dias, N., Gonser, R., Yang, C., Everitt, J., & Fletcher, R. (2007). Spectral analysis of coastal vegetation and land cover using AISA+ hyperspectral data. *Geocarto International*, *22*(1), 17–28. doi:10.1080/10106040701204354

Johns, G. M., Leeworthy, V. R., Bell, F. W., & Bonn, M. A. (2001) Socioeconomic study of reefs in southeast Florida: final report: for Broward County, Palm Beach County, Miami-Dade County, Monroe County, Florida Fish and Wildlife, & National Oceanic and Atmospheric Administration. Hazen and Sawyer, Miami, U.S.A.

Johnson, A. G., Glenn, C. R., Burnett, W. C., Peterson, R. N., & Lucey, P. G. (2008). Aerial infrared imaging reveals large nutrient-rich groundwater inputs to the ocean. *Geophysical Research Letters*, *35*(15), L15606. doi:10.1029/2008GL034574

Jollineau, M. Y., & Howarth, P. J. (2008). Mapping an inland wetland complex using hyperspectral imagery. *International Journal of Remote Sensing*, *29*(12), 3609–3631. doi:10.1080/01431160701469099

Jones, G. P., McCormick, M. I., Srinivasan, M., & Eagle, J. V. (2004). Coral decline threatens fish biodiversity in marine reserves. *Proceedings of the National Academy of Sciences*, *101*(21), 8251–8253. doi:10.1073/pnas.0401277101

Judd, C., Steinberg, S., Shaughnessy, F., & Crawford, G. (2007). Mapping salt marsh vegetation using aerial hyperspectral imagery and linear unmixing in Humboldt Bay, California. *Wetlands*, *27*(4), 1144–1152. doi:10.1672/0277-5212(2007)27[1144:MSMVUA]2.0.CO;2

Kallio, K., Kutser, T., Hannonen, T., Koponen, S., Pulliainen, J., Vepsäläinen, J., & Pyhälahti, T. (2001). Retrieval of water quality from airborne imaging spectrometry of various lake types in different seasons. *Science of The Total Environment*, *268*(1-3), 59–77. doi:10.1016/S0048-9697(00)00685-9

Kalma J. D, McVicar, T. R., & McCabe, M. F. (2008). Estimating land surface evaporation: A review of methods using remotely sensed surface temperature data. *Surveys in Geophysics*, *29*, 421–469.

Kanai, Y., Ueta, M., Germogenov, N., Nagendran, M., Mita, N., & Higuchi, H. (2002). Migration routes and important resting areas of Siberian cranes (Grus leucogeranus) between northeastern Siberia and China as revealed by satellite tracking. *Biological Conservation*, *106*(3), 339–346. doi:10.1016/S0006-3207(01)00259-2

Karl, D., Letelier, R., Tupas, L., Dore, J., Christian, J., & Hebel, D. (1997). The role of nitrogen fixation in biogeochemical cycling in the subtropical North Pacific Ocean. *Nature*, *388*, 533–538.

Kelly, M., & Tuxen, K. (2009). Remote sensing support for tidal wetland vegetation Research and management. In: Yang, X. (Ed). *Remote Sensing and Geospatial Technologies for Coastal Ecosystem Assessment and Management*. Springer-Verlag, Berlin, Germany, 341-364.

Kelly, M., Tuxen, K. A., & Stralberg, D. (2011). Mapping changes to vegetation pattern in a restoring wetland: Finding pattern metrics that are consistent across spatial scale and time. *Ecological Indicators*, *11*(2), 263–273. doi:10.1016/j.ecolind.2010.05.003

Kildow, J., Colgan, C., & Scorse, J. (2009). *State of the U.S. Ocean and Coastal Economies 2009; Report of the National Ocean Economics Program (NOEP)* (pp. 1–60).

Kinsey, D. W. (1983). Standards of performance in coral reef primary production and carbon turnover. In: *Perspectives on coral reefs.* Brian Clouston Publisher, Manuka, Australia, 209-220.

Kinsey, D. W. (1985). Metabolism, calcification and carbon production I: Systems level studies. *Fifth International Coral Reef Congress*, *4*, 505-526.

Klemas V. (2001). Remote sensing of landscape-level coastal environmental indicators. *Environmental Management*, 27, *1*,47-57.

Klemas, V. (2011). Remote sensing of wetlands: case studies comparing practical techniques. *Journal of Coastal Research*, *27*, 418–427. doi:10.2112/JCOASTRES-D-10-00174.1

Klemas, V. (2013a). Remote Sensing of Coastal Wetland Biomass: An Overview. *Journal of Coastal Research*, *290*, 1016–1028. doi:10.2112/JCOASTRES-D-12-00237.1

Klemas, V. (2013b). Remote sensing of emergent and submerged wetlands: an overview. *International Journal of Remote Sensing*, *34*(18), 6286–6320. doi:10.1080/01431161.2013.800656

Kleypas, J. A. (1997). Modeled estimates of global reef habitat and carbonate production since the Last Glacial Maximum. *Paleoceanography*, *12*(4), 533–545. doi:10.1029/97PA01134

Kleypas, J. A., McManus, J. W., & Meñez, L. A. B. (1999). Environmental limits to coral reef development: Where do we draw the line? *American Zoologist*, *39*(1), 146–159. doi:10.1093/icb/39.1.146

Klonowski, W. M., Fearns, P. R., Lynch, M. J. (2007). Retrieving key benthic cover types and bathymetry from hyperspectral imagery. *Journal of Applied Remote Sensing*, *1*(1), 011505. doi:10.1117/1.2816113

Kogan, F. N. (1998). A typical pattern of vegetation conditions in southern Africa during El Niño years detected from AVHRR data using three-channel numerical index. *International Journal of Remote Sensing*, *19*(18), 3688–3694. doi:10.1080/014311698213902

Kolokoussis, P., Karathanassi, V., Rokos, D., Argialas, D., Karageorgis, A. P., & Georgopoulos, D. (2011). Integrating thermal and hyperspectral remote sensing for the detection of coastal springs and submarine groundwater discharges. *International Journal of Remote Sensing*, *32*(23), 8231–8251. doi:10.1080/01431161.2010.533209

Kostadinov T. S., Siegel D. A., & Maritorena S. (2009). Retrieval of the particle size distribution from satellite ocean color observations. *Journal of Geophysical Research: Oceans*, *114*(C9), 2156-2202. 10.1029/2009JC005303

Kovacs, J. M., Wang, J., & Blanco-Correa, M. (2001). Mapping disturbances in a mangrove forest using multi-date Landsat TM imagery. *Environmental Management*, *27*(5), 763–776. doi:10.1007/s002670010186

Kuchler, D. A., Biña, R. T., & Claasen, D.vR. (1988). Status of high-technology remote sensing for mapping and monitoring coral reef environments. *Proceedings of the Sixth International Coral Reef Symposium*, *1,* 97-101.

Laist, D. W. (1987). Overview of the biological effects of lost and discarded plastic debris in the marine environment. *Marine Pollution Bulletin*, *18*(6), 319–326. doi:10.1016/S0025-326X(87)80019-X

Lapointe, B. (1995). A comparison of nutrient-limited productivity in *Sargassum natans* from neritic vs. oceanic waters of the western North Atlantic Ocean. *Limnology and Oceanography*, *40*(3), 625–633.

Law, K. L., Morét-Ferguson, S., Maximenko, N. A, Proskurowski, G., Peacock, E. E., Hafner, J., & Reddy, C. M. (2010). Plastic accumulation in the North Atlantic subtropical gyre. *Science*, *329*(5996), 1185–1188. doi:10.1126/science.1192321

Lee, S. H., Stockwell, D.A., Joo, H.-M., Son, Y. B., Kang, C.-K. & Whitledge, T. E. (2012). Phytoplankton production from melting ponds on Arctic sea ice. *Journal of Geophysical Research*, *117*, C04030. doi:10.1029/2011JC007717

Lee, Y.W., & Kim, G. (2007). Linking groundwater-borne nutrients and dinoflagellate red-tide outbreaks in the southern sea of Korea using a Ra tracer. *Estuarine, Coastal and Shelf Science*, *71*(1-2), 309–317. doi:10.1016/j.ecss.2006.08.004

Lee, Z., Carder, K. L., Hawes, S. K., Steward, R. G., Peacock, T. G., & Davis, C. O. (1994). Model for the interpretation of hyperspectral remote-sensing reflectance. *Applied Optics*, *33*(24), 5721–5732. doi:10.1364/AO.33.005721

Lee, Z., Carder, K. L., Mobley, C. D., Steward, R. G., & Patch, J. S. (1998). Hyperspectral remote sensing for shallow waters. I. A semianalytical model. *Applied Optics*, *37*(27), 6329–6338. doi:10.1364/AO.37.006329

Lee, Z., Carder, K. L., Mobley, C. D., Steward, R. G., & Patch, J. S. (1999). Hyperspectral remote sensing for shallow waters. 2. Deriving bottom depths and water properties by optimization. *Applied Optics*, *38*(18), 3831–3843. doi:10.1364/AO.38.003831

Lee, Z., Carder, K. L., & Arnone, R. A. (2002). Deriving inherent optical properties from water color: a multiband quasi-analytical algorithm for optically deep waters. *Applied Optics*, *41*(27), 5755–5772. doi:10.1364/AO.41.005755

Lee Z., Rhea W. J., Arnone R., and Goode W. (2005). Absorption coefficients of marine waters: expanding multiband information to hyperspectral data. *IEEE Transactions on Geoscience and Remote Sensing*, *43*(1), 118-124.

Lee, Z., Carder, K. L., Arnone, R. A., & He, M. (2007a). Determination of primary spectral bands for remote sensing of aquatic environments. *Sensors*, *7*(12), 3428–3441. doi:10.3390/s7123428

Lee, Z., Casey, B., Arnone, R., Weidemann, A., Parsons, R., Montes, M. J., Gao, B-C., Goode, W., Davis, C. O., Dye, J. (2007b). Water and bottom properties of a coastal environment derived from Hyperion data measured from the EO-1 spacecraft platform. *Journal of Applied Remote Sensing*, *1*(011502), 1-16.

Leet, W. S., Dewees, C. M., Klingbeil, R., & Johnson, E. J. (Eds). (2001). California's living marine resources: a status report. California Department of Fish and Game, Resources Agency, 277-281.

Leote, C., Ibánhez, J., & Rocha, C. (2008). Submarine groundwater discharge as a nitrogen source to the Ria Formosa studied with seepage meters. *Biogeochemistry*, *88*(2), 185–194. doi:10.1007/s

Lesser, M. P., & Mobley, C. D. (2007). Bathymetry, water optical properties, and benthic classification of coral reefs using hyperspectral remote sensing imagery. *Coral Reefs*, *26*(4), 819–829. doi:10.1007/s00338-007-0271-5

Li, L., Ustin, S. L., & Lay, M. (2005). Application of multiple endmember spectral mixture analysis (MESMA) to AVIRIS imagery for coastal salt marsh mapping: a case study in China Camp, CA, USA. *International Journal of Remote Sensing*, *26*(23), 5193–5207. doi:10.1080/01431160500218911

Liu, Y., Weisberg, R. H., Hu, C., & Zheng, L. (2011). Tracking the Deepwater Horizon oil spill: A modeling perspective. *Eos, Transactions American Geophysical Union*, *92*(6), 45–46. doi:10.1029/2011EO060001

Lobo, F. L., Novo, E. M. L. M., Barbosa, C. C. F., & Galvao, L. S. (2012). Reference spectra to classify Amazon water types. *International Journal of Remote Sensing, 33,* 3422-3442.

Loisel, H., Nicolas, J.-M., Sciandra, A., Stramski, D., & Poteau, A. (2006). Spectral dependency of optical backscattering by marine particles from satellite remote sensing of the global ocean. *Journal of Geophysical Research, 111,* C09024. doi:10.1029/2005JC003367

Louchard, E., Reid, R., Stephens, F., Davis, C., Leathers, R. A., & Downes, T. V. (2003). Optical remote sensing of benthic habitats and bathymetry in coastal environments at Lee Stocking Island, Bahamas: A comparative spectral classification approach. *Limnology and Oceanography, 48*(1), 511–521.

Lubac, B., Loisel, H., Guiselin, N., Astoreca, R., Artigas, L. F.,& Mériaux, X. (2008). Hyperspectral versus multispectral remote sensing approach to detect phytoplankton blooms in coastal waters : application to a *Phaeocystis globosa* bloom. *Journal of Geophysical Research, 113,* C06026, doi:10.1029/2007JC004451.

Lucke, R. L., Corson, M., McGlothlin, N. R., Butcher, S. D., Wood, D. L., Korwan, D. R., Li, R. R., et al. (2011). Hyperspectral Imager for the Coastal Ocean: instrument description and first images. *Applied Optics, 50*(11), 1501–1516. doi:10.1364/AO.50.001501

Lunetta, R. S. & Balogh, M. E. (1999). Application of multi-temporal Landsat 5 TM imagery for wetland identification. *Photogrammetric Engineering and Remote Sensing, 65,* 1303-1310.

Lunetta, R. S., Knight, J. F., Ediriwickrema, J., Lyon, J. G., & Worthy, L. D. (2006). Land-cover change detection using multi-temporal MODIS NDVI data. *Remote Sensing of Environment, 105*(2), 142–154. doi:10.1016/j.rse.2006.06.018

Lyon, J. G., & McCarthy, J. (1995). *Wetland and environmental applications of GIS*. Lewis Publishers, New York, U.S.A., 400 p.

Lyzenga, D.R. (1981). Remote sensing of bottom reflectance and water attenuation parameters in shallow water using aircraft and Landsat data. *International Journal of Remote Sensing, 2*(1), 71-82. doi:10.1080/01431168108948342

Mann, K. H. (2000). *Ecology of coastal waters: with implications for management*. Blackwell, Malden, Massachusetts, U.S.A. 192-218.

Mannino, A., Russ, M. E., & Hooker, S. B. (2008). Algorithm development and validation for satellite-derived distributions of DOC and CDOM in the US Middle Atlantic Bight. *Journal of Geophysical Research: Oceans, 113,* C07051.

Mariotto, I., Thenkabail, P.S., Huete, A., Slonecker, E.T., & Platonov, A. (2013). Hyperspectral versus multispectral crop-productivity modeling and type discrimination for the HyspIRI mission. *Remote Sensing of Environment, 139,* 291-305.

Marshall, B. R., & Smith, R. C. (1990). Raman scattering and in-water ocean optical properties. *Applied Optics, 29*(1), 71–84. doi:10.1364/AO.29.000071

Marshall, M., Tu, K., Funk, C., Michaelsen, J., Williams, P., Williams, C., Ardö, J., et al. (2013). Improving operational land surface model canopy evapotranspiration in Africa using a direct remote sensing approach. *Hydrology and Earth System Sciences, 17*(3), 1079–1091. doi:10.5194/hess-17-1079-2013

Martinez-Vicente, V., Land, P. E., Tilstone, G. H., Widdicombe, C., & Fishwick, J. R. (2010). Particulate scattering and backscattering related to water constituents and seasonal changes in the Western English Channel. *Journal of Plankton Research*, *32*(5), 603–619. doi:10.1093/plankt/fbq013

Matthews, M. W. (2011). A current review of empirical procedures of remote sensing in inland and near-coastal transitional waters. *International Journal of Remote Sensing*, *32*(21), 6855–6899. doi:10.1080/01431161.2010.512947

McFeeters, S. K. (1996). The use of the Normalized Difference Water Index (NDWI) in the delineation of open water features. *International Journal of Remote Sensing*, *17*(7), 1425-1432. doi:10.1080/01431169608948714

McGowan, J. A. (1998). Climate-Ocean Variability and Ecosystem Response in the Northeast Pacific. *Science*, *281*(5374), 210–217. doi:10.1126/science.281.5374.210

McInnes, K., Walsh, K., Hubbert, G., & Beer, T. (2003). Impact of sea-level rise and storm surges on a coastal community. *Natural Hazards*, *30*, 187–207.

McKee, D., Cunningham, A., Wright, D., & Hay, L. (2007). Potential impacts of nonalgal materials on water-leaving sun induced chlorophyll fluorescence signals in coastal waters. *Applied Optics*, *46*(31), 7720–7729. doi:10.1023/A1026118417752

McKenna, T., Andres, A., & DeLiberty, T. (2001). Mapping locations of ground-water discharge in Rehoboth and Indian River bays, Delaware using thermal imagery. *Geological Society of America, Abstracts with Programs, November 1–10, Boston, Massachusetts, U.S.A.*

McPhee-Shaw, E. E., Siegel, D. A., Washburn, L., Brzezinski, M. A., Jones, J. L., Leydecker, A., & Melack, J. (2007). Mechanisms for nutrient delivery to the inner shelf: Observations from the Santa Barbara Channel. *Limnology and Oceanography*, *52*(5), 1748–1766.

Meijerink, A. (2002). Satellite eco-hydrology: a review. *Tropical Ecology*, *43*(1), 91–106.

Mendelssohn, I., McKee, K., & Kong, T. (2001). A comparison of physiological indicators of sublethal cadmium stress in wetland plants. *Environmental and Experimental Botany*, *46*(3), 263–275. doi:10.1016/S0098-8472(01)00106-X

Mestres M., Sierra J. P., Sánchez-Arcilla A. (2007). Factors influencing the spreading of a lowdischarge river plume. *Continental Shelf Research*, *27*(16-15), 2116-2134.

Miller, D. C., & Ullman, W. J. (2004). Ecological Consequences of Ground Water Discharge to Delaware Bay, United States. *Ground Water*, *42*(7), 959–970. doi:10.1111/j.1745-6584.2004.tb02635.x

Miller, R. L., & Fujii, R. (2010). Plant community, primary productivity, and environmental conditions following wetland re-establishment in the Sacramento-San Joaquin Delta, California. *Wetlands Ecology and Management*, *18*(1), 1–16. doi:10.1007/s11273-009-9143-9

Milzow, C., Kgotlhang, L., Kinzelbach, W., Meier, P., & Bauer-Gottwein, P. (2009). The role of remote sensing in hydrological modelling of the Okavango Delta, Botswana. *Journal of Environmental Management*, *90*(7), 2252–60. doi:10.1016/j.jenvman.2007.06.032

Mishra, D.R., Cho, H.J., Ghosh, S., Fox, A., Downs, C., Merani, P.B.T., Kirui, P., Jackson, N., & Mishra, S. (2012). Post-spill state of the marsh: Remote estimation of the ecological impact of the Gulf of Mexico oil spill on Louisiana Salt Marshes. *Remote Sensing of Environment, 118,* 176-185.

Moberg, F., & Folke, C. (1999). Ecological goods and services of coral reef ecosystems. *Ecological Economics*, *29*(2), 215–233. doi:10.1016/S0921-8009(99)00009-9

Mobley, C. D., Sundman, L. K., Davis, C. O., Bowles, J. H., Downes, T. V., Leathers, R. A., Montes, M. J., et al. (2005). Interpretation of hyperspectral remote-sensing imagery by spectrum matching and look-up tables. *Applied Optics*, *44*(17), 3576–3592. doi:10.1364/AO.44.003576

Moffett, K. B. (2010). Groundwater-vegetation-atmosphere interactions in an intertidal salt marsh. Ph.D. dissertation, *Department of Environmental Earth System Science, Stanford University, Stanford, CA.*

Mohamed, Y. A., Bastiaanssen, W. G. M., & Savenije, H. H. G. (2004). Spatial variability of evaporation and moisture storage in the swamps of the upper Nile studied by remote sensing techniques. *Journal of Hydrology*, *289*(1-4), 145–164. doi:10.1016/j.jhydrol.2003.11.038

Moisan, J. R., Moisan, T. A. H., & Linkswiler, M. A. (2011). Estimating phytoplankton pigment concentrations from phytoplankton absorption spectra. *Journal of Geophysical Research, 116,* 148-227.

Moisan, T., Olaizola, M., & Mitchell, B. (1998). Xanthophyll cycling in *Phaeocystis antarctica*: Changes in cellular fluorescence. *Marine Ecology Progress Series*, *169,* 113–121. doi:10.3354/meps169113

Morel, A., & Gentili, B. (2009). A simple band ratio technique to quantify the colored dissolved and detrital organic material from ocean color remotely sensed data. *Remote Sensing of Environment*, *113*(5), 998–1011. doi:10.1016/j.rse.2009.01.008

Morris, J. T., Sundareshwar, P. V., Nietch, C. T., Kjerfve, B., & Cahoon, D. R. (2002). Responses of coastal wetlands to rising sea level. *Ecology*, *83*(10), 2869–2877. doi:10.1890/0012-9658(2002)083[2869:ROCWTR]2.0.CO;2

Moses, C., Andréfouët, S., Kranenburg, C., & Müller-Karger, F. (2009a). Regional estimates of reef carbonate dynamics and productivity using Landsat 7 ETM+, and potential impacts from ocean acidification. *Marine Ecology Progress Series*, *380,* 103–115. doi:10.3354/meps07920

Moses, W. J., Gitelson, A. A., Berdnikov, S., & Povazhnyy, V. (2009b). Satellite estimation of chlorophyll-*a* concentration using the red and NIR bands of MERIS — The Azov Sea case study. *IEEE Geoscience and Remote Sensing Letters*, *6*(4), 845–849. doi:10.1109/LGRS.2009.2026657

Moses, W. J., Bowles, J. H., Lucke, R. L., & Corson, M. R. (2012a). Impact of signal-to-noise ratio in a hyperspectral sensor on the accuracy of biophysical parameter estimation in case II waters. *Optics Express, 20*(4), 4309-4330.

Moses, W. J., Gitelson, A. A., Berdnikov, S., Saprygin, V., & Povazhnyi, V. (2012b). Operational MERIS-based NIR-red algorithms for estimating chlorophyll-*a* concentrations in coastal waters — The Azov Sea case study. *Remote Sensing of Environment, 121,* 118–124. doi:10.1016/j.rse.2012.01.024

Moses, W. J., Gitelson, A. A., Berdnikov, S., Bowles, J. H., Povazhnyi, V., Saprygin, V., & Wagner, E. J. (2014). HICO-Based NIR-red Algorithms for Estimating Chlorophyll-*a* Concentration in Productive Coastal Waters. *IEEE Geoscience and Remote Sensing Letters, 11*(6), 1111-1115.

Mueller, J. L., & Trees, C. C. (1997). Revised SeaWiFS prelaunch algorithm for the diffuse attenuation coefficient K (490). In: Hooker, S. B., & Firestone, E. R. (Eds). *Case Studies for SeaWiFS Calibration and Validation, Part 4. NASA Tech. Memo. 104566,* Vol. 41, NASA Goddard Space Flight Center, Greenbelt, Maryland, 18–21.

Müller-Karger, F. E. (1984). Lower trophic level studies in the marginal sea ice zone. MS Thesis, University of Alaska, Fairbanks. 145 p.

Müller-Karger, F. E., Alexander, V. (1987a). Nitrogen dynamics in a marginal sea-ice zone. *Continental Shelf Research, 7,* 805-823.

Müller-Karger, F. E., McClain, C. R., & Ray, G. C. (1987b). Primary Productivity. Chapter in the Strategic Atlas of Economic Resources of the Bering Sea. NOAA Strategic Assessment Branch, Rockville, MD.

Müller-Karger, F. E., McClain, C.R., & Richardson, P. L. (1988). The dispersal of the Amazon's water. *Nature, 333,* 56-59.

Müller‐Karger, F. E., McClain, C. R., Sambrotto, R., & Ray, G. (1990). A comparison of ship and Coastal Zone Color Scanner mapped distribution of phytoplankton in the southeastern Bering Sea. *Journal of Geophysical Research*, *95*(C7), 11.483–11,499.

Mumby, P. J., Skirving, W., Strong, A. E., Hardy, J. T., LeDrew, E. F., Hochberg, E. J., Stumpf, R. P., et al. (2004). Remote sensing of coral reefs and their physical environment. *Marine Pollution Bulletin*, *48*(3-4), 219–228. doi:10.1016/j.marpolbul.2003.10.031

Murray, S. J., Watson, I. M., & Prentice, I. C. (2012). The use of dynamic global vegetation models for simulating hydrology and the potential integration of satellite observations. *Progress in Physical Geography*, *37*(1), 63–97. doi:10.1177/0309133312460072

Mutanga, O., Adam, E., & Cho, M.A. (2012). High density biomass estimation for wetland vegetation using WorldView-2 imagery and random forest regression algorithm. *International Journal of Applied Earth Observation and Geoinformation, 18,* 399-406.

NASA /GSFC. (2010). Hurricane Ike: storm surge flooding image of the Gulf Coast. NASA image courtesy Jeff Schmaltz, MODIS Rapid Response Team at NASA GSFC.

National Research Council (2007). *Earth science and applications from space: National imperatives for the next decade and beyond*. Committee on Earth Science and Applications from Space: A Community Assessment and Strategy for the Future. The National Academic Press, Washington, DC, USA, pp. 1–456.

Nikolakopoulos, K. G., Karathanassi, V., & Rokos, D. (2006). Hyperspectral data and methods for coastal water mapping. *Proceedings of SPIE, 6359,* 1–10. doi:10.1117/12.688998

O'Reilly, J. E., Maritorena, S., Mitchell, B. G., Siegel, D. A., Carder, K. L., Garver, S. A., Kahru, M., et al. (1998). Ocean color chlorophyll algorithms for SeaWiFS. *Journal of Geophysical Research, 103*(C11), 24937–24953. doi:10.1029/98JC02160

Odermatt, D., Gitelson, A., Brando, V. E., & Schaepman, M. (2012). Review of constituent retrieval in optically deep and complex waters from satellite imagery. *Remote Sensing of Environment, 118*, 116–126. doi:10.1016/j.rse.2011.11.013

Odriozola, A. L., Varela, R., Hu, C., Astor, Y., Lorenzoni, L., & Müller-Karger, F. E. (2007). On the absorption of light in the Orinoco River plume. Continental Shelf Research, *27*, 1447-1464. doi.10.1016/j.csr.2007.01.012.

Odum, E. P., (1993). *Ecology and our endangered life-support systems*. 2nd Edition. Sinauer Associates, Inc., Sunderland, Massachusetts, U.S.A. 320 p.

Odum, H., & Odum, E. (1955). Trophic structure and productivity of a windward coral reef community on Eniwetok Atoll. *Ecological Monographs, 25*(3), 291–320.

Oey, L-Y, Ezer, T., Hu, C., Müller-Karger, F.E. (2007). Baroclinic tidal flows and inundation processes in Cook Inlet, Alaska: Numerical modeling and satellite observations. *Ocean Dynamics, 57*(3), 205-221. doi:10.1007/s10236-007-0103-8

Okin, G. S., Painter, T. H. (2004). Effect of grain size on remotely sensed spectral reflectance of sandy desert surfaces. *Remote Sensing of Environment, 89*, 272-280.

Ostlund, C., Flink, P., Strömbeck, N., Pierson, D., & Lindell, T. (2001). Mapping of the water quality of Lake Erken, Sweden, from imaging spectrometry and Landsat Thematic Mapper. *The Science of the Total Environment, 268*(1-3), 139–154. doi:10.1016/S0048-9697(00)00683-5

Ouma, Y. O., & Tateishi, R. (2006). A water index for rapid mapping of shoreline changes of five East African Rift Valley lakes: an empirical analysis using Landsat TM and ETM+ data. *International Journal of Remote Sensing, 27*(15), 3153–3181. doi:10.1080/01431160500309934

Ozesmi, S. L., & Bauer, M. E. (2002). Satellite remote sensing of wetlands. *Wetlands Ecology and Management, 10*, 381–402. doi:10.1023/A:1020908432489

Pandolfi, J. M., Bradbury, R. H., Sala, E., Hughes, T. P., Bjorndal, K. a, Cooke, R. G., McArdle, D., et al. (2003). Global trajectories of the long-term decline of coral reef ecosystems. *Science, 301*(5635), 955–958. doi:10.1126/science.1085706

Papeş, M., Tupayachi, R., Martínez, P., Peterson, A. T., & Powell, G. V. N. (2010). Using hyperspectral satellite imagery for regional inventories: a test with tropical emergent trees in the Amazon Basin. *Journal of Vegetation Science, 21*(2), 342–354. doi:10.1111/j.1654-1103.2009.01147.x

Pendleton, L., Donato, D.C., Murray, B.C., Crooks, S., Jenkins, W.A., Sifleet, S., Craft, C., Fourqurean, J.W., Kauffman, J.B., Marbà, N., Megonigal, P., Pidgeon, E., Herr, D., Gordon, D., & Baldera, A. (2012). Estimating global "Blue Carbon" emissions from conversion and degradation of vegetated coastal ecosystems. *PLoS ONE, 7*, e43542.

Pengra, B. W., Johnston, C. A., & Loveland, T. R. (2007). Mapping an invasive plant, *Phragmites australis*, in coastal wetlands using the EO-1 Hyperion hyperspectral sensor. *Remote Sensing of Environment*, *108*(1), 74–81. doi:10.1016/j.rse.2006.11.002

Perrette, M., A. Yool, G. D. Quartly and E. E. Popova (2011). Near-ubiquity of ice-edge blooms in the Arctic. *Biogeosciences*, *8*, 515-524.

Petropoulos, G., Carlson, T. N., Wooster, M. J., & Islam, S. (2009). A review of Ts/VI remote sensing based methods for the retrieval of land surface energy fluxes and soil surface moisture. *Progress in Physical Geography*, *33*(2), 224–250. doi:10.1177/0309133309338997

Philpot, W. D. (1989). Bathymetric mapping with passive multispectral imagery. *Applied Optics*, *28*(8), 1569–1578. doi:10.1364/AO.28.001569

Phinn, S., Roelfsema, C., Dekker, A., Brando, V., & Anstee, J. (2008). Mapping seagrass species, cover and biomass in shallow waters: An assessment of satellite multi-spectral and airborne hyper-spectral imaging systems in Moreton Bay (Australia). *Remote Sensing of Environment*, *112*(8), 3413-3425. doi: 10.1016/j.rse.2007.09.017

Pinet, P.R., (2009). *Invitation to oceanography*. 5th Edition. Jones & Bartlett, Sudbury, Massachussetts, U.S.A., 620 p.

Polcyn, F.C., Brown, W. L., & Sattinger, I. J. (1970). *The measurement of water depth by remote-sensing techniques*. University of Michigan Press, Ann Arbor, Michigan, U.S.A. 47 p.

Portnoy, J. W., Nowicki, B. L., Roman, C. T., & Urish, D. W. (1998). The discharge of nitrate-contaminated groundwater from developed shoreline to marsh-fringed estuary. *Water Resources Research*, *34*(11), 3095–3104. doi:10.1029/98WR02167

Pozdnyakov, D., Korosov,A., Grassl, H., & Pettersson, L. (2005). An advanced algorithm for operational retrieval of water quality from satellite data in the visible. *International Journal of Remote Sensing*, *26*(12), 2669–2687. doi:10.1080/01431160500044697

Pu, R., Bell, S., Meyer, C., Baggett, L., & Zhao, Y. (2012). Mapping and assessing seagrass along the western coast of Florida using Landsat TM and EO-1 ALI/Hyperion imagery. Estuarine, *Coastal and Shelf Science*, *115*, 234-245. doi: 10.1016/j.ecss.2012.09.006

Purkis, S. & Klemas, V. (2011). *Remote Sensing and Global Environmental Change.* Wiley-Blackwell, Oxford, U.K. 384 pp.

Raitsos D. E., Lavender S. J., Maravelias C. D., Haralambous J., Richardson A. J., & Reid P. C. (2008). Identifying phytoplankton functional groups from space: An ecological approach. *Limnology and Oceanography, 53*(2), 605-613.

Ramsey, E., & Rangoonwala, A. (2005). Leaf optical property changes associated with the occurrence of *Spartina alterniflora* dieback in coastal Louisiana related to remote sensing mapping. *Photogrammetric Engineering and Remote Sensing*, *71*(3), 299–311.

Ramsey, E., & Rangoonwala, A. (2006). Canopy reflectance related to marsh dieback onset and progression in coastal Louisiana. *Photogrammetric Engineering and Remote Sensing*, *72*(6), 641–652.

Reed, D. C., Rassweiler, A., & Arkema, K. K. (2008). Biomass rather than growth rate determines variation in net primary productivity by giant kelp. *Ecology*, *89*(9), 2493–2505. doi:10.1890/07-1106.1

Reed, D. C., Rassweiler, A., Carr, M. H., Cavanaugh, K. C., Malone, D. P., & Siegel, D. A. (2011). Wave disturbance overwhelms top-down and bottom-up control of primary production in California kelp forests. *Ecology*, *92*(11), 2108–2116. doi:10.1890/11-0377.1

Riegl, B. M., Purkis, S. J. (2009). Model of coral population response to accelerated bleaching and mass mortality in a changing climate. *Ecological Modelling*, *220*, 192–208.

Ritchie, J.C., Schiebe, F. R., & McHenry, J. R. (1976). Remote sensing of suspended sediment in surface water. *Photogrammetric Engineering and Remote Sensing*, *42*, 1539-1545.

Rivas, P. & Caselles, V., 2004. A simplified equation to estimate spatial reference evaporation from remote sensing-based surface temperature and local meteorological data. *Remote Sensing of Environment*, *93*, 68-76.

Roberts, D. A., Quattrochi, D. A., Hulley, G. C., Hook, S. J., & Green, R. O. (2012). Synergies between VSWIR and TIR data for the urban environment: An evaluation of the potential for the Hyperspectral Infrared Imager (HyspIRI) Decadal Survey mission. *Remote Sensing of Environment*, *117*(2012), 83–101. doi:10.1016/j.rse.2011.07.021

Roesler, C. S. & Perry, M. J. (1995). *In situ* phytoplankton absorption, fluorescence emission, and particulate backscattering spectra determined from reflectance. *Journal of Geophysical Research*, *100*(13), 279-294.

Rooker, J., Turner, J., & Holt, S. (2006). Trophic ecology of *Sargassum*-associated fishes in the Gulf of Mexico determined from stable isotopes and fatty acids. *Marine Ecology Progress Series*, *313*, 249–259. doi:10.3354/meps313249

Roseen, R. M., Brannaka, L. K., & Ballestero, T. P. (2001). Determination of nutrient loading from groundwater discharge into an inland estuary using airborne thermal imagery. *Proceedings of the 12th Biennial Coastal Zone Conference*, Cleveland, OH, USA.

Rosso, P. H., Ustin, S. L., & Hastings, A. (2005). Mapping marshland vegetation of San Francisco Bay, California, using hyperspectral data. *International Journal of Remote Sensing*, *26*(23), 5169–5191. doi:10.1080/01431160500218770

Running, S. W., Nemani, R. R., Heinsch, F. A., Zhao, M., Reeves, M., & Hashimoto, H. (2004). A continuous satellite-derived measure of global terrestrial primary production. *BioScience*, *54*(6), 547–560. doi:10.1641/0006-3568(2004)054[0547:ACSMOG]2.0.CO;2

Sadeghi, A., Dinter, T., Vountas, M., Taylor, B., Altenburg-Soppa, M., and Bracher, A. (2012). Remote sensing of coccolithophore blooms in selected oceanic regions using the PhytoDOAS method applied to hyper-spectral satellite data. *Biogeosciences, 9*, 2127-2143. doi:10.5194/bg-9-2127-2012

Saito, H., Bellan, M., Al-Habshi, A., Aizpuru, M., & Blasco, F. (2003). Mangrove research and coastal ecosystem studies with SPOT-4 HRVIR and TERRA ASTER in the Arabian

Gulf. *International Journal of Remote Sensing*, *24*(21), 4073–4092. doi:10.1080/0143116021000035030

Salvat, B. (1992). Coral reefs — a challenging ecosystem for human societies. *Global Environmental Change*, *2*(1), 12–18. doi:10.1016/0959-3780(92)90032-3

Sandholt, I., Rasmussen, K., & Andersen, J. (2002). A simple interpretation of the surface temperature/vegetation index space for assessment of surface moisture status. *Remote Sensing of Environment*, *79*(2-3), 213–224. doi:10.1016/S0034-4257(01)00274-7

Sathyendranath, S., Hoge, F. E., Platt, T., & Swift, R. N. (1994). Detection of phytoplankton pigments from ocean color: improved algorithms. *Applied Optics*, *33*(6), 1081–1089. doi:10.1364/AO.33.001081

Sathyendranath, S., Watts, L., & Devred, E. (2004). Discrimination of diatoms from other phytoplankton using ocean-colour data. *Marine Ecology Progress Series*, *272*, 59–68.

Schalles, J. F., Gitelson, A. A., Yacobi, Y. Z., & Kroenke, A. E. (1998). Estimation of Chlorophyll *a* from time series measurements of high spectral resolution reflectance in a eutrophic lake. *Journal of Phycology*, *34*(2), 383–390. doi:10.1046/j.1529-8817.1998.340383.x

Schiller, H., & Doerffer, R. (1999). Neural network for emulation of an inverse model operational derivation of Case II water properties from MERIS data. *International Journal of Remote Sensing*, *20*(9), 1735–1746. doi:10.1080/014311699212443

Schmidt, K. S., & Skidmore, A. K. (2003). Spectral discrimination of vegetation types in a coastal wetland. *Remote Sensing of Environment*, *85*(1), 92–108. doi:10.1016/S0034-4257(02)00196-7

Schmidt, K. S., Skidmore, A. K., Kloosterman, E., Van Oosten, H., Kumar, L., & Janseen, J. (2004). Mapping coastal vegetation using an expert system and hyperspectral imagery. *Photogrammetric Engineering and Remote Sensing*, *70*(6), 703–715.

Schofield, O., Bergmann, T., Oliver, M. J., Irwin, A., Kirkpatrick, G., Bissett, P. W., Moline, M. A., & Orrico, C. (2004). Inversion of spectral absorption in the optically complex coastal waters of the Mid-Atlantic Bight. *Journal of Geophysical Research, 109*, C12S04. doi:10.1029/2003JC002071

Schroeder, T., Devlin, M. J., Brando, V. E., Dekker, A. G., Brodie, J. E., Clementson, L. A., & McKinna, L. (2012). Inter-annual variability of wet season freshwater plume extent into the Great Barrier Reef lagoon based on satellite coastal ocean colour observations. *Marine Pollution Bulletin*, *65*(4–9): 210-223.

Scott, J. W., Moore, L .R., Harris, W. M. & Reed, M. D. (2003). Using the Landsat 7 Enhanced Thematic Mapper tasseled cap transformation to extract shoreline. Open-File Report, OF 03-272, US Geological Survey.

Seher, S. S., & Tueller, P.T. (1973). Color aerial photos for marshland. *Photogrammetric Engineering 38*(6), 489-499.

Settle, J. J., & Drake, N. A. (1993). Linear mixing and the estimation of ground cover proportions. *International Journal of Remote Sensing*, *14*(6), 1159–1177. doi:10.1080/01431169308904402

Shih, S., & Jordan, J. (1993). Use of Landsat thermal-IR data and GIS in soil moisture assessment. *Journal of Irrigation and Drainage Engineering*, *119*(5), 868–879. doi:10.1061/(ASCE)0733-9437(1993)119%3A5(868)

Short, F., Carruthers, T., Dennison, W., & Waycott, M. (2007). Global seagrass distribution and diversity: A bioregional model. *Journal of Experimental Marine Biology and Ecology*, *350*(1), 3-20. doi: 10.1016/j.jembe.2007.06.012

Silvestri, S., Marani, M., & Marani, A. (2003). Hyperspectral remote sensing of salt marsh vegetation, morphology and soil topography. *Physics and Chemistry of the Earth*, *28*(1-3), 15–25. doi:10.1016/S1474-7065(03)00004-4

Small, A., Adey, W., & Spoon, D. (1998). Are current estimates of coral reef biodiversity too low? The view through the window of a microcosm. *Atoll Research Bulletin*, *458*, 1–20.

Smith, S. V. (1978). Coral-reef area and the contributions of reefs to processes and resources of the world's oceans. *Nature*, *273*(5659), 225–226. doi:10.1038/273225a0

Smith, S. V, & Buddemeier, R. W. (1992). Global change and coral reef ecosystems. *Annual Review of Ecology and Systematics*, *23*(1), 89–118. doi:10.1146/annurev.es.23.110192.000513

Sone, C., Saito, K., & Futakuchi, K. (2009). Comparison of three methods for estimating leaf Area Index of Upland Rice Cultivars. *Crop Science*, *49*(4), 1438–1443. doi:10.2135/cropsci2008.09.0520

Sonnentag, O., Detto, M., Vargas, R., Ryu, Y., Runkle, B. R. K., Kelly, M., & Baldocchi, D. D. (2011). Tracking the structural and functional development of a perennial pepperweed (*Lepidium latifolium L.*) infestation using a multi-year archive of webcam imagery and eddy covariance measurements. *Agricultural and Forest Meteorology*, *151*(7), 916–926. doi:10.1016/j.agrformet.2011.02.011

South Atlantic Fishery Council. (2002). Fishery management plan for pelagic *Sargassum* habitat of the South Atlantic region. (Online) http://www.safmc.net/Portals/6/Library/FMP/Sargassum/SargFMP.pdf

Spalding, M. D., & Grenfell, A. M. (1997). New estimates of global and regional coral reef areas. *Coral Reefs*, *16*(4), 225–230. doi:10.1007/s003380050078

Steinmetz, F., Deschamps, P.-Y. & Ramon, D. (2001). Atmospheric correction in presence of sun glint: application to MERIS. *Optics Express*, *19*(10), 9783-9800.

Sterckx, S., Knaeps, E., Bollen M., Trouw K., & Houthuys, R. (2007). Retrieval of suspended sediment from Advanced Hyperspectral Sensor data in the Scheldt Estuary at different stages in the tidal cycle. *Marine Geodesy, 30*(1), 97–108.

Stoddart, D. R. (1969). Ecology and morphology of recent coral reefs. *Biological Reviews*, *44*(4), 433–498. doi:10.1111/j.1469-185X.1969.tb00609.x

Stumpf, R. P., Gelfenbaum, G., & Pennock, J. R. (1993). Wind and tidal forcing of a buoyant plume, Mobile Bay, Alabama. *Continental Shelf Research, 13*, 1281−1301.

Stumpf, R. P., & Holderied, K., Sinclair, M. (2003). Determination of water depth with high-resolution satellite imagery over variable bottom types. *Limnology and Oceanography*, *48*, 547–556.

Subranamiam, A., Brown, C. W., Hood, R. R., Carpenter, E. J., & Capone, D. G. (2001). Detecting *Trichodesmium* blooms in SeaWiFS imagery. *Deep Sea Research Part II: Topical Studies in Oceanography*, *49*(1-3), 107–121. doi:10.1016/S0967-0645(01)00096-0

Svejkovsky, J., & Muskat, J. (2009). Development of a portable multispectral aerial sensor for real-time oil spill thickness mapping in coastal and offshore waters. Final Report, U.S. Department of the Interior, Mineral Management Service.

Szmant, A. M. (2002). Nutrient enrichment on coral reefs: Is it a major cause of coral reef decline? *Estuaries*, *25*(4), 743–766. doi:10.1007/BF02804903

Terchunian, A., Klemas, V., Segovia, A., Alvarez, A., Vasconez, B., & Guerrero, L. (1986). Mangrove mapping in Ecuador: The impact of shrimp pond construction. *Environmental Management*, *10*(3), 345–350. doi:10.1007/BF01867258

Thenkabail, P.S., Enclona, E.A., Ashton, M.S., Legg, C., & De Dieu, M.J. (2004). Hyperion, IKONOS, ALI, and ETM+ sensors in the study of African rainforests. *Remote Sensing of Environment, 90*, 23-43.

Thompson, R. C., Olsen, Y., Mitchell, R. P., Davis, A., Rowland, S. J., John, A. W. G., McGonigle, D., et al. (2004). Lost at sea: where is all the plastic? *Science*, *304*(5672), 838. doi:10.1126/science.1094559

Tian, Y. C., Yao, X., Yang, J., Cao, W. X., Hannaway, D. B., & Zhu, Y. (2011). Assessing newly developed and published vegetation indices for estimating rice leaf nitrogen concentration with ground- and space-based hyperspectral reflectance. *Field Crops Research*, *120*(2), 299–310. doi:10.1016/j.fcr.2010.11.002

Tilley, D. R., Ahmed, M., Son, J. H., & Badrinarayanan, H. (2003). Hyperspectral reflectance of emergent macrophytes as an indicator of water column ammonia in an oligohaline, subtropical marsh. *Ecological Engineering*, *21*(2-3), 153–163. doi:10.1016/j.ecoleng.2003.10.004

Townsend, P., & Walsh, S. (2001). Remote sensing of forested wetlands: Application of multitemporal and multispectral satellite imagery to determine plant community composition and structure in Southeastern USA. *Plant Ecology*, *157*(2), 129–149. doi:10.1023/A:1013999513172

Tsoar, H. (2005). Sand dunes mobility and stability in relation to climate. *Physica A: Statistical Mechanics and its Applications*, *357*(1), 50–56. doi:10.1016/j.physa.2005.05.067

Turpie, K. R. (2012). Enhancement of a canopy reflectance model for understanding the specular and spectral effects of an aquatic background in an inundated tidal canopy. Ph.D. dissertation, *Department of Geography, University of Maryland, College Park, Maryland.*

Turpie, K. R. (2013). Explaining the spectral red-edge features of inundated marsh vegetation, *Journal of Coastal Research, in press.* doi:10.2112/JCOASTRES-D-12-00209.1

Tuxen, K. A., Schile, L. M., Kelly, M., & Siegel, S. W. (2008). Vegetation colonization in a restoring tidal marsh: A remote sensing approach. *Restoration Ecology*, *16*(2), 313–323. doi:10.1111/j.1526-100X.2007.00313.x

Tuxen, K. A., Schile, L. M., Stralberg, D., Siegel, S. W., Parker, T., Vasey, M., Callaway, J., et al. (2011). Mapping changes in tidal wetland vegetation composition and pattern across a salinity gradient using high spatial resolution imagery. *Wetlands Ecology and Management*, *19*(2), 141–157. doi:10.1007/s11273-010-9207-x

Underwood, E. C., Mulitsch, M. J., Greenberg, J. A., Whiting, M. L., Ustin, S. L., & Kefauver, S. C. (2006). Mapping invasive aquatic vegetation in the Sacramento-San Joaquin delta using hyperspectral imagery. *Environmental Monitoring and Assessment, 121*(1-3), 47-64.

UNEP (2006). Marine and coastal ecosystems and human well-being: A synthesis report based on findings of the millennium ecosystem assessment. Nairobi, Kenya: UNEP.

UNEP-WCMC, WorldFish Centre, WRI and TNC (2010). Global distribution of warm- water coral reefs, compiled from multiple sources, including the Millennium Coral Reef Mapping Project. See attribute table for details. UNEP World Conservation Monitoring Centre. Cambridge (UK), http://data.unep- wcmc.org/datasets/13

Ustin, S. L., Roberts, D. A., Gamon, J. A., Asner, G. P., & Green, R. O. (2004). Using Imaging Spectroscopy to Study Ecosystem Processes and Properties. *BioScience*, *54*(6), 523–534. doi:10.1641/0006-3568(2004)054[0523:UISTSE]2.0.CO;2

Vaesen, K., Gilliams, S., Nackaerts, K., & Coppin, P. (2001). Ground-measured spectral signatures as indicators of ground cover and leaf area index: The case of paddy rice. *Field Crops Research*, *69*(1), 13–25. doi:10.1016/S0378-4290(00)00129-5

Vaiphasa, C., Ongsomwang, S., Vaiphasa, T., & Skidmore, A. K. (2005). Tropical mangrove species discrimination using hyperspectral data: A laboratory study. *Estuarine, Coastal and Shelf Science*, *65*(1-2), 371–379. doi:10.1016/j.ecss.2005.06.014

Vanderbilt, V. C., Perry, G. L., Livingston, G. P., Ustin, S. L., Barrios, M. C-D., Beron, F. M., Leroy, M. M., Balois, J. Y., Morrissey, L. A., Shewchuk, S. R., et al. (2002). Inundation discriminated using sun glint. *IEEE Transactions on Geoscience and Remote Sensing, 40*(6), 1279-1287.

Varni, M., Usunoff, E., Weinzettel, P., and Rivas, R. (1999). The groundwater recharge in the Azul aquifer, central Buenos Aires Province, Argentina. *Physics and Chemistry of the Earth, 24*, 349-352.

Venrick, E. L., Backman, T. W., Bartram, W. C., Platt, C. J., Thornhill, M. S., & Yates, R. E. (1973). Man-made objects on the surface of the Central North Pacific Ocean. *Nature, 241*(5387), 271–271. doi:10.1038/241271a0

Walsh, J. J., & Steidinger, K. A. (2001). Saharan dust and Florida red tides: The cyanophyte connection. *Journal of Geophysical Research*, *106*(C6), 11597–11612. doi:10.1029/1999JC000123

Wang, M., & Shi, W. (2007). The NIR-SWIR combined atmospheric correction approach for MODIS ocean color processing. *Optics Express*, *15*(24), 15722–15733. doi:10.1364/OE.15.015722

Wang, F., Huang, J., Tang, Y., & Wang, X. (2007). New vegetation index and its application in estimating leaf area index of rice. *Rice Science*, *14*(3), 195–203. doi:10.1016/S1672-6308(07)60027-4

Wang, L. T., McKenna, T. E., & Deliberty, T. L. (2008). Report of Investigations No. 74: Locating ground-water discharge areas in Rehoboth and Indian River Bays and Indian River Delaware using Landsat 7 imagery. Delaware Geological Survey, Newark, Delaware, U.S.A.

Wang, L. T., & Sousa, W. P. (2009). Distinguishing mangrove species with laboratory measurements of hyperspectral leaf reflectance. *International Journal of Remote Sensing*, *30*(5), 1267–1281. doi:10.1080/01431160802474014

Wang, Y. (2010). Remote sensing of coastal environments: An overview. In: Wang, J. (Ed). *Remote Sensing of Coastal Environments*. CRC Press, Boca Raton, Florida, U.S.A. 1-24.

Werdell, P. J., Bailey, S., McClain, C., & Fargion, S. (2002). The SeaWiFS Bio-Optical Archive and Storage Current Architecture and Implementation System (SeaBASS): Current Architecture and Implementation. *NASA/TM*, 211617.

Werdell, P. J., Bailey, S., Thomas, D., & McClain, C. (2005). *In situ* marine bio-optical data analysis and archival at NASA. American Geophysical Union Meeting, Fall Meeting, December, 2005. San Francisco, CA, USA.

Westberry, T. K., & Siegel, D. A. (2003). Phytoplankton natural fluorescence variability in the Sargasso Sea. *Deep Sea Research Part I: Oceanographic Research Papers*, *50*(3), 417–434. doi:10.1016/S0967-0637(03)00019-0

Westberry, T. K., & Siegel, D. A., & Subramaniam, A. (2005). An improved bio-optical model for the remote sensing of *Trichodesmium* spp. blooms. *Journal of Geophysical Research*, *110*, 1–11. doi:10.1029/2004JC002517

Wettle, M., Daniel, P. J., Logan, G. A., & Thankappan, M. (2009). Assessing the effect of hydrocarbon oil type and thickness on a remote sensing signal: A sensitivity study based on the optical properties of two different oil types and the HYMAP and Quickbird sensors. *Remote Sensing of Environment*, *113*(9), 2000–2010. doi:10.1016/j.rse.2009.05.010

White, A. T., Vogt, H. P., & Arin, T. (2000). Philippine coral reefs under threat: The economic losses caused by reef destruction. *Marine Pollution Bulletin*, *40*(7), 598–605. doi:10.1016/S0025-326X(00)00022-9

Whitmire, A., Pegau, W., Karp-Boss, L., Boss, E., & Cowles, T. (2010). Spectral backscattering properties of marine phytoplankton cultures. *Optics Express*, *18*(14), 1680–1690. doi:10.1029/2003RG000148.D.

Wilkinson, C. R. (Ed). (2008). *Status of coral reefs of the world*. Global coral reef monitoring network and reef and rainforest research centre, Townsville, Australia, 296 p.

Wiseman Jr., W. J., & Garvine, R. W. (1995). Plumes and coastal currents near large river mouths. *Estuaries, 18*(3), 509–517.

Witherington, B., Hirama, S., & Hardy, R. (2012). Young sea turtles of the pelagic *Sargassum*-dominated drift community: habitat use, population density, and threats. *Marine Ecology Progress Series, 463*, 1–22. doi:10.3354/meps09970

Wolfe, R. E., Nishihama, M., Fleig, A. J., Kuyper, J. A., Roy, D. P., Storey, J. C., & Patt, F. S. (2002). Achieving sub-pixel geolocation accuracy in support of MODIS land science. *Remote Sensing of Environment, 83*(1-2), 31–49. doi:10.1016/S0034-4257(02)00085-8

Wu, W. (2007). Coastline evolution monitoring and estimation — a case study in the region of Nouakchott, Mauritania. *International Journal of Remote Sensing, 28*(24), 5461–5484. doi:10.1080/01431160701227612

Xavier, A. C., & Vettorazzi, C. A. (2004). Mapping leaf area index through spectral vegetation indices in a subtropical watershed. *International Journal of Remote Sensing, 25*(9), 1661–1672. doi:10.1080/01431160310001620803

Xiao, X., He, L., Salas, W., Li, C., Moore, B., Zhao, R., Frolking, S., et al. (2002). Quantitative relationships between field-measured leaf area index and vegetation index derived from vegetation images for paddy rice fields. *International Journal of Remote Sensing, 23*(18), 3595–3604. doi:10.1080/01431160110115799

Xin, S. (2004). Inferring wetland hydrological conditions from remote sensing: A case study of Lake Baiyang, China. M.S. thesis, *International Institute for Geo-Information Science and Earth Observation, Enschede, The Netherlands*.

Xu, H. (2006). Modification of normalised difference water index (NDWI) to enhance open water features in remotely sensed imagery. *International Journal of Remote Sensing, 27*(14), 3025–3033. doi:10.1080/01431160600589179

Yang, C., Everitt, J. H., Fletcher, R. S., Jensen, J. R., & Mausel, P.W. (2009). Evaluating AISA+ hyperspectral imagery for mapping black mangrove along the south Texas gulf coast. *Photogrammetric Engineering and Remote Sensing, 75*(4), 425-436.

Yang, D., & Pan, D. (2007). Hyperspectral retrieval model of phycocyanin in Case II waters. *Chinese Science Bulletin, 51*(2), 149–153.

Yentsch, C. (2013). CZCS—Its Role in the Study of the Growth of Oceanic Phytoplankton. In *Ocean. Colour: Theory and Applications*. Barale, V., Ed., Springer: Berlin, Germany.

Yu, K., Hu, C., Müller-Karger, F. E., Lu, D., & Soto, I. (2011). Shoreline changes in west-central Florida between 1987 and 2008 from Landsat observations. *International Journal of Remote Sensing, 32*(23), 8299–8313. doi:10.1080/01431161.2010.535045

Zepp, R. G., Shank, G. C., Vahätälo, A., Bartels, E., & Jones, R. P. (2008). Photobiogeochemistry of *Sargassum*: a potentially important source of chromophoric dissolved organic matter in the upper ocean. Ocean Science Meeting, 2-7 March, 2008. Orlando, Florida, U.S.A.

Zhang, X., & Hu, L. (2010). Effects of temperature and salinity on light scattering by water. *SPIE Proceedings*, Vol. 7678L, 1-6. doi:10.1117/12.850803

Zhao, B., Yan, Y., Guo, H., He, M., Gu, Y., & Li, B. (2009). Monitoring rapid vegetation succession in estuarine wetland using time series MODIS-based indicators: An application in the Yangtze River Delta area. *Ecological Indicators*, *9*(2), 346–356. doi:10.1016/j.ecolind.2008.05.009

Zhao J., Barnes B., Melo N., English D., Lapointe B., Müller-Karger F., Schaeffer, B. & Hu, C. (2013). Assessment of satellite-derived diffuse attenuation coefficients and euphotic depths in south Florida coastal waters. *Remote Sensing of Environment, 131,* 38-50. doi: 10.1016/j.rse.2012.12.009

Zhu, W. N., Yu, Q., Tian, Y. Q., Chen, R. F., & Gardner, G. B. (2011). Estimation of chromophoric dissolved organic matter in the Mississippi and Atchafalaya river plume regions using above-surface hyperspectral remote sensing. *Journal of Geophysical Research: Oceans*, *116*, C02011.

Zhu, W. N., & Yu, Q. (2013). Inversion of chromophoric dissolved organic matter (CDOM) from EO-1 Hyperion imagery for turbid estuarine and coastal waters. *IEEE Transactions on Geoscience & Remote Sensing*, *51*, 3286–3298.

Zimmerman, R. C., & Kremer, J. N. (1984). Episodic nutrient supply to a kelp forest ecosystem in Southern California. *Journal of Marine Research*, *42*(3), 591–604. doi:10.1357/002224084788506031

Zomer, R. J., Trabucco, A., & Ustin, S. L. (2009). Building spectral libraries for wetlands land cover classification and hyperspectral remote sensing. *Journal of Environmental Management*, *90*(7), 2170–2177. doi:10.1016/j.jenvman.2007.06.02